Supplementary Information (SI) for Journal of Materials Chemistry C.

Supplementary information file: Closed-to-open-shell photoswitching in solid state and electric fields of thienyl-based acylhydrazones for catalysis and optical memories

Martin Šetek,[a] Valentino L. P. Guerra,[a] Harry Robson,[a] Anna O. Geleverya,[a] Ondřej Maxa,[a] Anna Lamancová,[a,b] Václav Eigner,[a] Dana Nachtigallová,[b,c] Ján Tarábek,[b] Petr Kovaříček [a,]*

[a] University of Chemistry and Technology Prague, Department of Organic Chemistry, Technická 5, 166 28, Prague 6, Czechia; *petr.kovaricek@vscht.cz, +420 220 444 165

[b] Institute of Organic Chemistry and Biochemistry, Flemingovo nám. 542/2, 160 00, Prague 6, Czechia

[c] IT4Innovations, VSB-Technical University of Ostrava, 17. listopadu 2172/15, 708 00 Ostrava Poruba, Czech Republic

1 GENERAL

Chemicals, which were used in this work, were provided by companies ABCR, Acros, Merck, Fluka, Fluorochem and Sigma-Aldrich and used without further purification.

The ^{1}H NMR spectra were measured on the spectrometers Agilent 400-MR DDR2 with frequency 400 MHz and Bruker Avance with frequency 500 MHz with a CRP probe. The ^{13}C NMR spectra were measured on the spectrometers Bruker Avance with frequency 126 MHz with a CRP probe and JEOL-ECZL400G with frequency 100 MHz. The chemical shift was referenced to the residual solvent signal according to the literature.[1]

Mass spectrometry was performed on facility Q-TOF (Micromass) in Central Laboratories of UCT Prague with ESI or APCI ionization methods.

UV-Vis analysis was performed on a Agilent Cary HP - 8454 Spectrophotometer. The spectra were processed using Origin 64 software.

Fluorescence analysis was performed using Varian Cary Eclipse.

The light for irradiation was provided with Quantum Design – Tunable monochromatic light source with Xenon lamp. Intensity: 375 μW @ 340 nm and bandwidth 4.8 nm.

The cyclic voltammetry was performed with PalmSens4 potentiostat with PSTrace software. The data were processed using Origin 64 software.

TLC analyses were performed on Alugram SIL G UV254 plates (aluminium sheets with 5-7 nm silica gel with 60 Å pore size, and 254 nm flourescenct indicator) or on Alugram Alox N Uv254 plates (aluminium sheets with neutral aluminium oxide with 60 Å pore size and 254 nm flourescent indicator). Technical grade Silica gel with 60 Å pore size, 40–63 µm particle size, in a 230–400 mesh (Merck) for column chromatography.

The flash chromatography was performed using Pure C-850 FlashPrep (BÜCHI).

2 SYNTHESIS, CHARACTERIZATION

2.1 General procedure A: Vilsmeier-Haack reaction

$POCl_3$ (1 equiv.) was added to a DMF (1 equiv.) solution in dichlormethane (3.0 mL) at 0 °C, and the reaction mixture was allowed to reach rt. The solution was then slowly added to a solution of thiophene derivative (1 equiv.) in dichlormethane (5.0 mL) at 0° C and allowed to reach rt. After stirring for 12 h, an excess of 3.0 M NaOH aqueous solution (5 equiv.) was added and stirred for 2h at rt. The reaction mixture was extracted with dichlormethane (25 ml × 3) and the combined organic layers were dried over $MgSO_4$. Purification of the residue was accomplished by flash chromatography on silica gel using hexane/ethyl acetate (3:1) as eluent to afford the product as a white solid.[2] 3,4-ethylenedioxythiophene-2-carbaldehyde, 3-hexylthiophene-2-carbaldehyde, thieno[2,3-b]thiophene-2-carbaldehyde and 4H-cyclopenta[2,1-b:3,4-b']dithiophene-2-carbaldehyde were synthesized according to the above mentioned procedure; thiophene-2-carbaldehyde, thiophene-3-carbaldehyde, thieno[3,2-b]thiophene-2-carbaldehyde, thieno[3,2-b]thiophene-2,5-dicarbaldehyde and thieno[2,3-b]thiophene-2,5-dicarbaldehyde were bought from Merck.

2.2 Syntheses of aldehyde precursors

2.2.1 Synthesis of 3,4-ethylenedioxythiophene-2-carbaldehyde

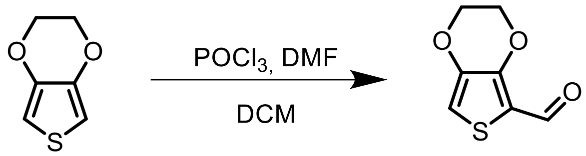

93 %

It was synthesized according to the general procedure A from $POCl_3$ (1.07 g, 7.03 mmol), DMF (0.51 g, 7.03 mmol) and 3,4-ethylenedioxythiophene (1.0 g, 7.03 mmol). Obtained as a white powder (1.11 g, 93 %). The analysis is in agreement with the literature.[3]

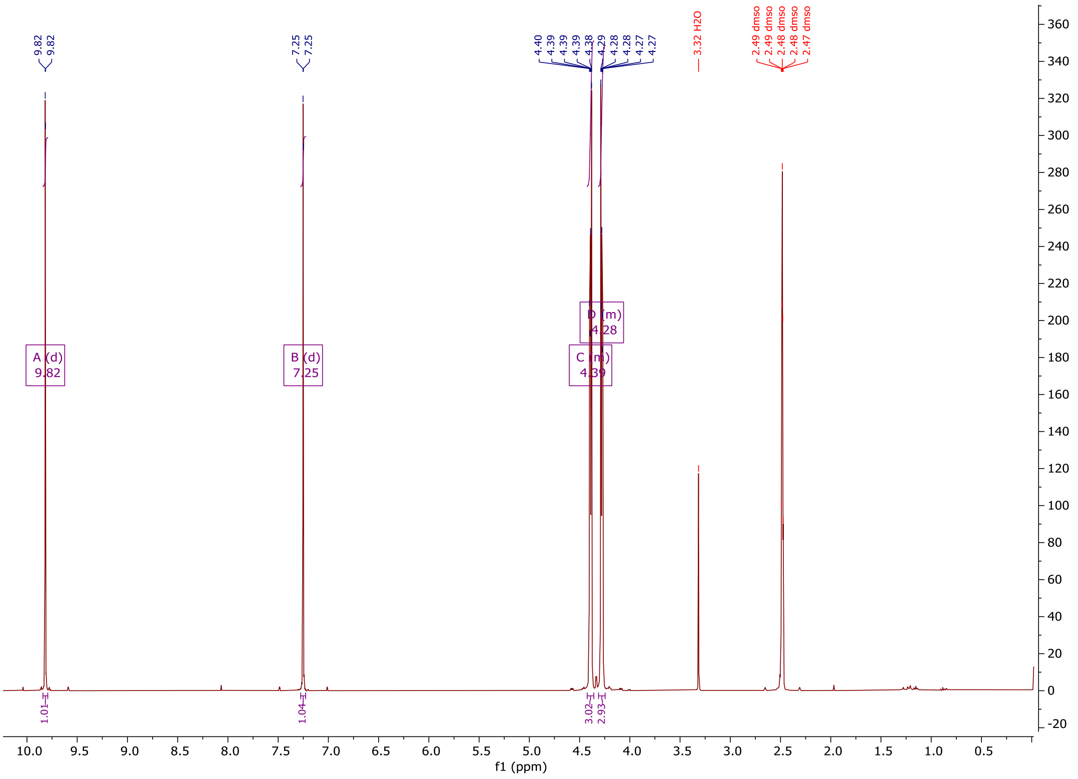

^{1}H NMR (400 MHz, DMSO-d_6, 298 K) δ (ppm) 10.47 (s, 1H), 7.90 (s, 1H), 5.07 – 5.01 (m, 2H), 4.96 – 4.89 (m, 2H)

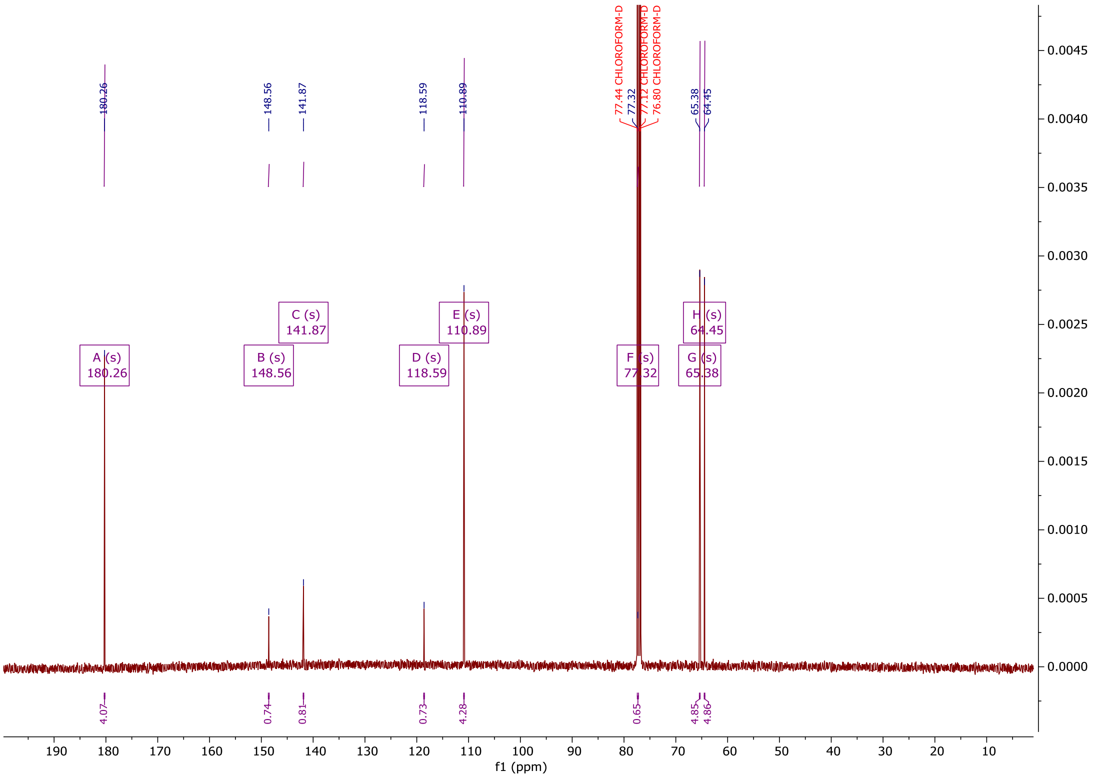

^{13}C NMR (101 MHz, chloroform-*d*, 298 K) δ (ppm) 180.3, 148.6, 141.9, 118.6, 110.9, 65.4, 64.5

HRMS (ESI+) m/z $[M + H]^+$: calculated for $[C_7H_6O_3S+H]^+$ 171.0110, found 171.0110

2.2.2 Synthesis of 3-hexylthiophene-2-carbaldehyde

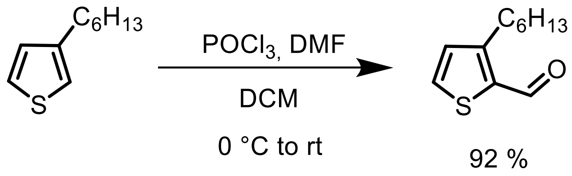

It was synthesized according to the general procedure A from $POCl_3$ (0.91 g, 5.94 mmol), DMF (0.43 g, 5.94 mmol) and 3-hexylthiophene (1.0 g, 5.94 mmol). Obtained as a white powder (1.07 g, 92 %). The product contained two formylated products and the ratio of 3-hexylthiophene-2-carbaldehyde/4-hexylthiophene-2-carbaldehyde of 5:1 was determined by ^{1}H NMR. The analysis is in agreement with the literature.[4]

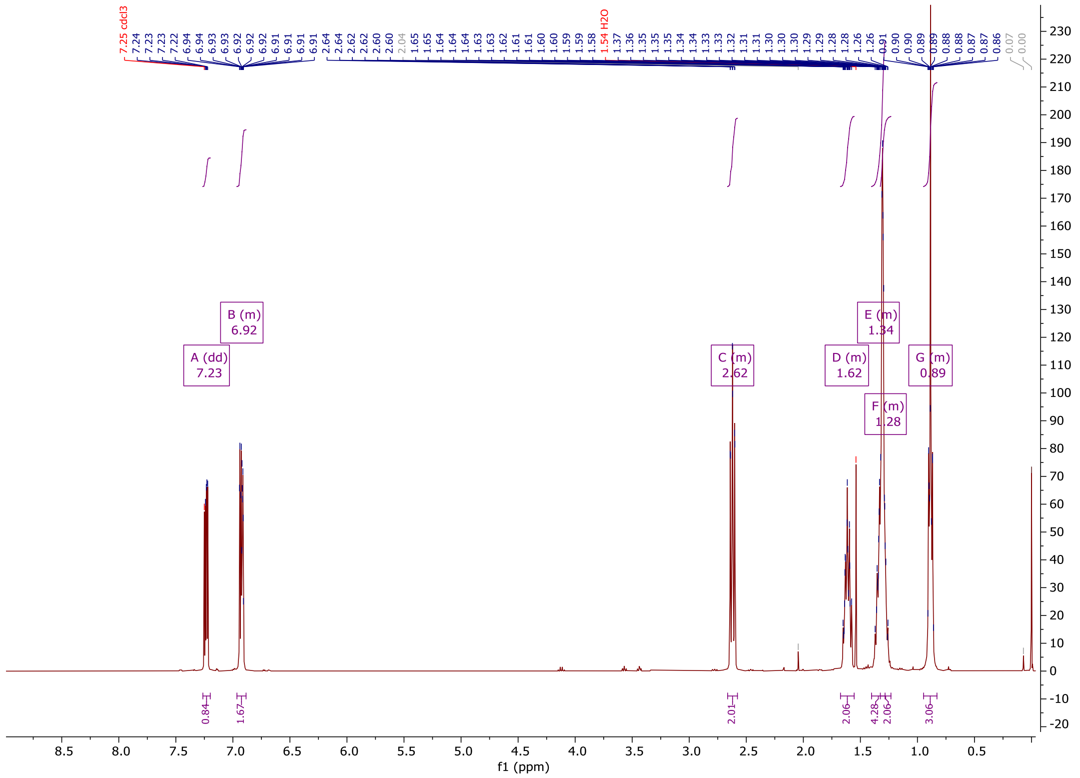

¹H NMR (400 MHz, chloroform-*d,* 298 K) δ (ppm) 10.00 (d, *J* = 1.1 Hz, 1H), 7.60 (dd, *J* = 4.9, 1.1 Hz, 1H), 6.97 (d, *J* = 5.0 Hz, 1H), 2.96 – 2.88 (m, 2H), 1.69 – 1.53 (m, 2H), 1.38 – 1.21 (m, 6H), 0.91 – 0.79 (m, 3H)

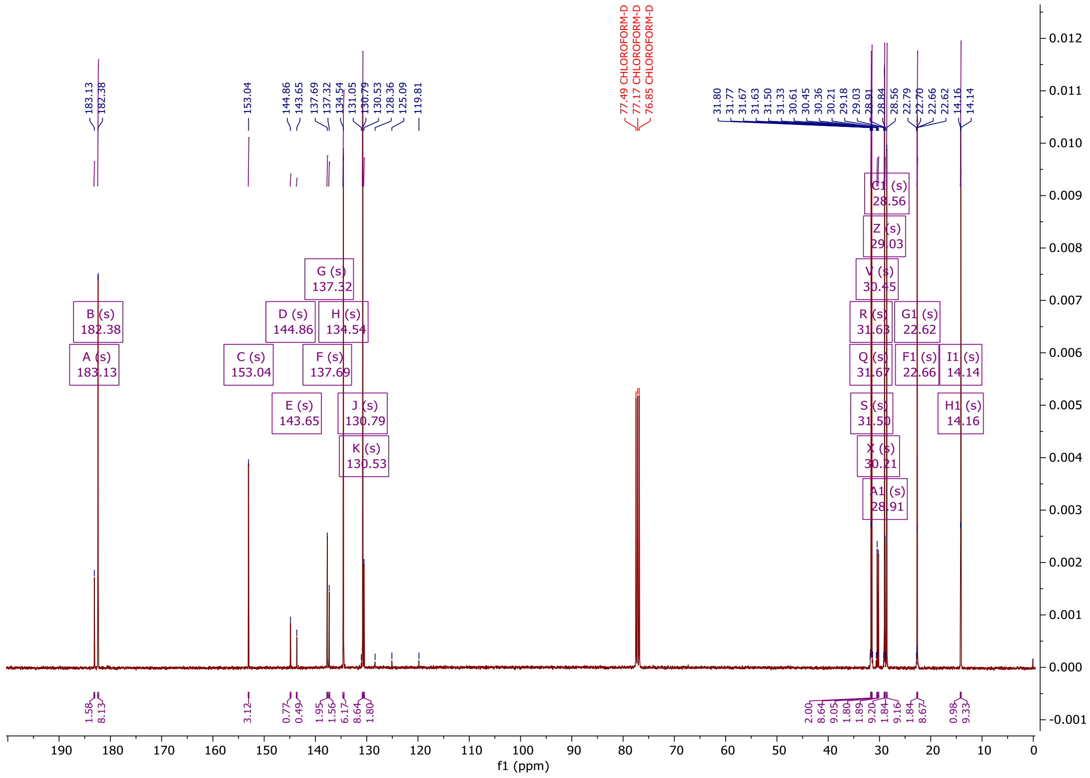

^{13}C NMR (101 MHz, chloroform-*d*, 298 K) δ (ppm) 182.4, 153.0, 137.7, 134.5, 130.8, 31.6, 31.5, 29.0, 28.6, 22.66, 14.14

HRMS (ESI+) m/z $[M + H]^+$: calculated for $[C_{11}H_{16}OS+H]^+$ 197.0995, found 197.0996

2.2.3 Synthesis of thieno[2,3-b]thiophene-2-carbaldehyde

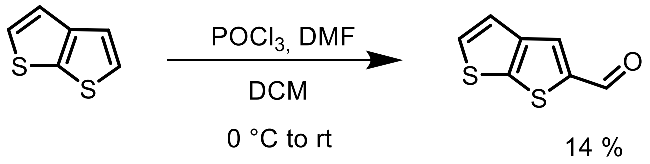

It was synthesized according to the general procedure A from $POCl_3$ (0.44 g, 2.85 mmol), DMF (0.21 g, 2.85 mmol) and thieno[2,3-*b*]thiophene (0.400 g, 2.85 mmol). Obtained as a white powder (70 mg, 14 %). The analysis is in agreement with the literature.[2]

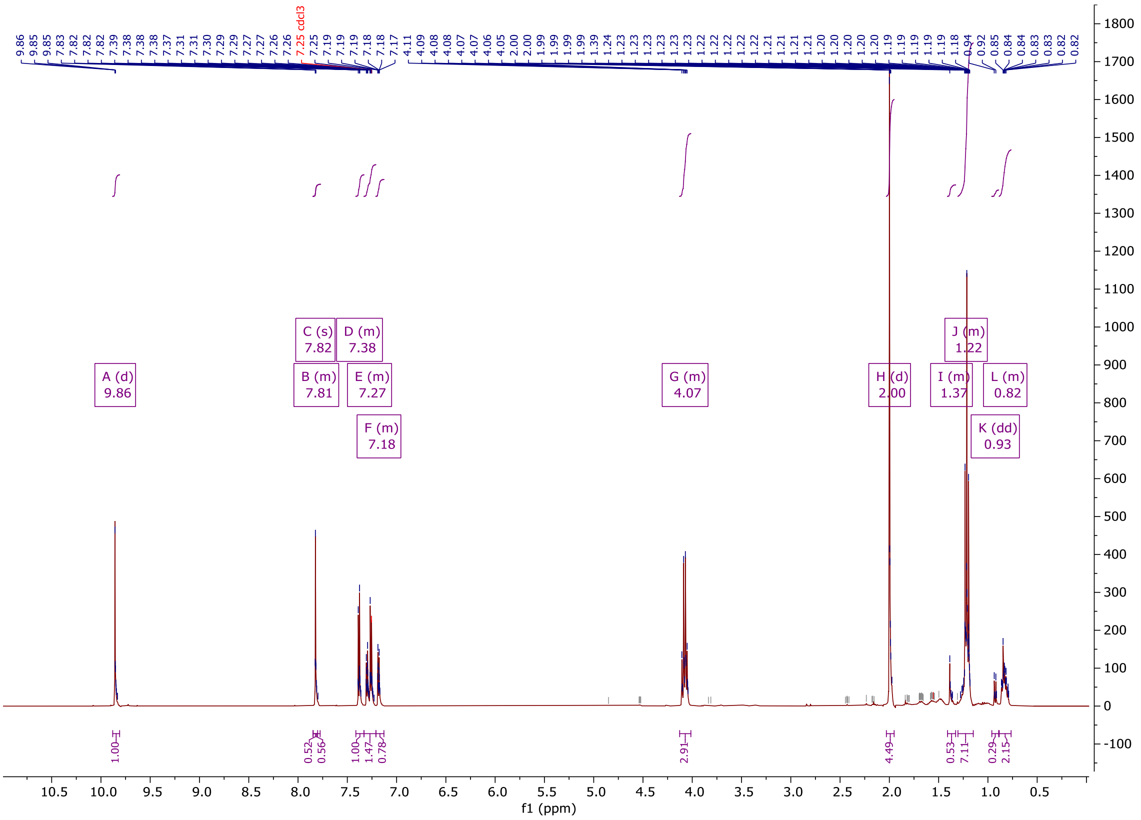

^{1}H NMR (400 MHz, chloroform-*d,* 298 K) δ (ppm) 9.86 (s, 1H), 7.82 (s, 1H), 7.38 (d, *J* = 5.3 Hz, 1H), 7.18 (d, *J* = 5.3 Hz, 1H)

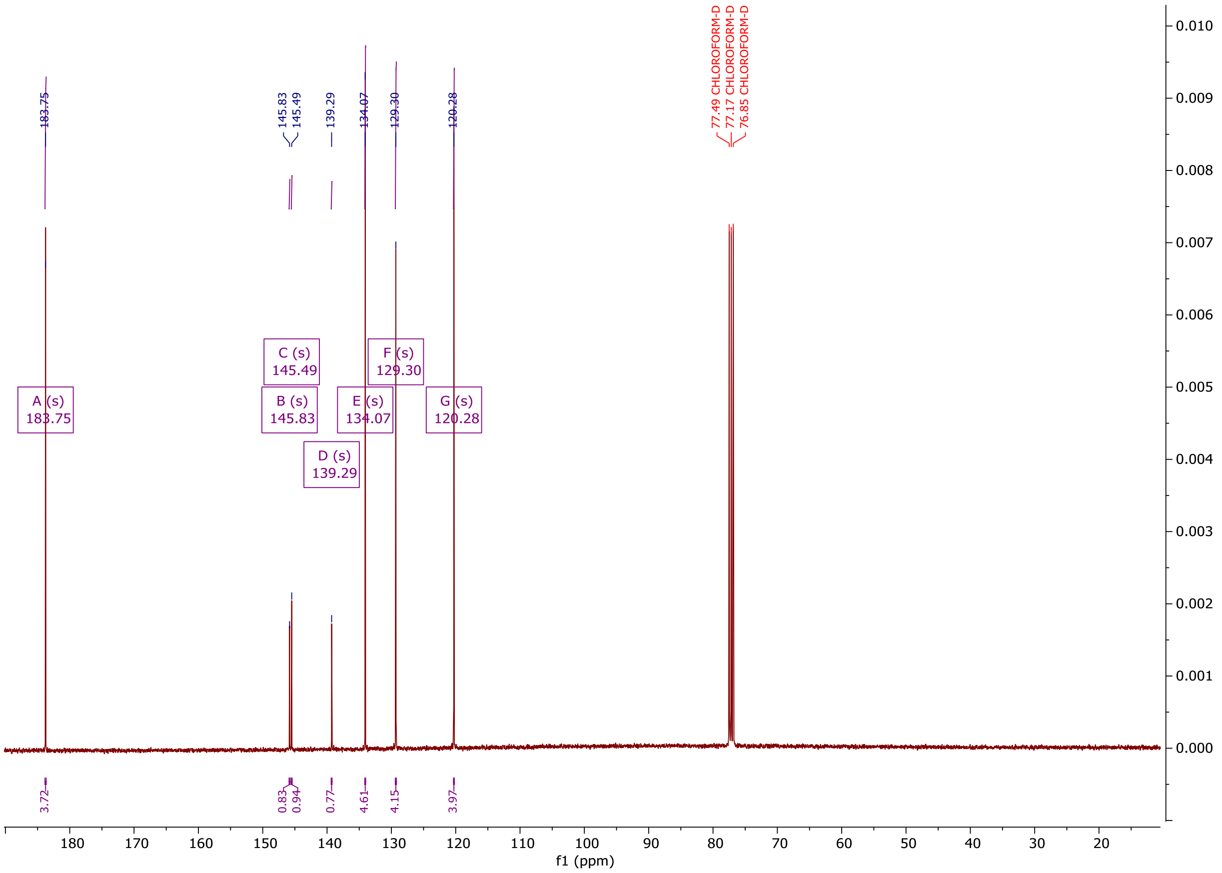

^{13}C NMR (101 MHz, chloroform-*d*, 298 K) δ (ppm) 183.3, 146.5, 146.2, 130.2, 129.5, 128.2, 121.0

HRMS (ESI+) m/z $[M + H]^+$: calculated for $[C_7H_4OS_2+H]^+$ 168.9776, found 168.9773

2.2.4 Synthesis of 4H-cyclopenta[2,1-b:3,4-b']dithiophene-2-carbaldehyde

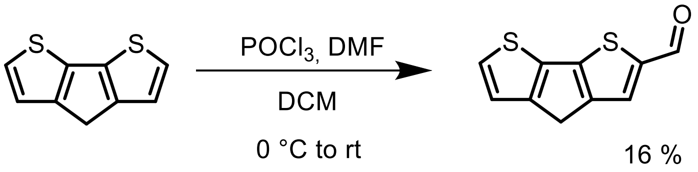

It was synthesized according to the general procedure A from $POCl_3$ (0.258 g, 1.68 mmol), DMF (0.123 g, 1.68 mmol) and thieno[2,3-*b*]thiophene (0.300 g, 1.68 mmol). Obtained as a white powder (54 mg, 16 %).

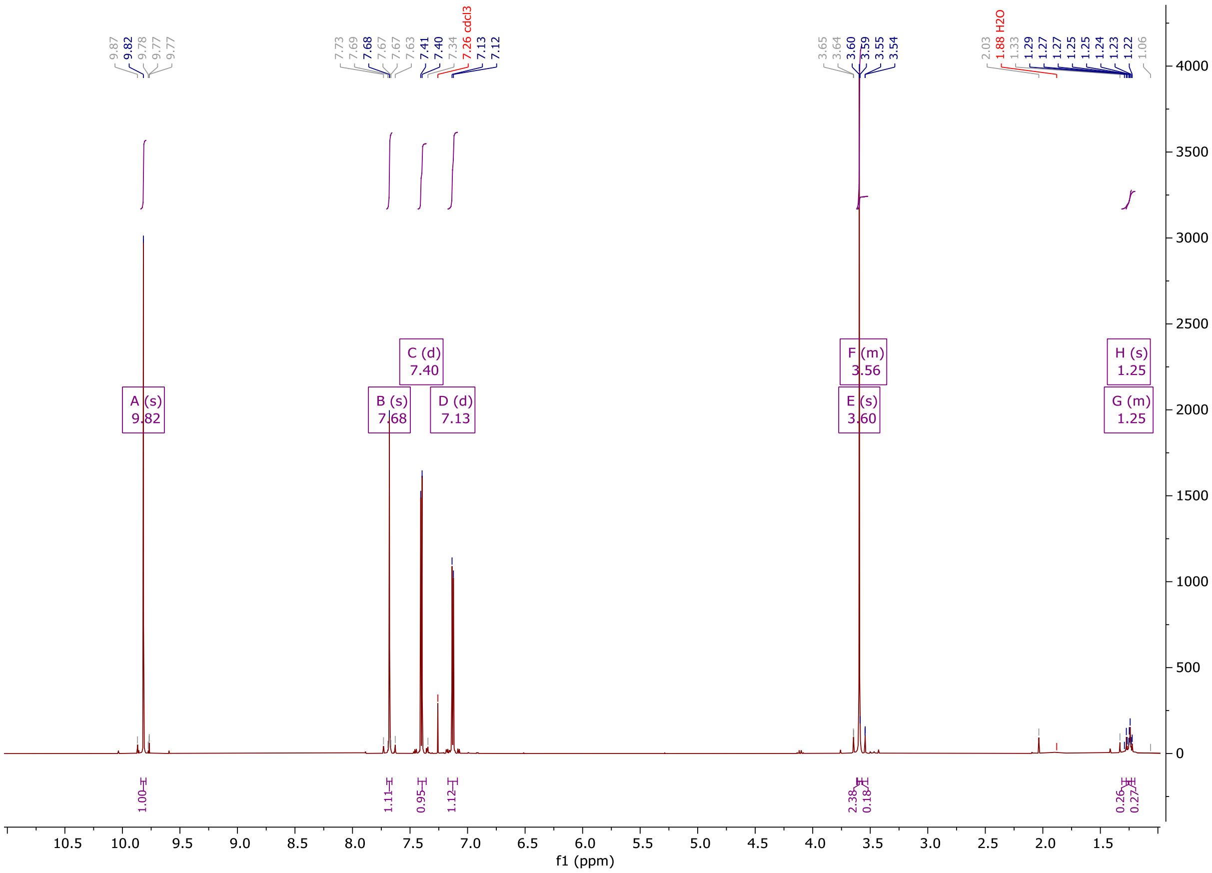

^{1}H NMR (400 MHz, chloroform-*d*, 298 K) δ (ppm) 9.82 (s, 1H), 7.68 (s, 1H), 7.40 (d, *J* = 4.9 Hz, 1H), 7.13 (d, *J* = 4.9 Hz, 1H), 3.60 (s, 2H)

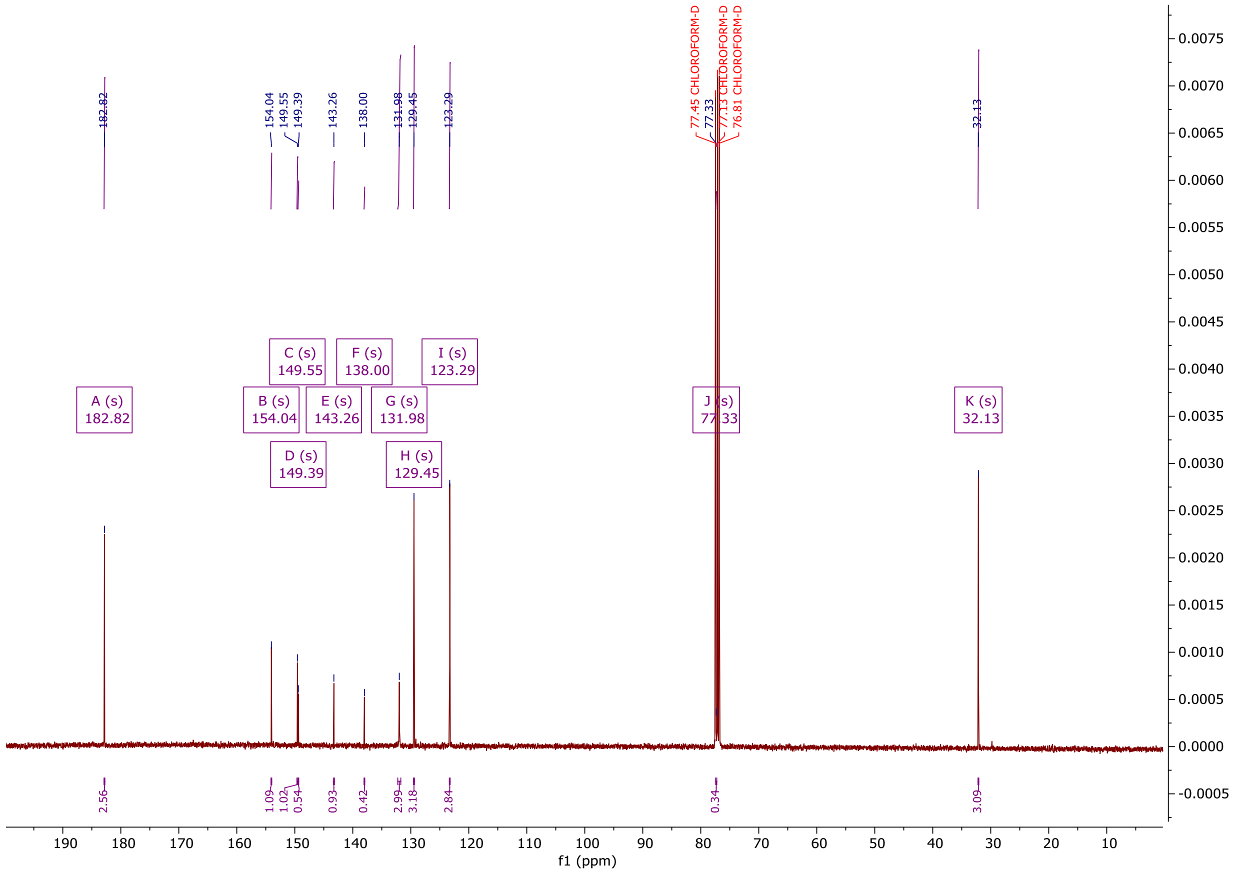

^{13}C NMR (101 MHz, chloroform-*d*, 298 K) δ (ppm) 182.8, 154.0, 149.6, 149.4, 143.3, 138.0, 132.0, 129.5, 123.3, 32.1

HRMS (ESI+) m/z $[M + H]^+$: calculated for $[C_{10}H_6OS_2+H]^+$ 206.9933, found 206.9932

2.2.5 Synthesis of 1,5-bis(5-chloro-2-methylthiophen-3-yl)pentane-1,5-dione

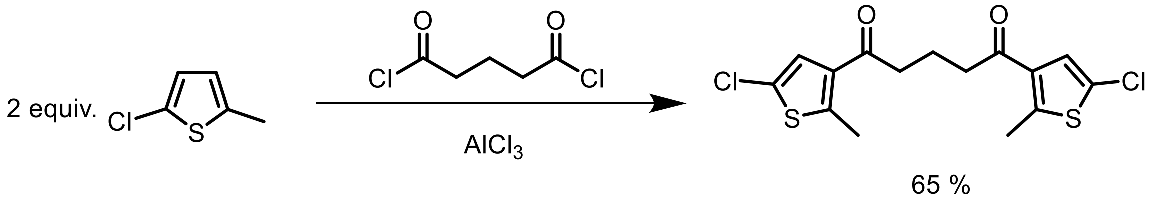

2-chloro-5-methylthiophene (19.6 g, 0.15 mol, 2 equiv.) and glutaroyl dichloride (12.5 g, 0.07 mol, 1 equiv.) were dissolved in $CHCl_3$ (130 mL). Solution was cooled to 0 °C in an ice bath and anhydrous $AlCl_3$ (23.6 g, 0.18 mol, 2.4 equiv.) was added in portions during 30 minutes. The reaction mixture was then stirred at rt for 2h. Then the reaction was quenched by slow addition of H_2O (80 mL). The product precipitated and was filtered off and washed with H_2O. Product was obtained as a brown powder (17.3 g, 65 %).[5]

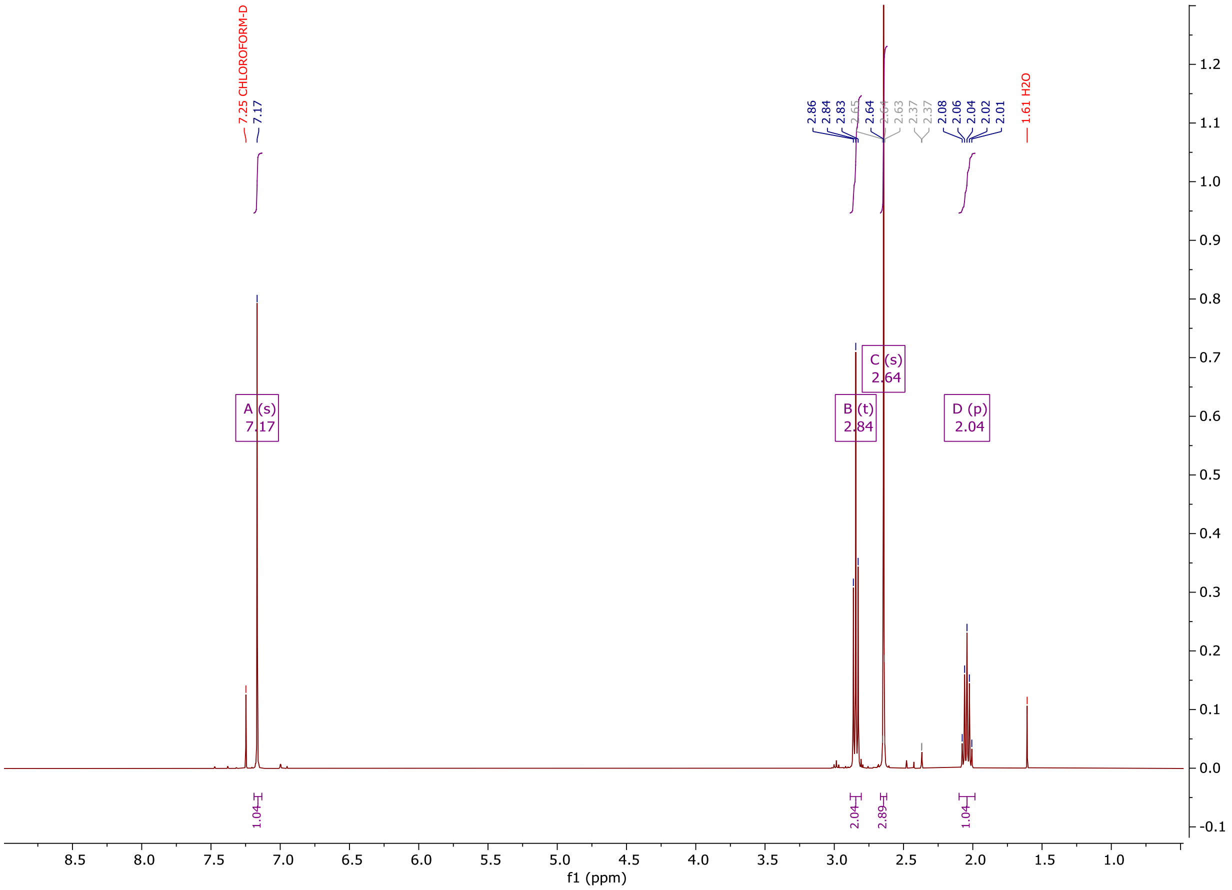

^{1}H NMR (400 MHz, chloroform-*d*, 298 K) δ (ppm) 7.17 (s, 2H), 2.84 (t, *J* = 6.9 Hz, 4H), 2.64 (s, 6H), 2.04 (p, *J* = 6.9 Hz, 2H)

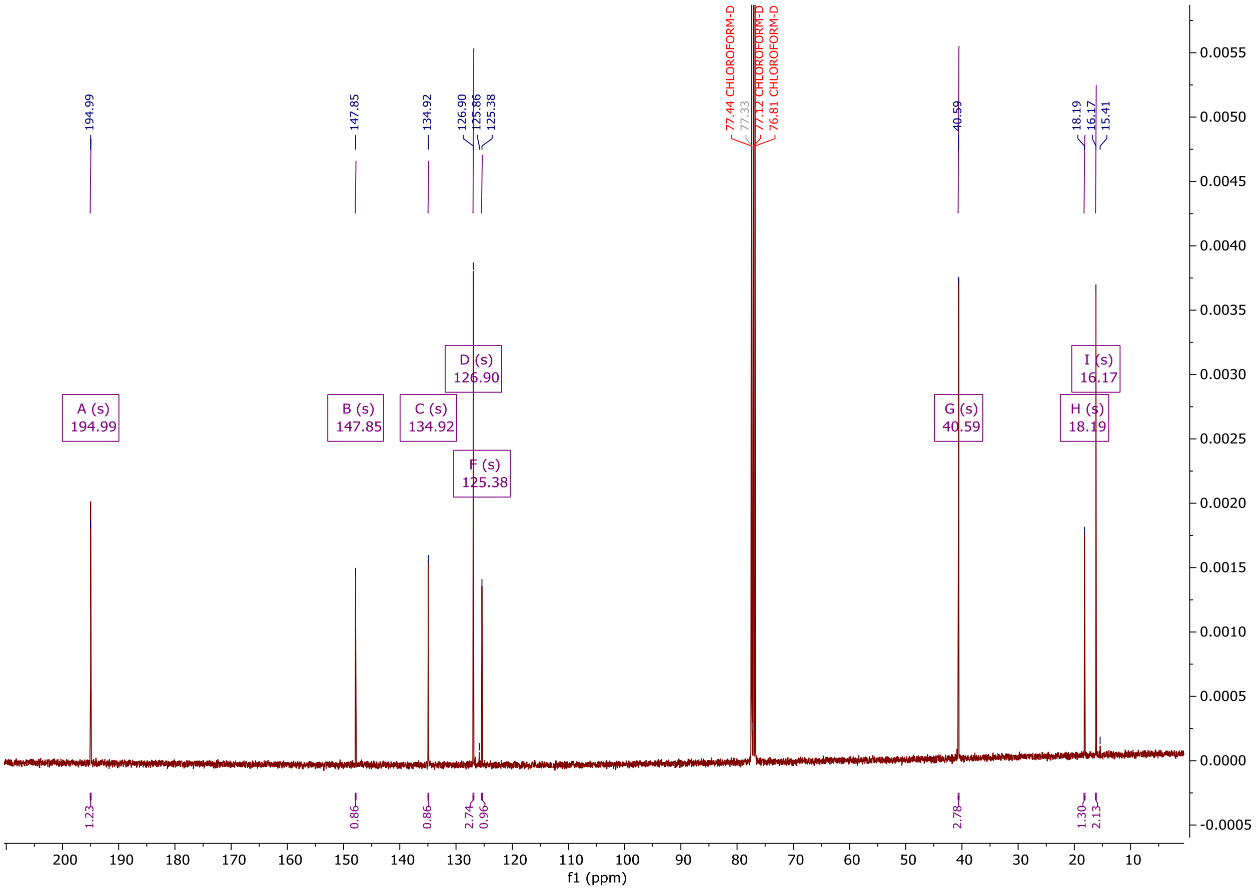

^{13}C NMR (101 MHz, chloroform-*d*, 298 K) δ (ppm) 195.01, 148.0, 134.9, 126.92, 125.40, 40.60, 18.20, 16.2

HRMS (APCI+) m/z $[M + H]^+$: calculated for $[C_{15}H_{14}Cl_2O_2S_2+H]^+$ 360.9885, found 360.9895

2.2.6 Synthesis of 1,2-bis(5-chloro-2-methylthiophen-3-yl)cyclopent-1-ene

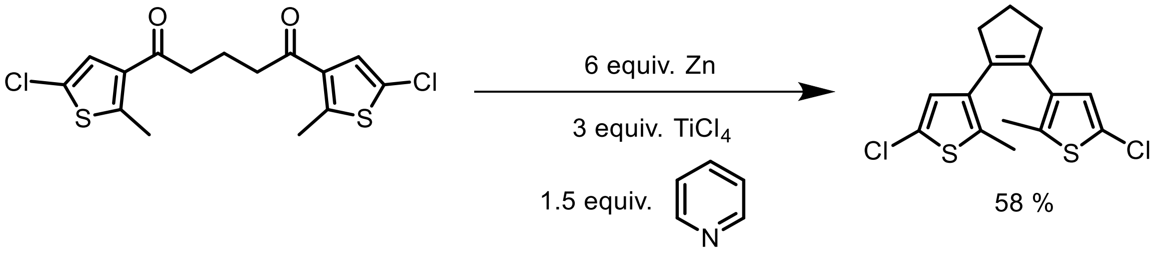

First, zinc (3.32 g, 0.05 mol) was activated my 1M HCl and then it was dried overnight in vacuum. Zinc was then placed in a three-neck flask with dry THF (80 mL) and it was evacuated and filled with Ar. $TiCl_4$ was added to the reaction mixture dropwise using a syringe. The reaction was then heated to 70 °C for 1h. After cooling to rt, the reaction mixture was cooled to 0 °C in an ice bath leading to a change of color to blue. Pyridine (0.013 mol, 1 mL) was added, and the reaction was stirred for 10 minutes. After addition of 1,5-bis(5-chloro-2-methylthiophen-3-yl)pentane-1,5-dione (3.1 g, 0.008 mol), the reaction mixture was again heated to 70 °C for 1.5h. After cooling to rt, the reaction mixture was diluted with Et_2O and it was washed with 1M HCl, followed by washing with 1M NH_4Cl. The organic layer was separated, dried over $MgSO_4$ and the solvent was evaporated. The crude product was purified by flash chromatography (hexane) resulting in a pale red product (1.6 g, 58 %).[6]

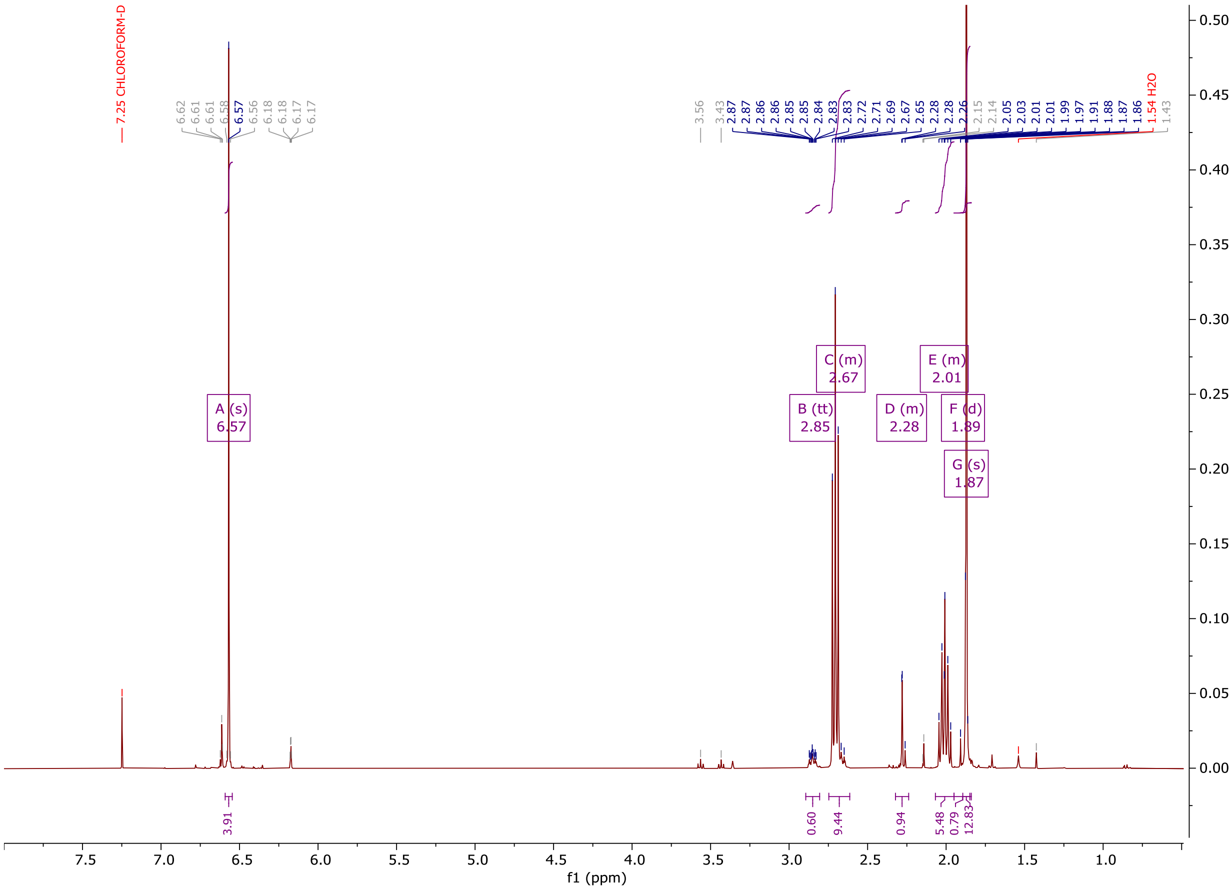

^{1}H NMR (400 MHz, chloroform-*d*, 298 K) δ (ppm) 6.57 (s, 2H), 2.71 (t, *J* = 7.3, 4H), 2.02 (m, 2H), 1.87 (s, 6H)

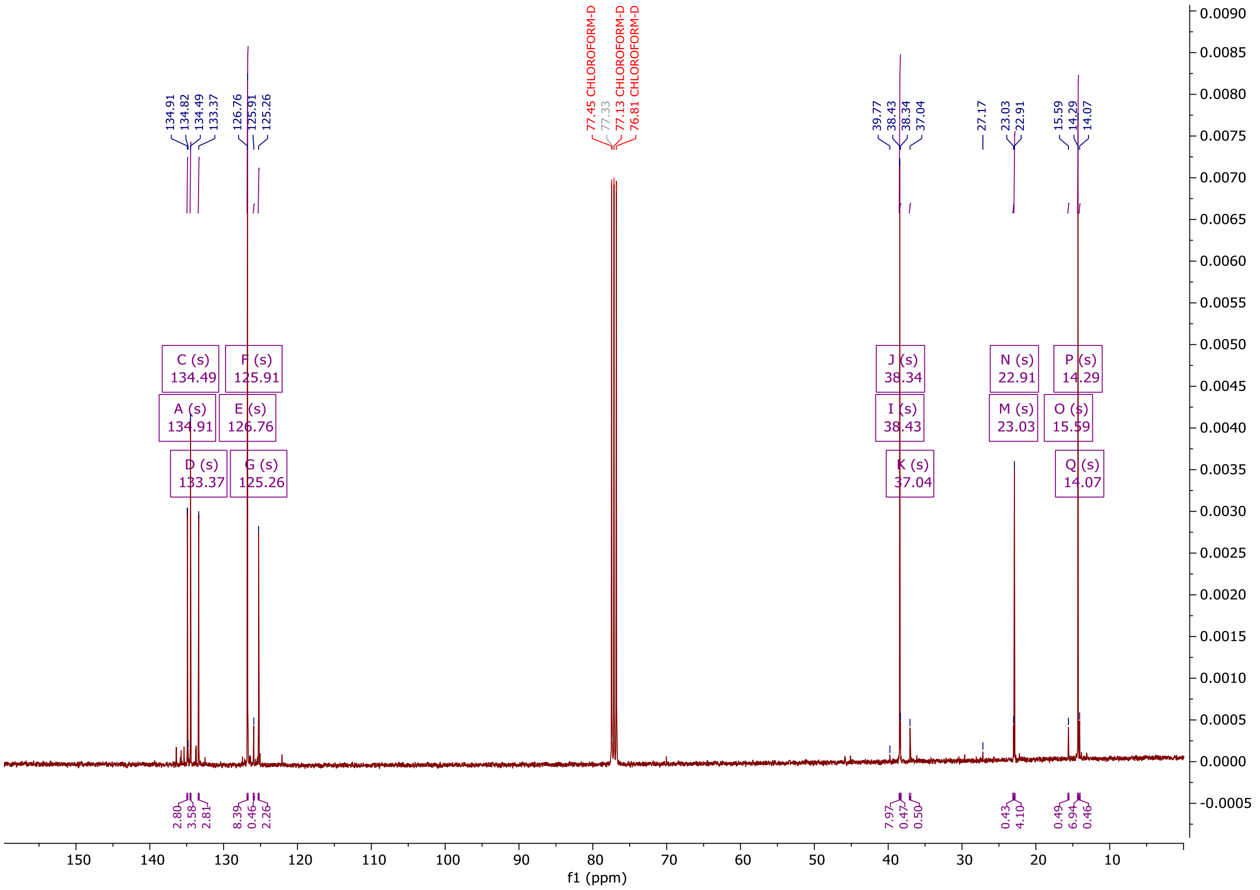

^{13}C NMR (101 MHz, chloroform-*d*, 298 K) δ (ppm) 134.9, 133.4, 125.3, 38.4, 38.3, 37.1, 22.9, 14.3

HRMS (APCI+) m/z $[M + H]^+$ **:** calculated for $[C_{15}H_{14}Cl_2S_2+H]^+$ 328.9987, found 328.9992

2.2.7 Synthesis of 4,4'-(cyclopent-1-ene-1,2-diyl)bis(5-methylthiophene-2-carbaldehyde)

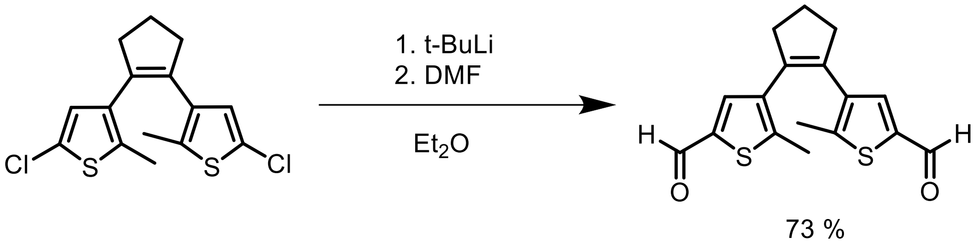

The starting 1,2-bis(5-chloro-2-methylthiophen-3-yl)cyclopent-1-ene (0.7 g, 2 mmol) was placed in a flask, which was then evacuated and filled with Ar. Then it was dissolved in dry Et$_2$O (50 mL) the flask was cooled to 0 °C in an ice bath. *t*-BuLi (3.5 mL, 6 mmol, 3 equiv.) was then added dropwise to the solution and it was kept stirring at 0 °C for 10 minutes. Then the ice bath was removed and the reaction was stirred at rt for 1 hour. The reaction mixture was then cooled again to 0 °C and dry DMF (0.34 mL, 4 mmol, 2 equiv.) was added dropwise and it was left to stir 0 °C for 10 minutes and the ice bath was removed. After 1 hour, the reaction was quenched by addition of 1M HCl (30 ml). The organic layer was separated and the aqueous layer was extracted with Et$_2$O. Combined organic layers were dried over MgSO$_4$ and the solvent was evaporated. Crude product was purified by flash chromatography (Hex:EtOAc, 8:2) resulting in a pale yellow product (0.46 g, 73 %).[7]

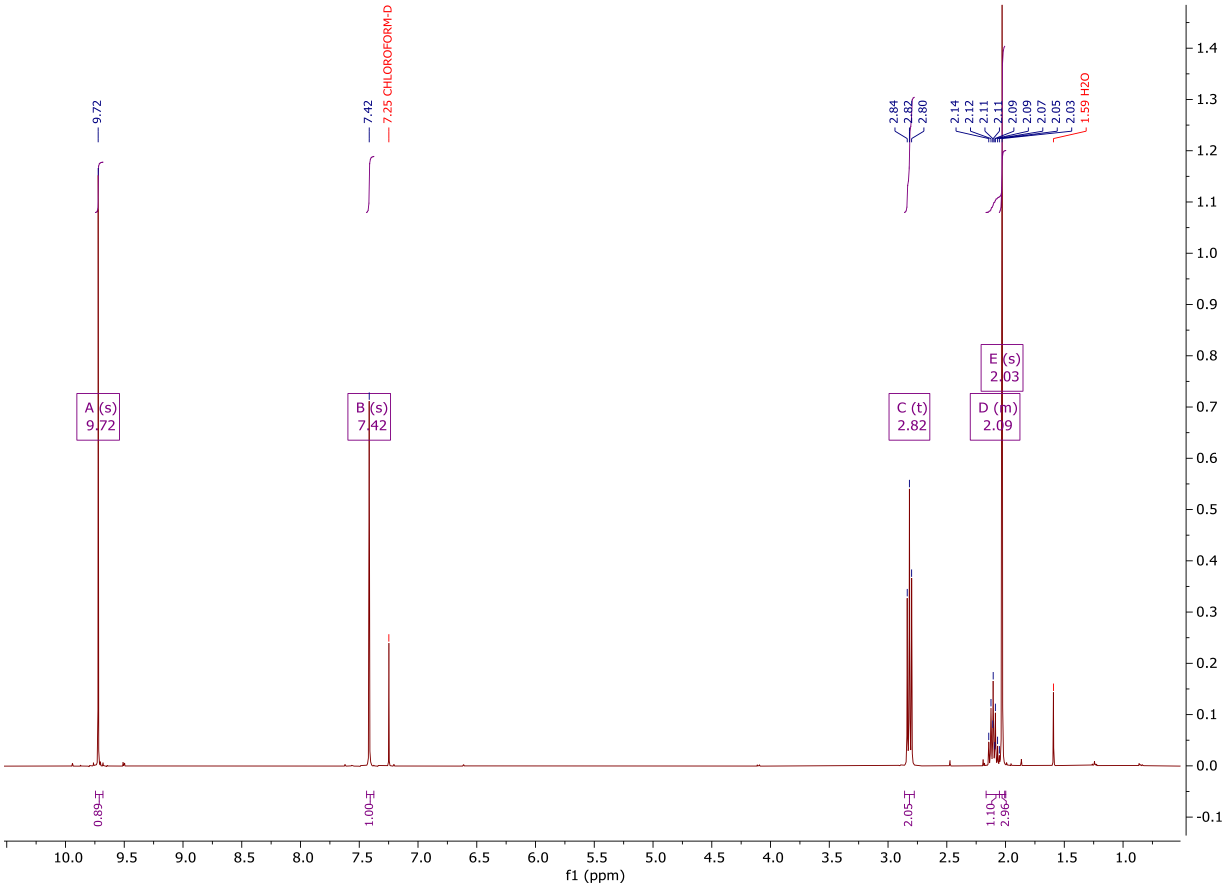

^{1}H NMR (400 MHz, chloroform-*d,* 298 K) δ (ppm) 9.72 (s, 2H), 7.41 (s, 2H), 2.82 (t, *J* = 7.5 Hz, 4H), 2.11 (p, J = 7.5 Hz, 2H), 2.03 (s, 6H)

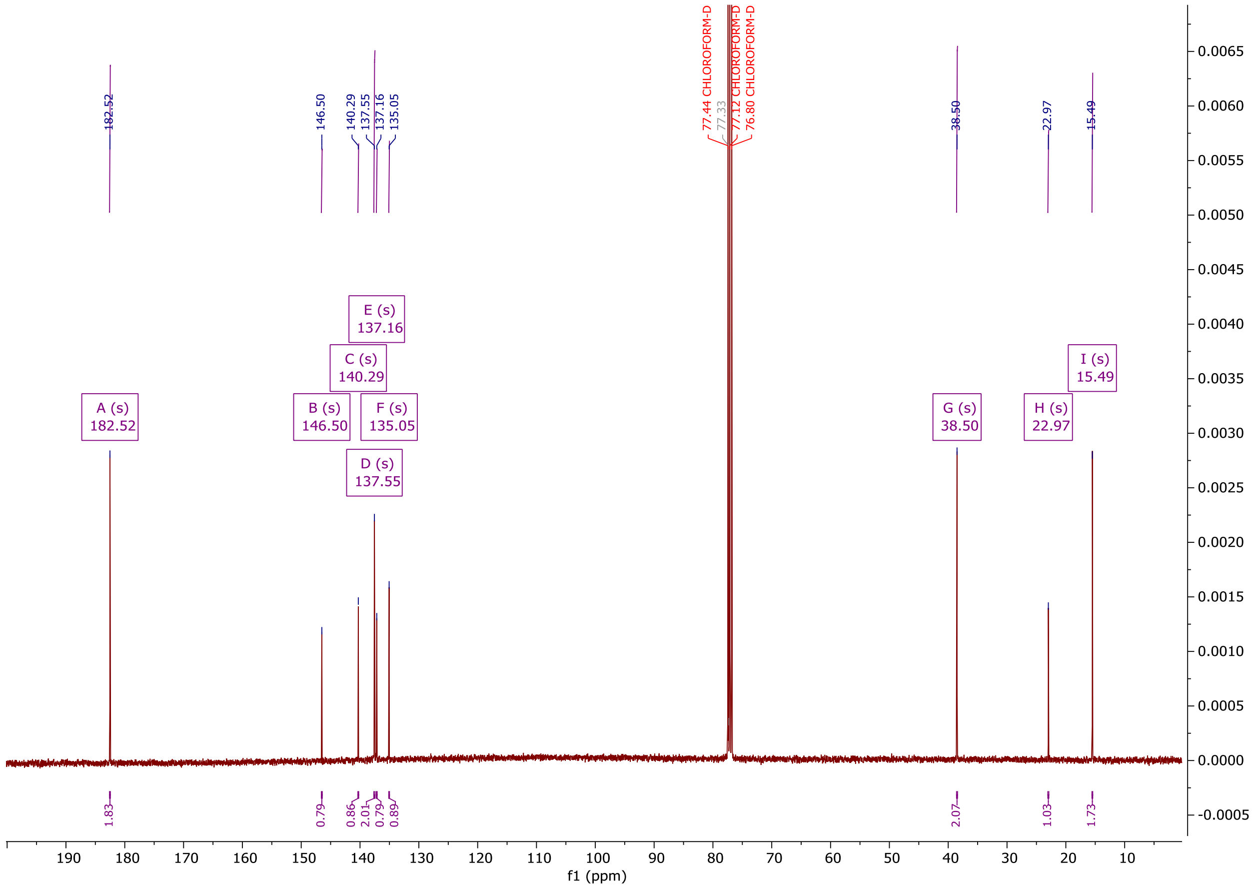

^{13}C NMR (101 MHz, chloroform-*d*, 298 K) δ (ppm) 182.5, 146.5, 140.3, 137.6, 137.2, 135.1, 38.5, 23.0, 15.5

HRMS (ESI+) m/z [M + Na]$^+$ **:** calculated for $[C_{17}H_{16}O_2S_2+Na]^+$ 339.0484, found 339.0489

Melting point: 135 – 139 °C

2.3 General procedure B: Condensation of the hydrazide and the carbonyl compound

The hydrazide (1.0 equiv) and the aldehyde (1.0 equiv) were suspended in EtOH. Subsequently, a catalytic amount (50 μL) of 1M HCl was added and the mixture was heated to reflux until all starting materials dissolved (< 10 min). The product precipitates from solution upon cooling to room temperature and was filtered off to yield the pure acylhydrazone without the need for further purification. Note: Precipitation can be further stimulated by either sonication or storing at 4 °C overnight.[8]

2.3.1 Synthesis of AH1

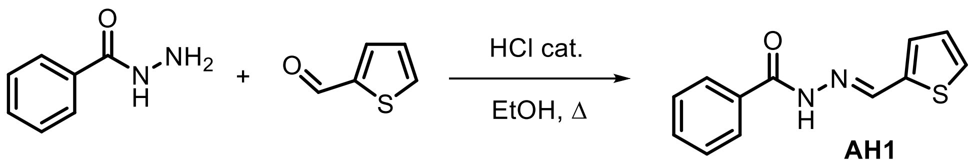

AH1

97 %

Synthesized according to general procedure B from benzhydrazide (0.20 g, 1.47 mmol, 1.0 equiv) and thiophene-2-carbaldehyde (0.16 g, 1.47 mmol, 1.0 equiv). Obtained as a white powder (0.33 g, 97 %).

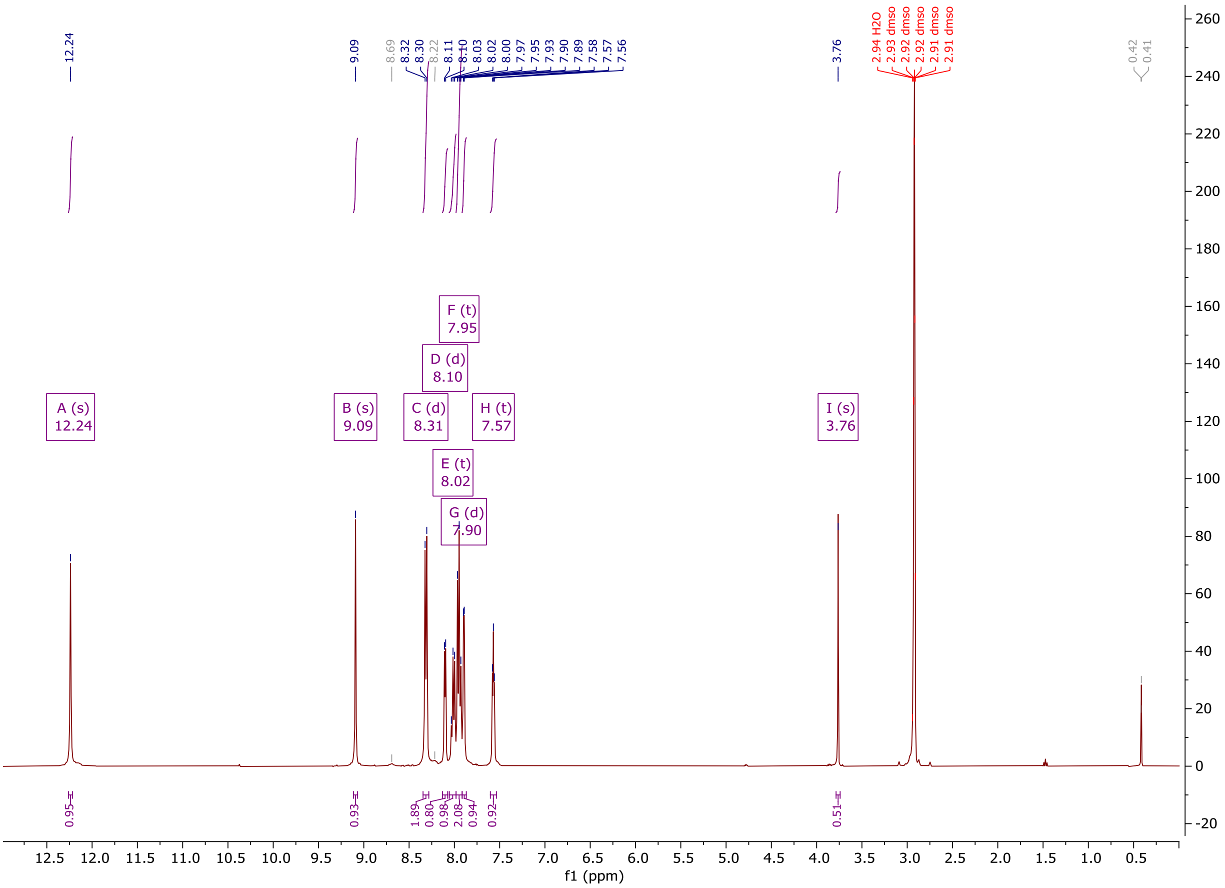

^{1}H NMR (400 MHz, DMSO-d_6, 298 K) δ (ppm) 12.24 (s, 1H), 9.09 (s, 1H), 8.31 (d, J = 7.5 Hz, 2H), 8.10 (d, J = 5.0 Hz, 1H), 8.02 (t, J = 7.2 Hz, 1H), 7.95 (t, J = 7.4 Hz, 2H), 7.90 (d, J = 3.6 Hz, 1H), 7.57 (t, J = 4.3 Hz, 1H).

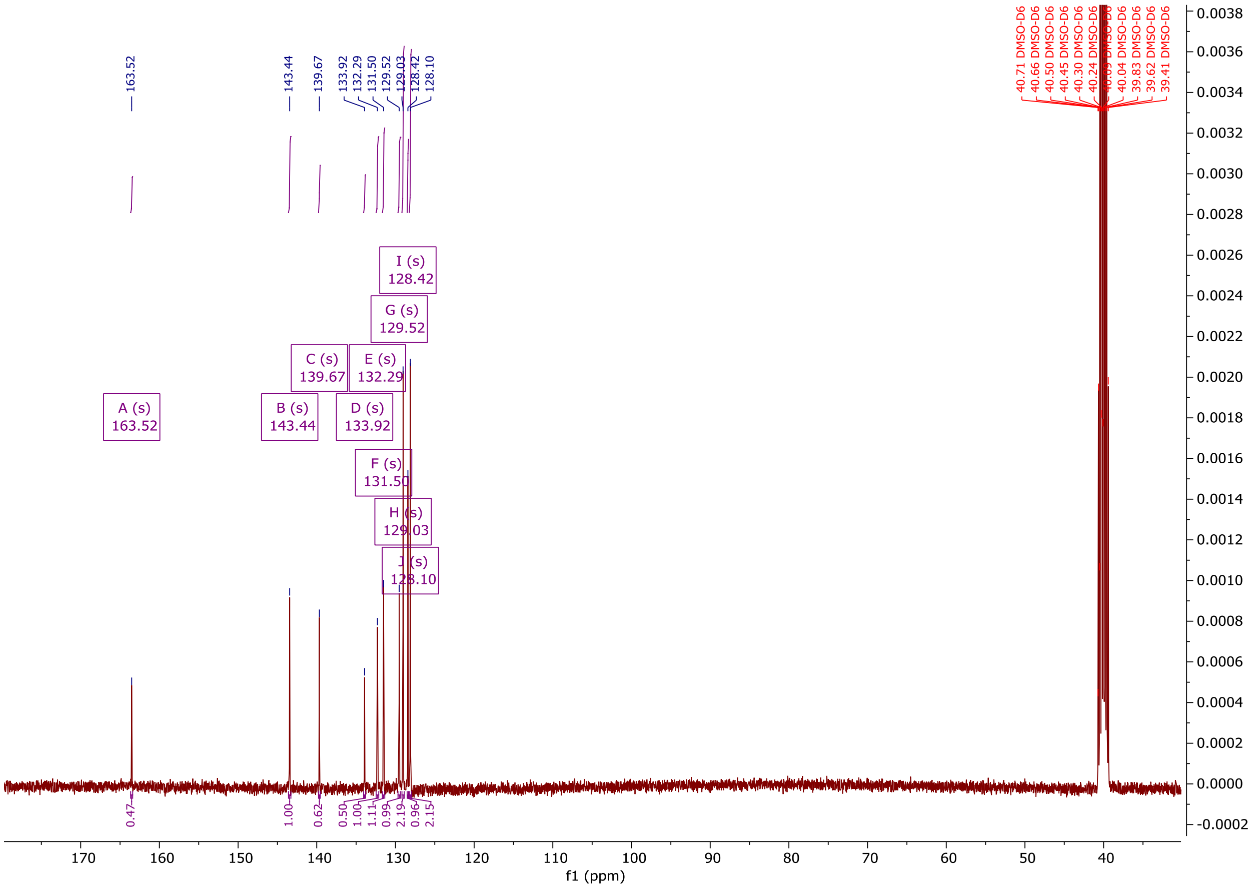

^{13}C NMR (101 MHz, DMSO-*d*$_6$, 298 K) δ (ppm) 163.5, 143.4, 139.7, 133.9, 132.3, 131.5, 129.5, 129.0, 128.4, 128.1

HRMS (ESI+) m/z $[M + H]^+$: calculated for $[C_{12}H_{10}N_2OS+H]^+$ 231.05875, found 231.05877

Melting point: 206 – 209 °C

2.3.2 Synthesis of AH2

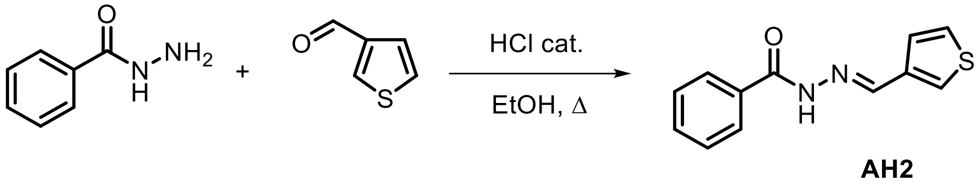

AH2

92 %

Synthesized according to general procedure B from benzhydrazide (0.20 g, 1.47 mmol, 1.0 equiv) and thiophene-3-carbaldehyde (0.16 g, 1.47 mmol, 1.0 equiv). Obtained as a white powder (0.31 g, 92 %).

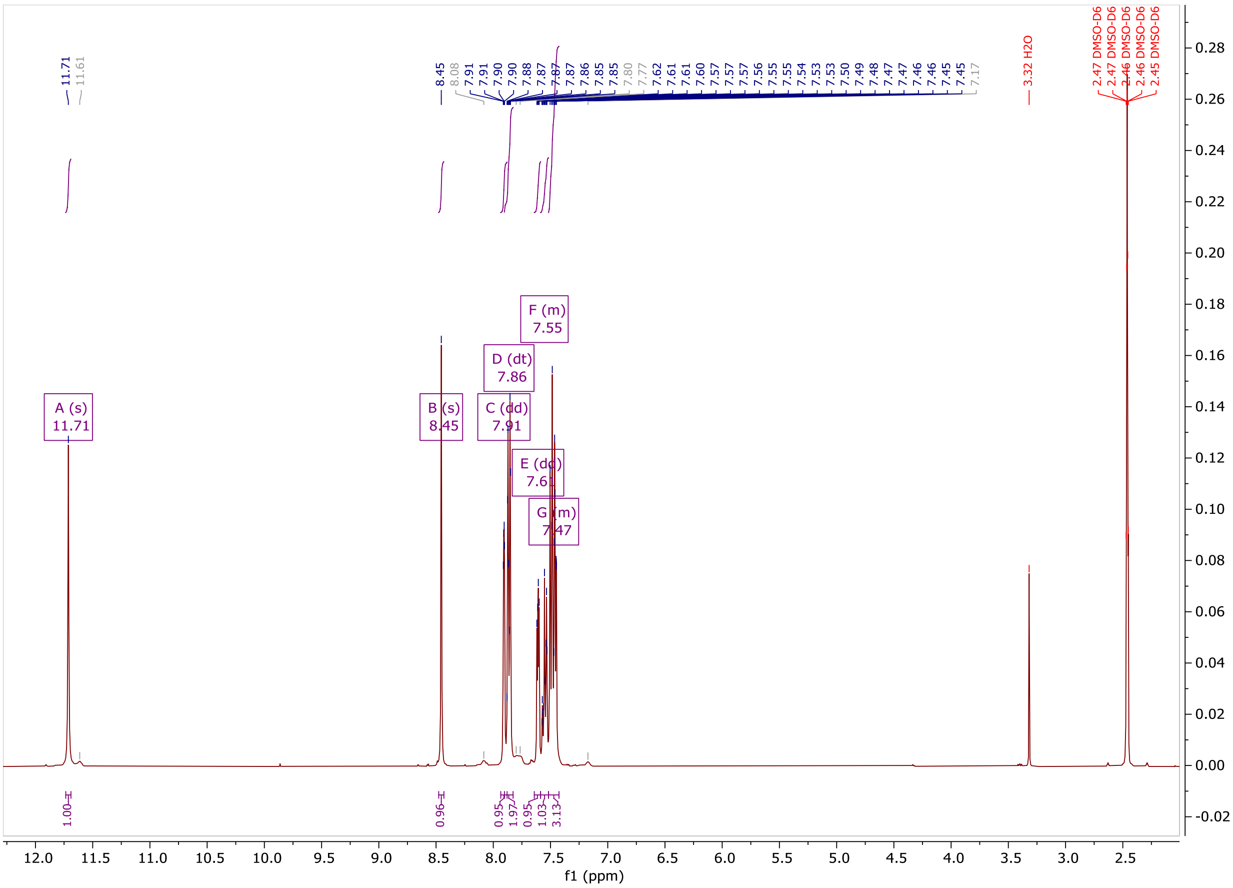

^{1}H NMR (400 MHz, DMSO-d_6, 298 K) δ (ppm) 11.71 (s, 1H), 8.45 (s, 1H), 7.91 (dd, *J* = 3.0, 1.2 Hz, 1H), 7.87 (d, *J* = 7.1 Hz, 2H), 7.62 (dd, *J* = 5.2, 2.9 Hz, 1H), 7.55 (d, *J* = 7.4 Hz, 1H), 7.49 (m, 3H)

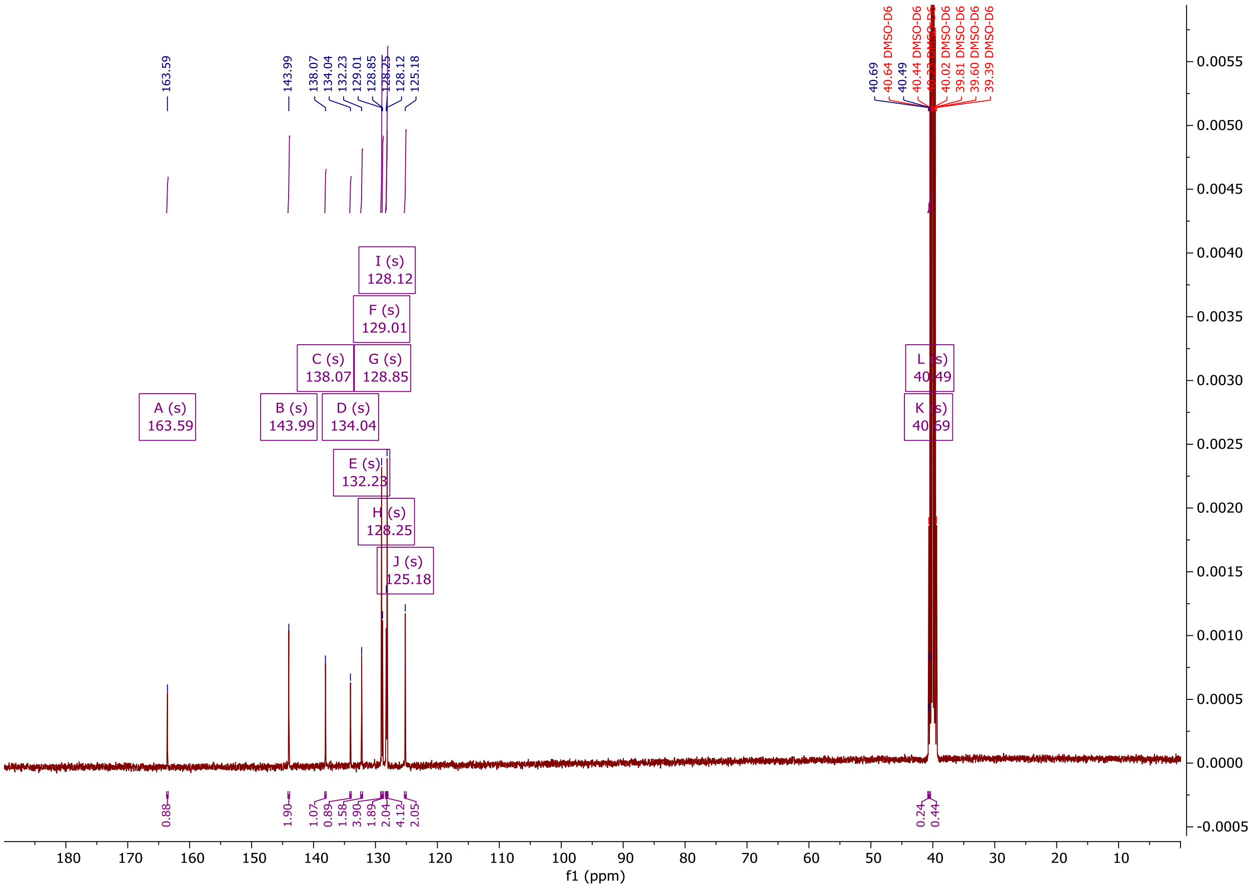

^{13}C NMR (101 MHz, DMSO-*d$_6$*, 298 K) δ (ppm)163.6, 144.0, 138.1, 134.1, 132.2, 129.0, 128.9, 128.3, 128.1, 125.2

HRMS (ESI+) m/z [M + Na]$^+$: calculated for [$C_{12}H_{10}N_2OS$+Na]$^+$ 253.0406, found 253.0406

Melting point: 199 – 203 °C

2.3.3 Synthesis of AH3

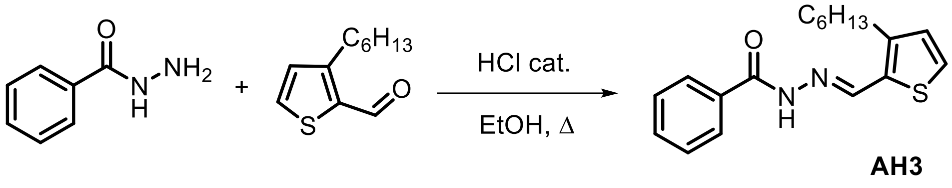

AH3

89 %

Synthesized according to general procedure B from benzhydrazide (0.901 g, 6.62 mmol, 1.0 equiv) and 3-hexylthiophene-2-carbaldehyde (1.30 g, 6.62 mmol, 1.0 equiv). Obtained as a white powder (1.86 g, 89 %).

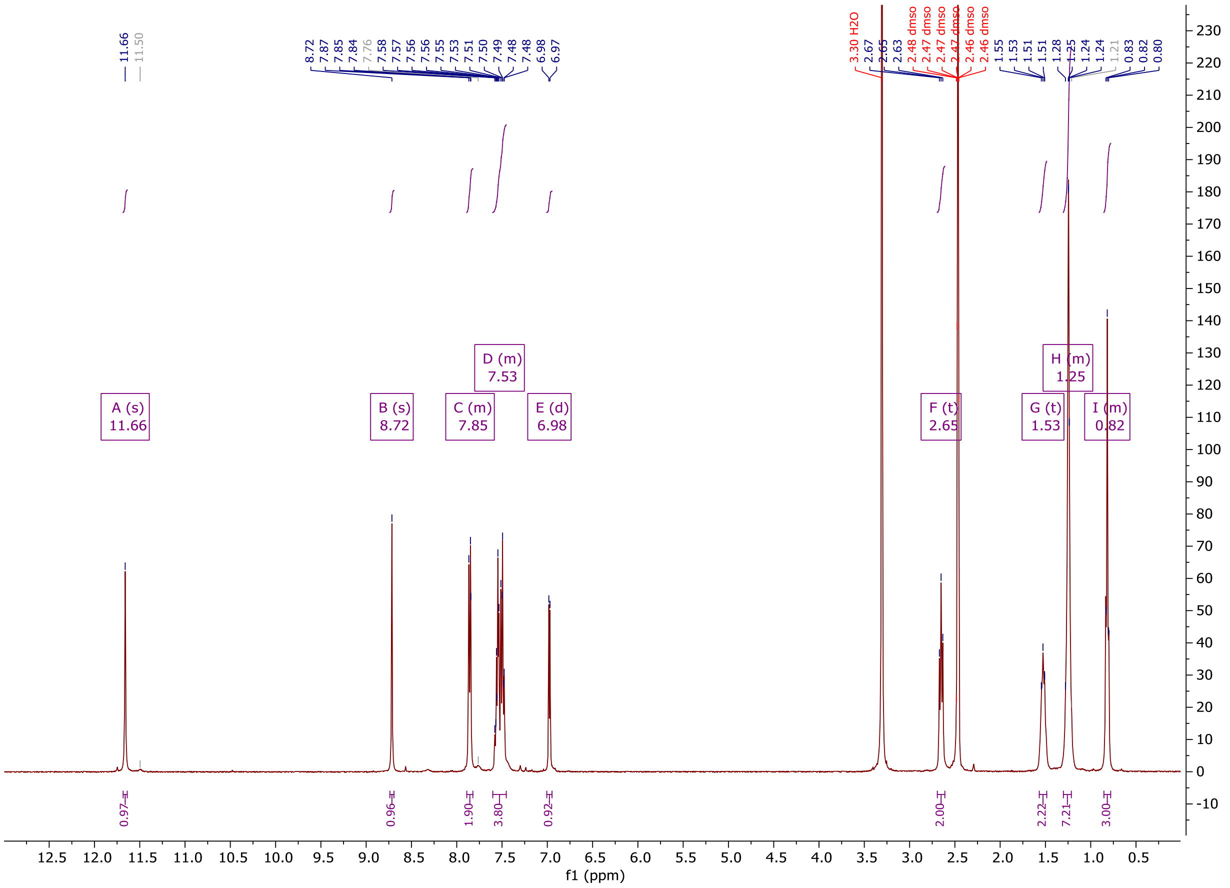

^{1}H NMR (400 MHz, DMSO-d_6, 298 K) δ (ppm) 11.66 (s, 1H), 8.72 (s, 1H), 7.86 (d, *J* = 7.4 Hz, 2H), 7.60 – 7.45 (m, 4H), 6.98 (d, *J* = 5.1 Hz, 1H), 2.65 (t, *J* = 7.6 Hz, 2H), 1.53 (m, 2H), 1.31 – 1.17 (m, 6H), 0.86-0.78 (m, 3H)

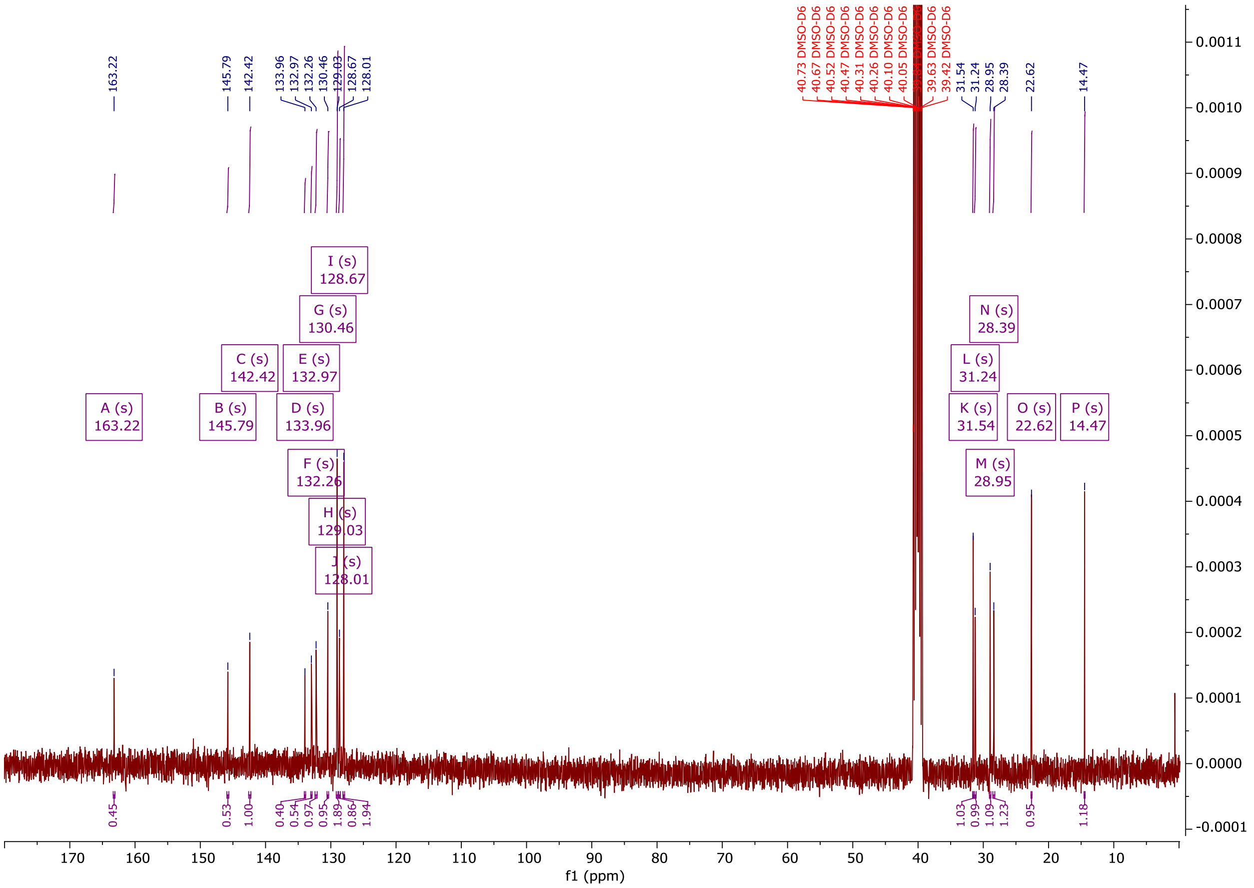

^{13}C NMR (101 MHz, DMSO-*d*$_6$, 298 K) δ (ppm) 163.2, 145.8, 142.4, 134.0, 133.0, 132.3, 130.5, 129.0, 128.7, 128.0, 31.6, 31.2, 29.0, 28.4, 14.5

HRMS (APCI+) m/z $[M + H]^+$: calculated for $[C_{18}H_{22}N_2OS+H]^+$ 315.1526, found 315.1526

Melting point: 124 – 128 °C

2.3.4 Synthesis of AH4

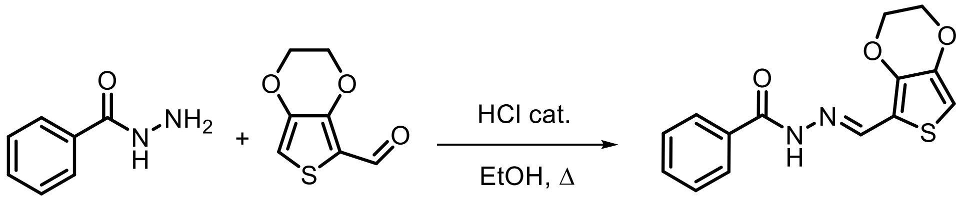

AH4

98 %

Synthesized according to general procedure B from benzhydrazide (0.20 g, 1.27 mmol, 1.0 equiv) and 3,4-ethylenedioxythiophene-2-carbaldehyde (0.25 g, 1.27 mmol, 1.0 equiv). Obtained as a white powder (0.41 g, 98 %).

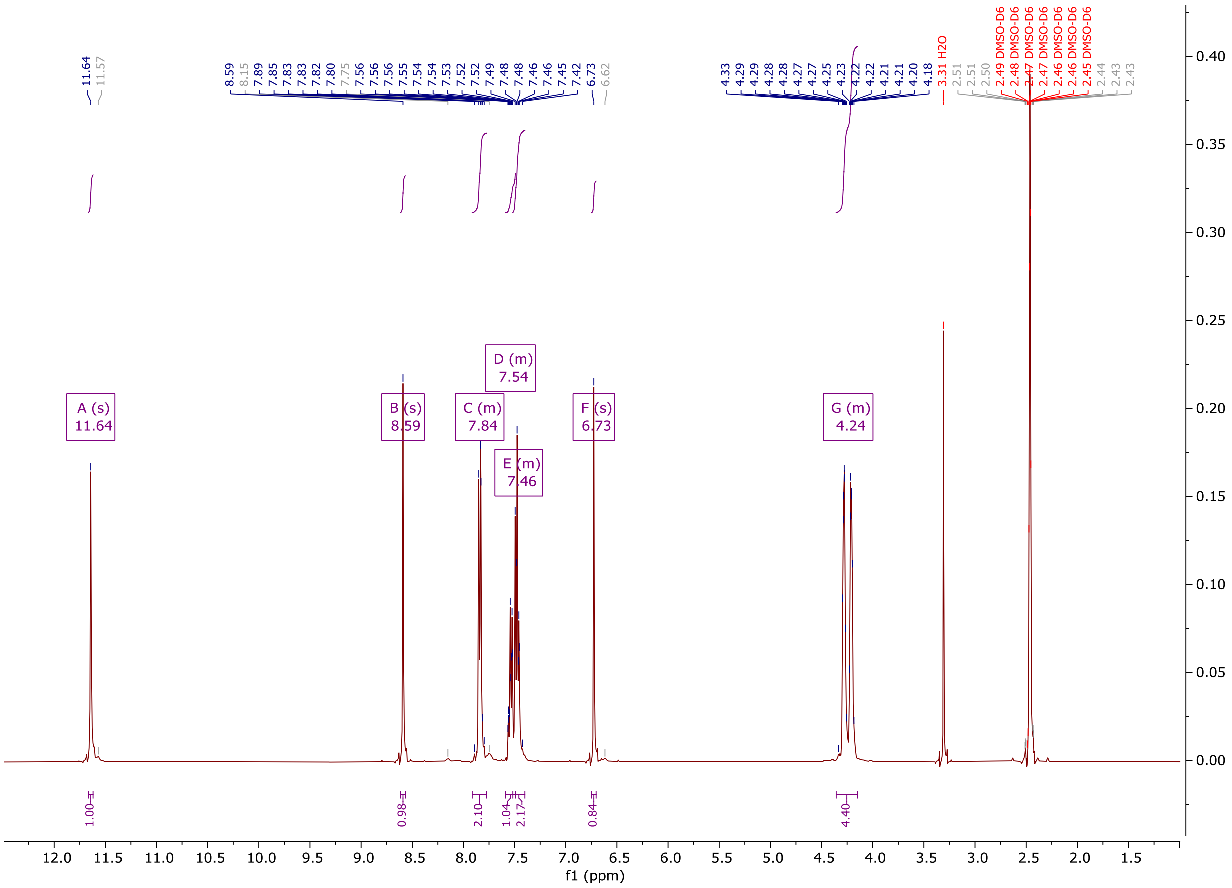

^{1}H NMR (400 MHz, DMSO-*d*$_6$, 298 K) δ (ppm) 11.64 (s, 1H), 8.59 (s, 1H), 7.84 (d, *J* = 7.7 Hz, 2H), 7.57 – 7.51 (m, 1H), 7.48 (t, J = 7.3 Hz, 2H), 6.73 (s, 1H), 4.25 (m, 4H)

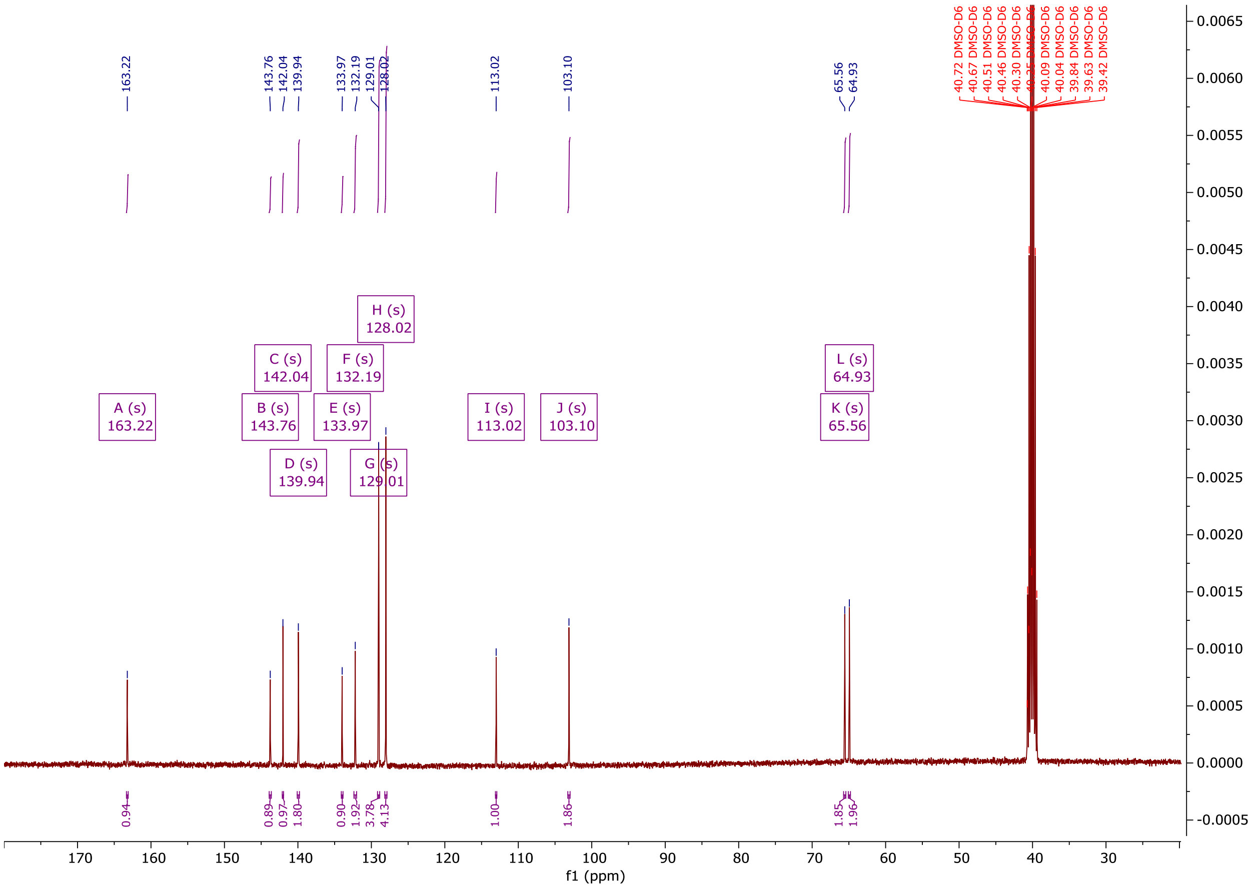

^{13}C NMR (101 MHz, DMSO-*d*$_6$, 298 K) δ (ppm) 163.2 143.8, 142.1, 140.0, 134.0, 132.2, 129.0, 128.0, 113.0, 103.1, 65.6, 64.9.

HRMS (ESI+) m/z [M + H]$^+$: calculated for [$C_{14}H_{12}N_2O_3S$+H]$^+$ 289.0641, found 289.0640

Melting point: 223 – 226 °C

2.3.5 Synthesis of AH5

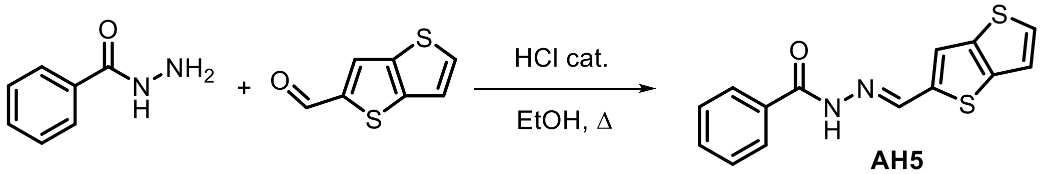

AH5

89 %

Synthesized according to general procedure B from benzhydrazide (0.52 g, 3.07 mmol, 1.0 equiv) and thieno(3,2-b)thiophene-2-carboxaldehyde (0.42 g, 3.07 mmol, 1.0 equiv). Obtained as a white powder (78.5 mg, 89 %).

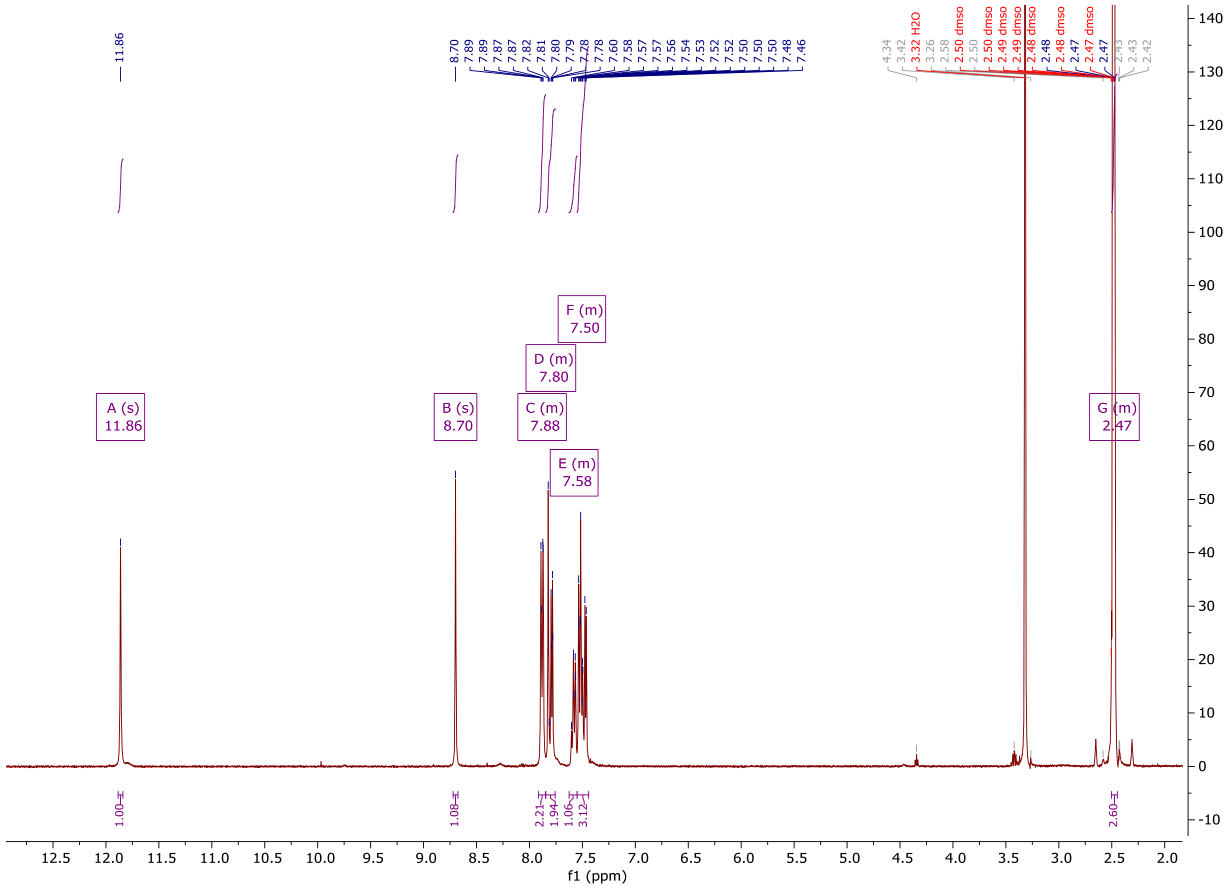

^{1}H NMR (400 MHz, DMSO-*d*$_6$, 298 K) δ (ppm) 11.88 (s, 1H), 8,73 (s, 1H), 7.91 (d, *J* = 7.5, 2H), 7.85 (s, 1H) 7.82 (d, *J* = 5.2, 1H), 7.61 (t, *J* = 7.1 1H), 7.55 (t, *J* = 7.6, 2H), 7.50 (d, *J* = 5.1, 1H)

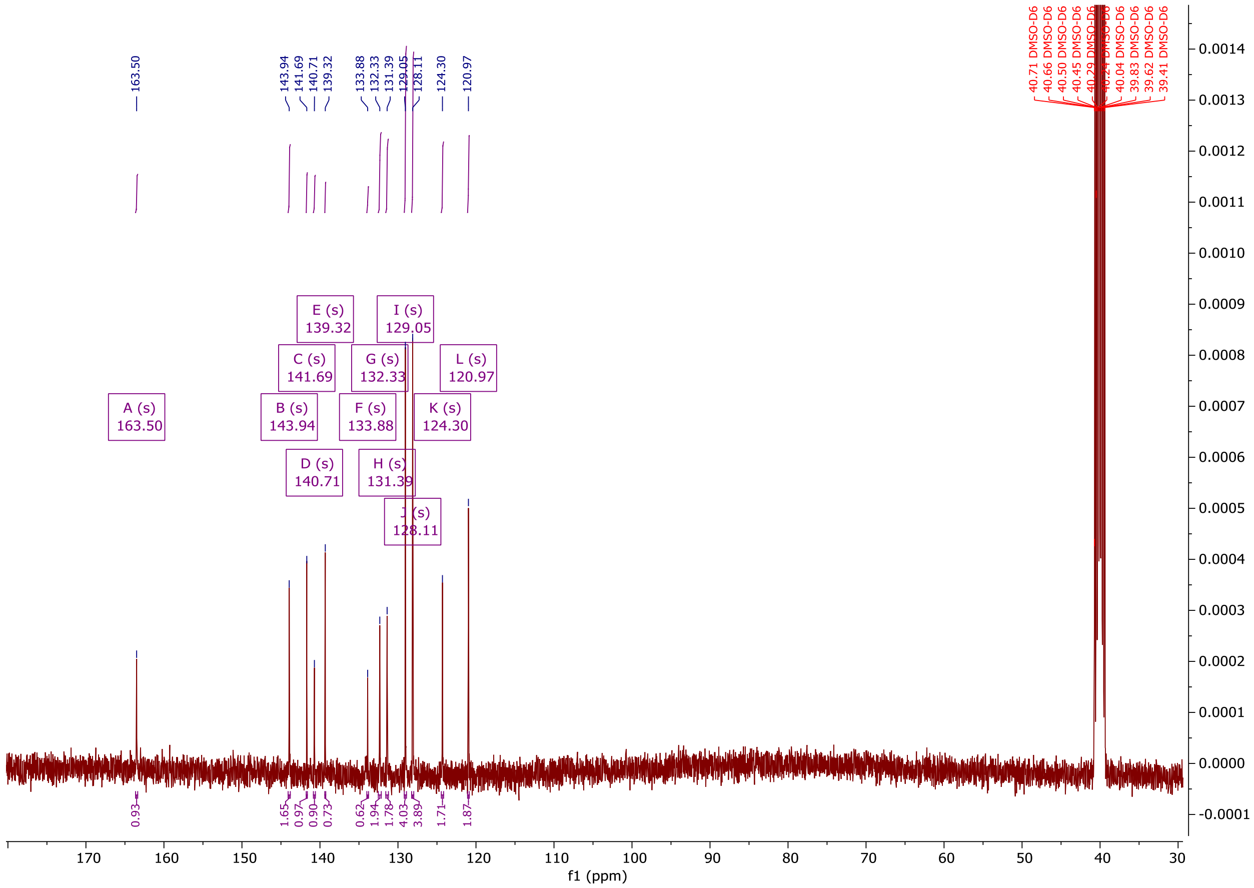

^{13}C NMR (101 MHz, DMSO-*d*$_6$, 298 K) δ (ppm) 163.5, 143.9, 141.7, 140.7, 139.3, 133.9, 132.3, 131.4, 129.1, 128.1, 124.3, 121.0

HRMS (ESI+) m/z [M + Na]$^+$ **:** calculated for [$C_{14}H_{10}N_2OS_2$+Na]$^+$ 309.0127, found 309.0128

Melting point: 233 – 236 °C

2.3.6 Synthesis of AH6

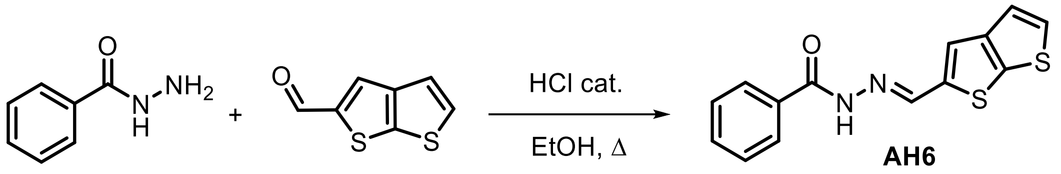

AH6

72 %

Synthesized according to general procedure B from benzhydrazide (54 mg, 0.4 mmol, 1.0 equiv) and thieno(2,3-*b*)thiophene-2-carbaldehyde (67 mg, 0.4 mmol, 1.0 equiv). Obtained as a white powder (82 mg, 72 %).

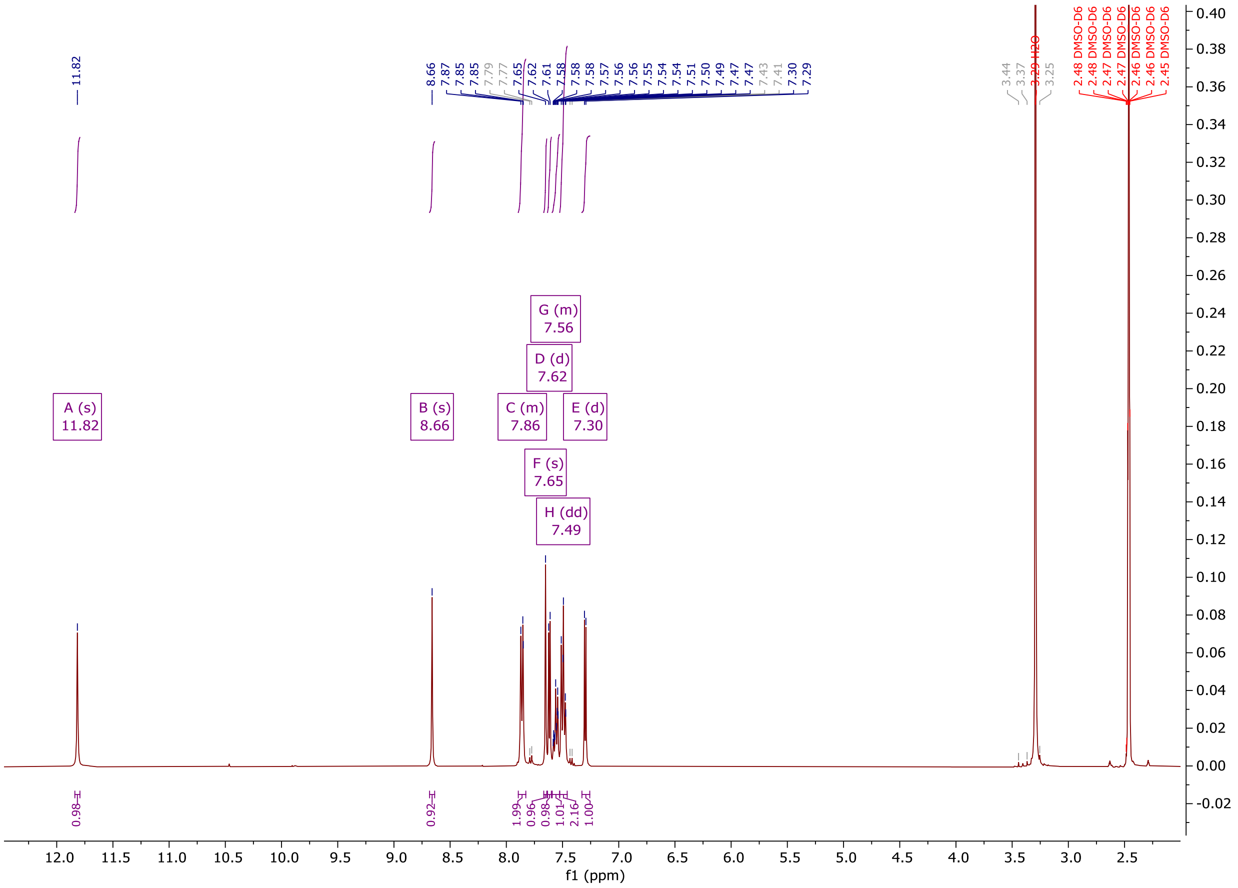

^{1}H NMR (400 MHz, DMSO-d_6, 298 K) δ (ppm) 11.82 (s, 1H), 8.66 (s, 1H), 7.86 (d, J = 7.0 Hz, 2H), 7.65 (s, 1H), 7.62 (d, J = 5.2 Hz, 1H), 7.56 (t, J = 7.2 Hz, 1H), 7.49 (dd, J = 8.3, 6.7 Hz, 2H), 7.30 (d, J = 5.2 Hz, 1H)

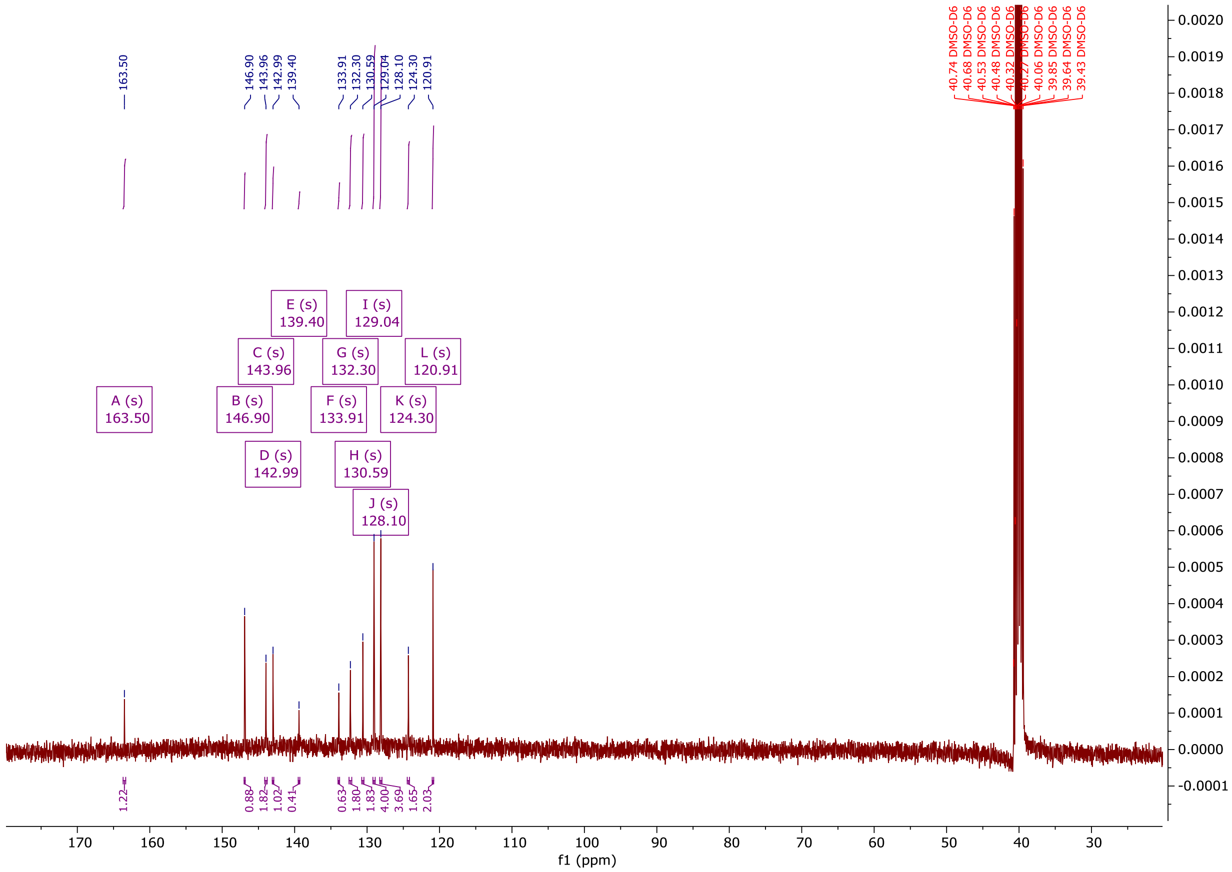

^{13}C NMR (101 MHz, DMSO-*d*$_6$, 298 K) δ ppm 163.5, 146.9, 144.0, 143.0, 133.9, 132.3, 130.6, 129.1, 128.1, 124.3, 120.9

HRMS (ESI+) m/z [M + Na]$^+$ **:** calculated for [$C_{14}H_{10}N_2OS_2$+Na]$^+$ 309.0127, found 309.0128

Melting point: 212 – 215 °C

2.3.7 Synthesis of AH7

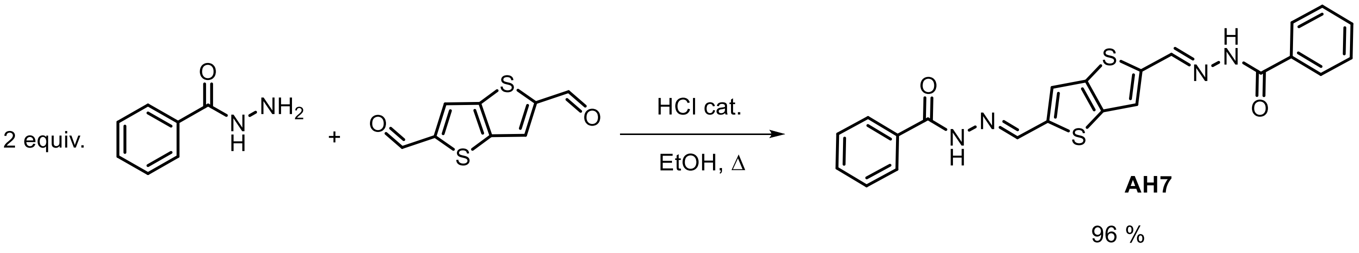

Synthesized according to general procedure B from benzhydrazide (0.200 g, 1.02 mmol, 1.0 equiv) and thieno[3,2-b]thiophene-2,5-dicarbaldehyde (0.278 g, 2.04 mmol, 2.0 equiv). Product obtained as a yellow powder (0.42 g, 96 %).

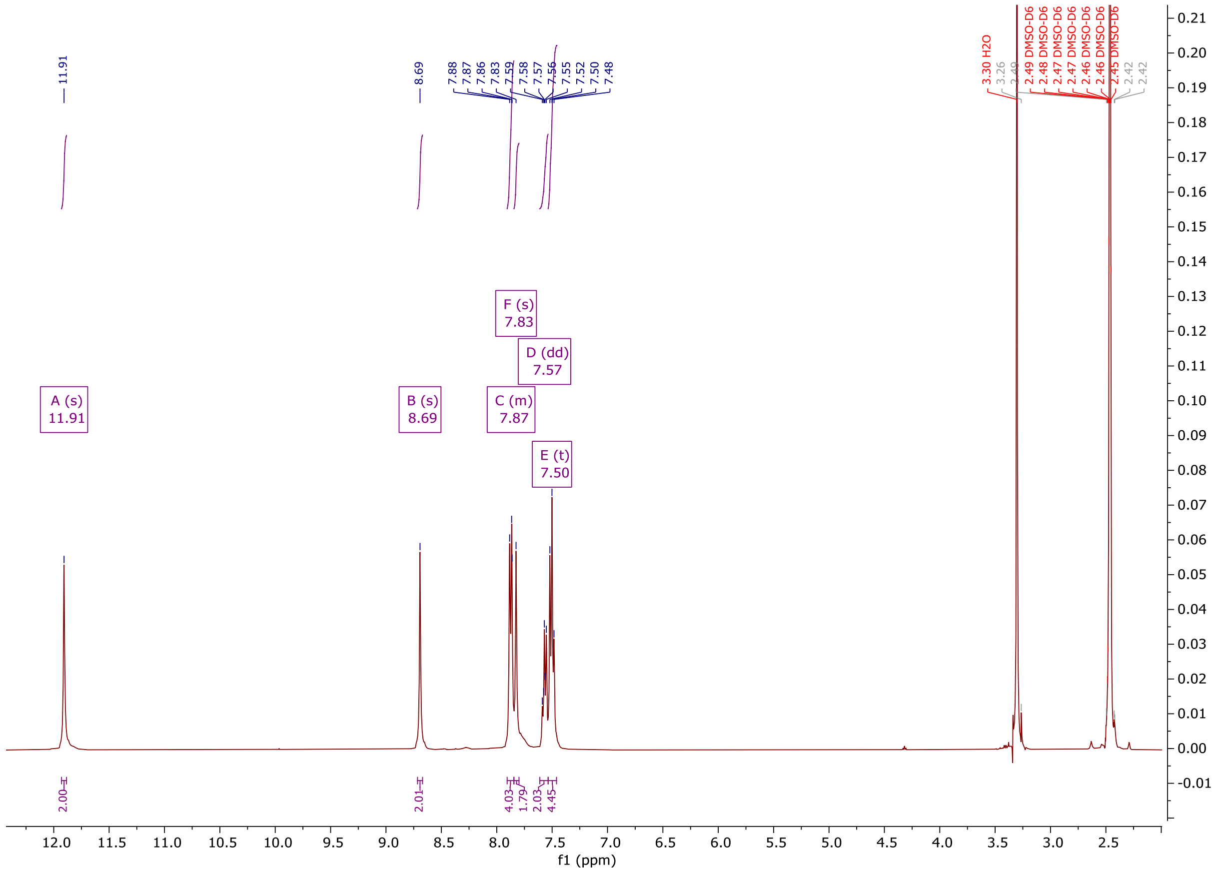

^{1}H NMR (400 MHz, DMSO-d_6, 298 K) δ (ppm) 11.91 (s, 2H), 8.69 (s, 2H), 7.87 (d, *J* = 7.1 Hz, 4H), 7.83 (s, 2H), 7.61 - 7.54 (m, 2H), 7.50 (t, *J* = 7.4 Hz, 4H)

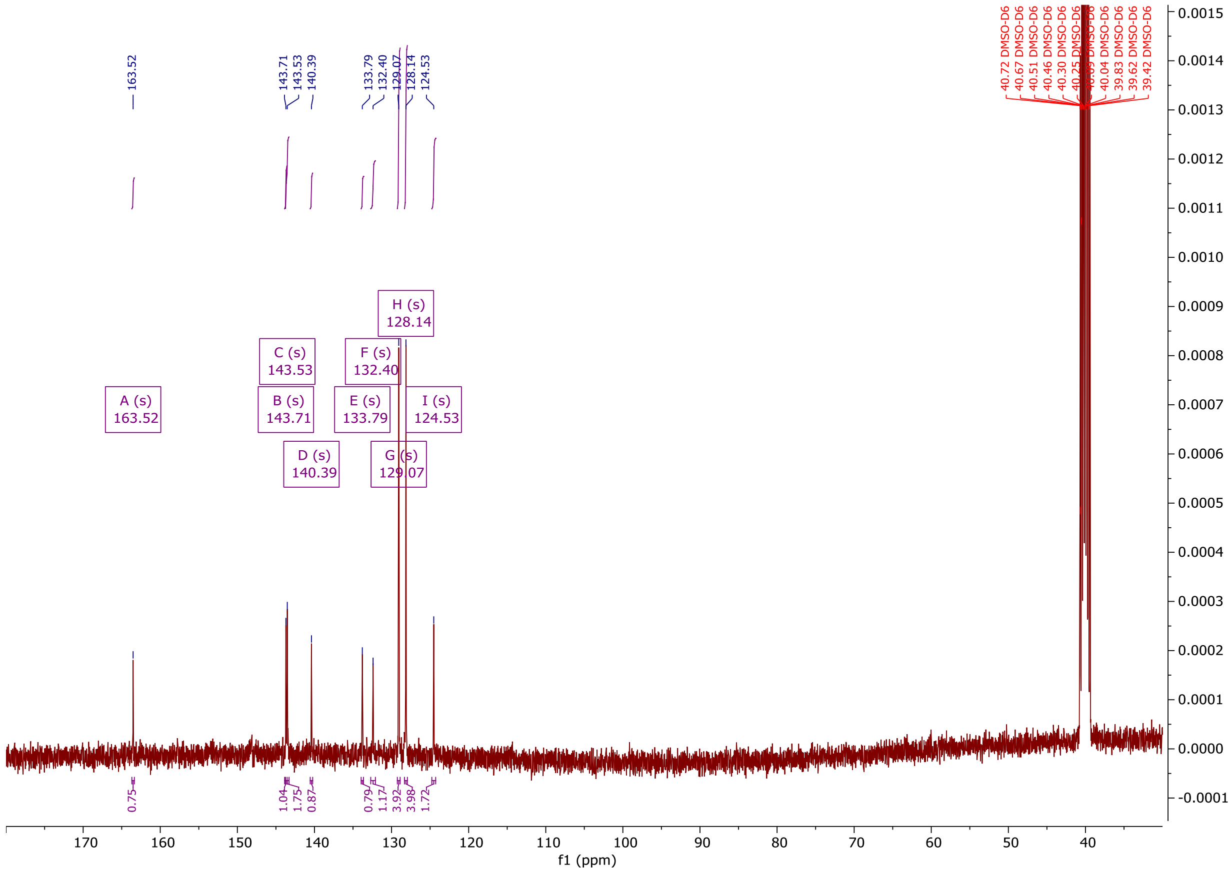

^{13}C NMR (101 MHz, DMSO-d_6, 298 K) δ (ppm) 163.5, 143.7, 143.5, 140.4, 133.8, 132.4, 129.1, 128.2, 124.5

HRMS (ESI-) m/z [M - H]$^-$ **:** calculated for $[C_{22}H_{15}N_4O_2S_2\text{-}H]^-$ 431.0642, found 431.0641

Melting point: 368 – 370 °C

2.3.8 Synthesis of AH8

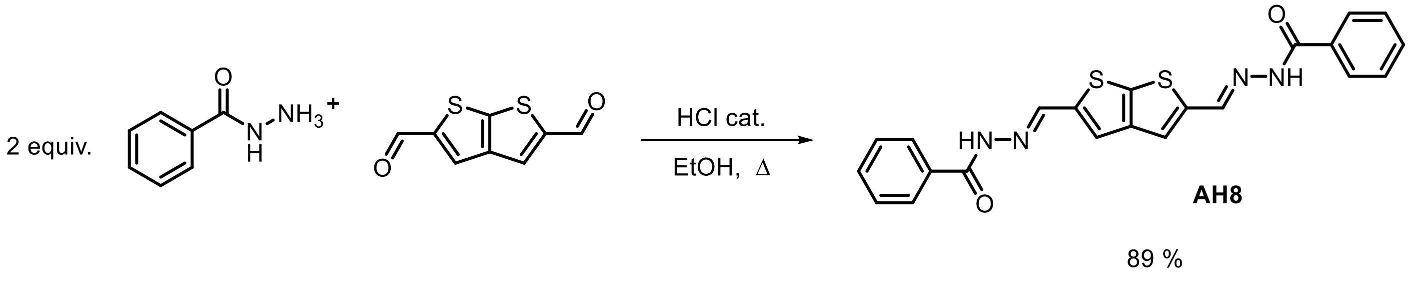

Synthesized according to general procedure B from benzhydrazide (0.200 g, 1.02 mmol, 1.0 equiv) and thieno[3,2-b]thiophene-2,5-dicarbaldehyde (0.278 g, 2.04 mmol, 2.0 equiv). Product obtained as a yellow powder (0.39 g, 89 %).

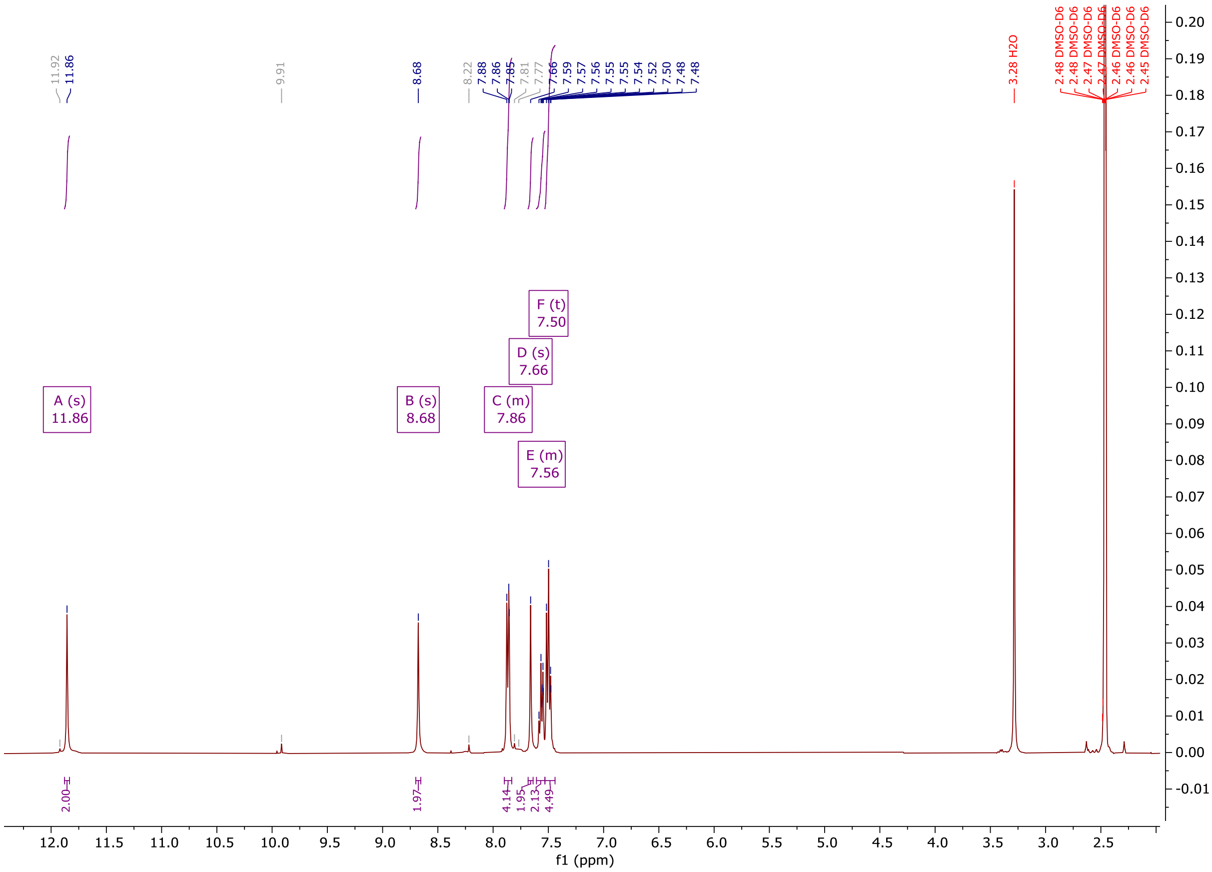

^{1}H NMR (400 MHz, DMSO-d_6, 298 K) δ (ppm) 11.86 (s, 2H), 8.68 (s, 2H), 7.86 (d, *J* = 7.5 Hz, 4H), 7.66 (s, 2H), 7.56 (m, 2H), 7.50 (t, *J* = 7.3 Hz, 4H)

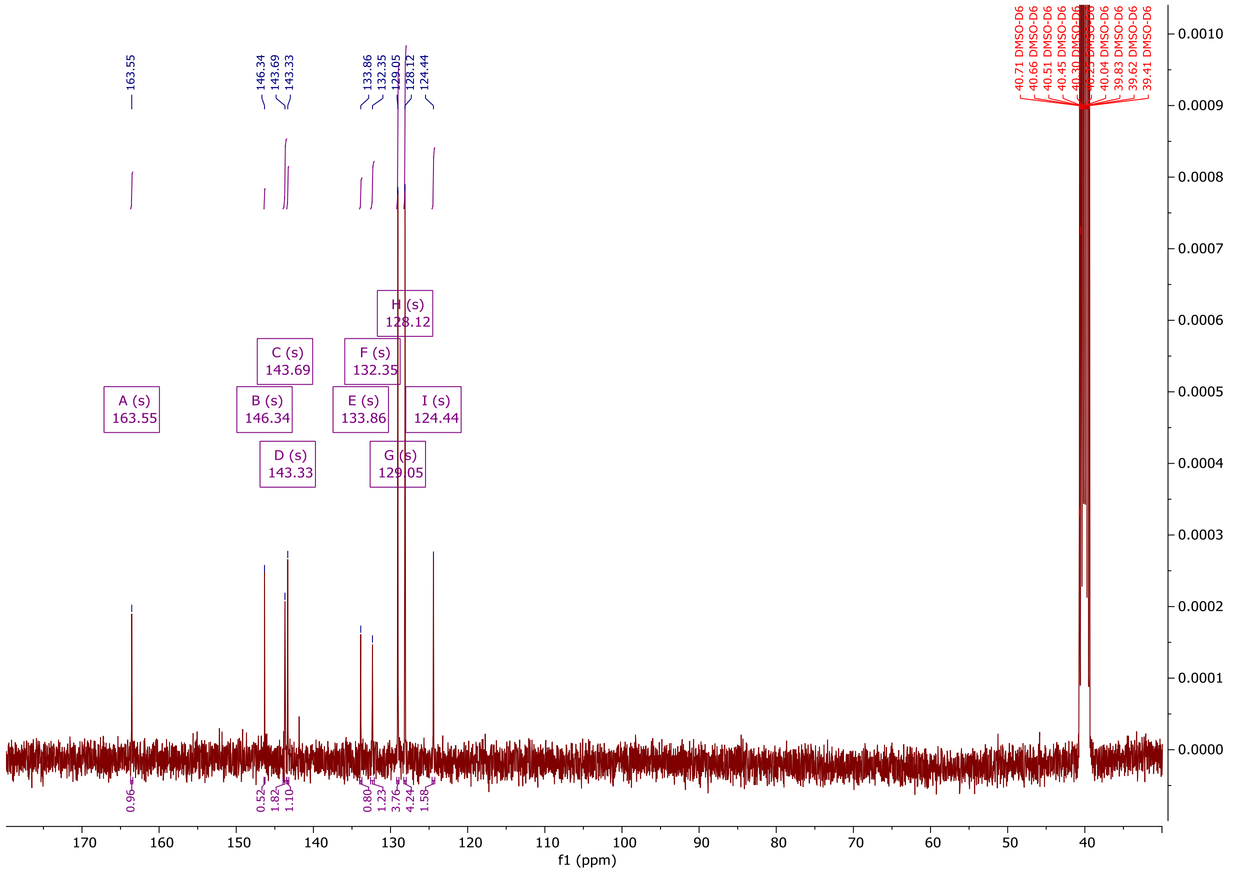

^{13}C NMR (101 MHz, DMSO-d_6, 298 K) δ (ppm) 163.6, 146.4, 143.7, 143.3, 133.9, 132.4, 129.1, 128.1, 124.5

HRMS (ESI+) m/z [M + Na]$^+$ **:** calculated for $[C_{22}H_{15}N_4O_2S_2+Na]^+$ 455.0607, found 455.0607

Melting point: 338 – 341 °C

2.3.9 Synthesis of AH9

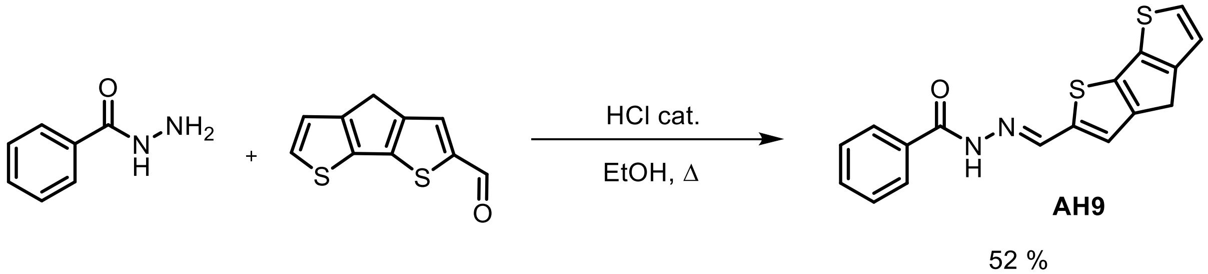

AH9

52 %

Synthesized according to general procedure B from benzhydrazide (0.056 g, 0.3 mmol, 1.0 equiv) and 4*H*-cyclopenta[2,1-b:3,4-b']dithiophene-2-carbaldehyde (0.037 g, 0.3 mmol, 1.0 equiv). Product obtained as a shiny yellow powder (0.051 g, 52 %).

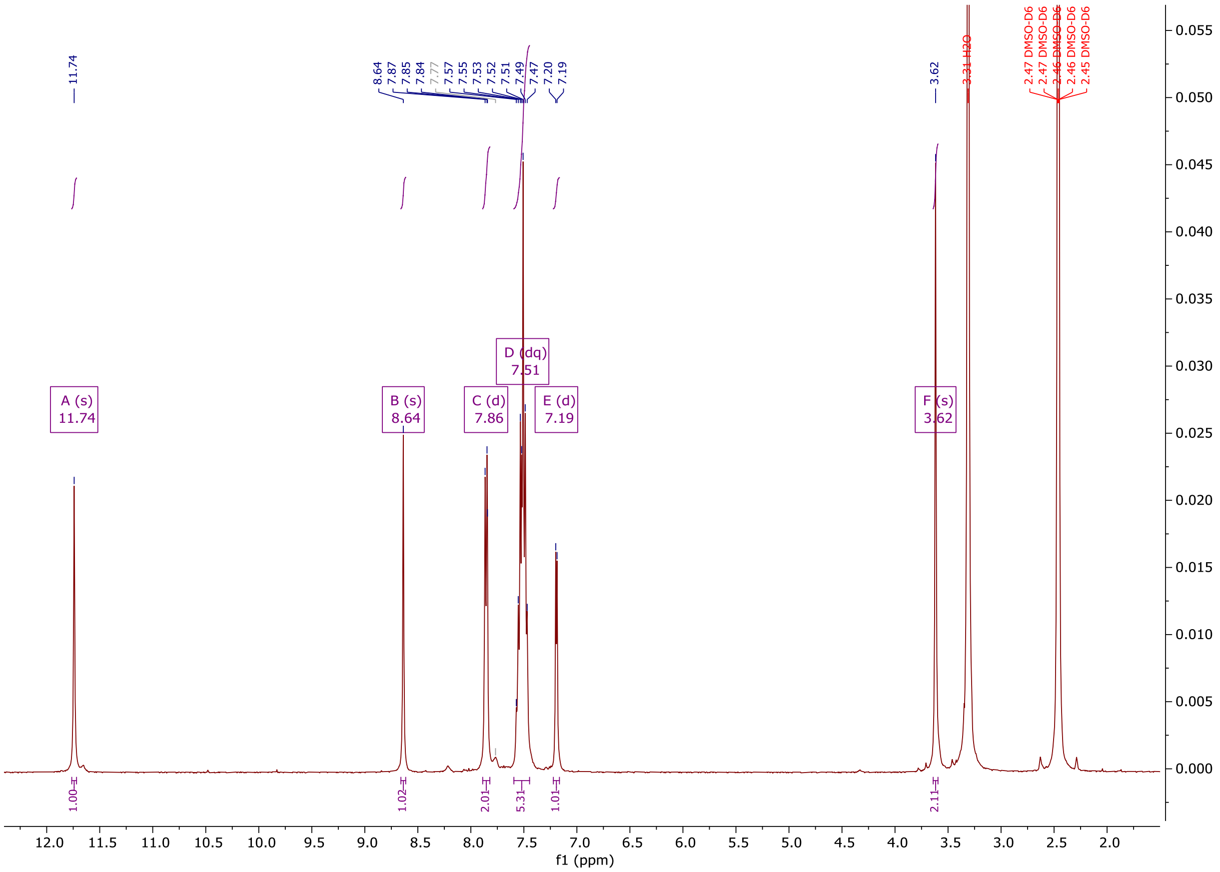

^{1}**H NMR** (400 MHz, DMSO-*d*$_6$, 298 K) δ (ppm) 11.74 (s, 1H), 8.64 (s, 1H), 7.86 (d, J = 7.2 Hz, 2H), 7.58 – 7.44 (m, 5H), 7.19 (d, J = 4.9 Hz, 1H), 3.62 (s, 2H)

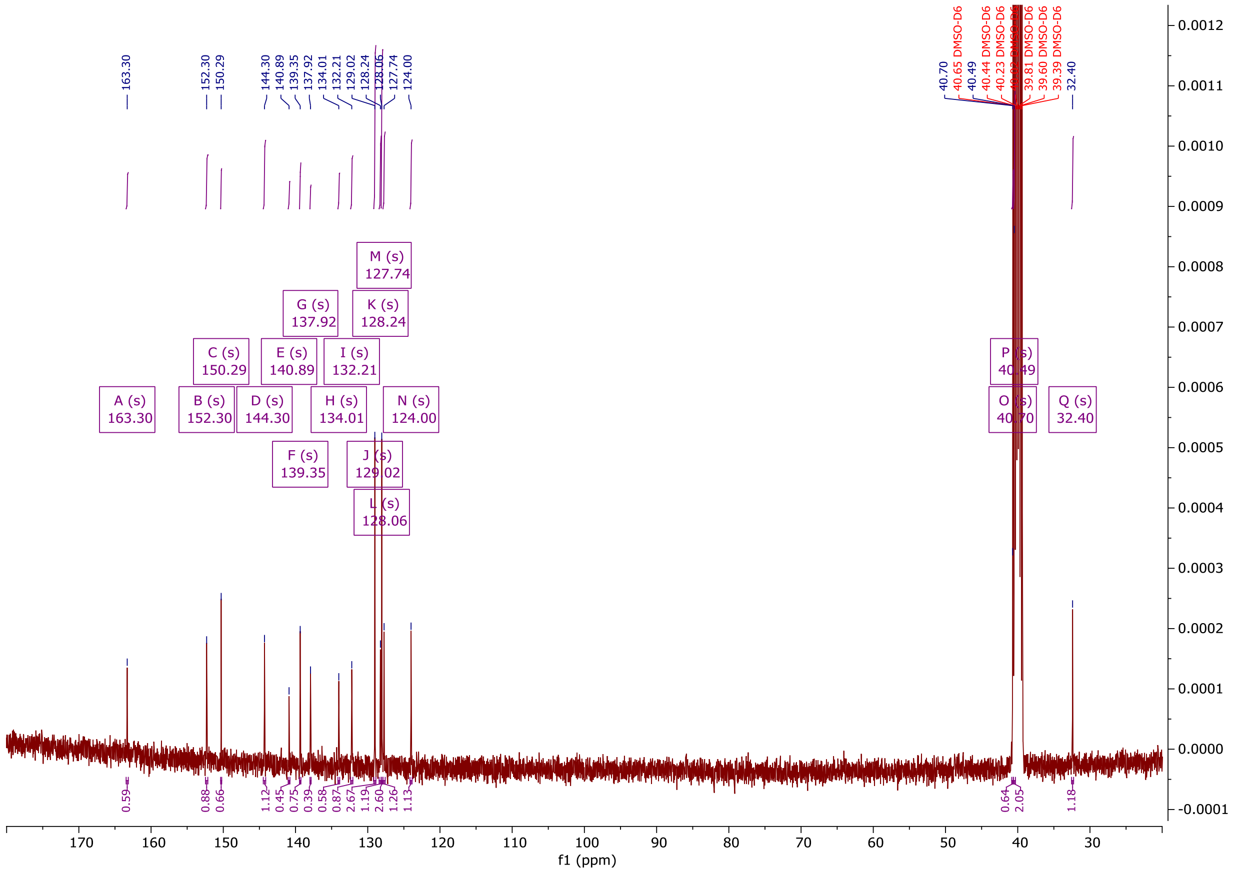

^{13}C NMR (101 MHz, DMSO-*d$_6$*, 298 K) δ (ppm) 163.6, 146.9, 144.1, 143.0, 134.0, 132.4, 129.1, 128.1, 124.5, 120.9, 109.4

HRMS (ESI+) m/z [M + Na]$^+$ **:** calculated for $[C_{17}H_{12}N_2OS_2+Na]^+$ 347.0283, found 347.0287

Melting point: 218 – 221 °C

2.3.10 Synthesis of DAE-2AH1

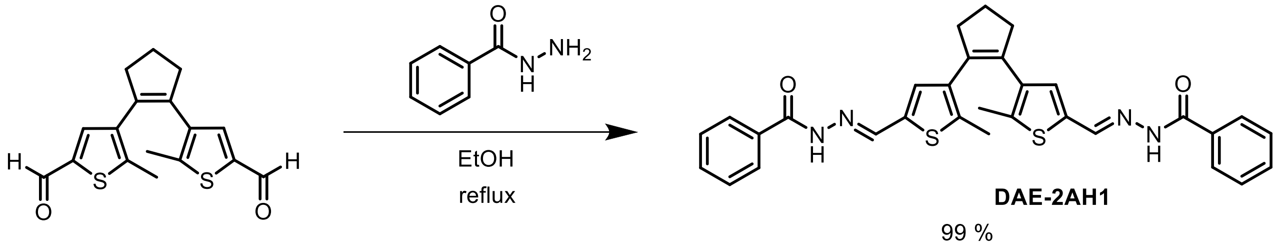

Synthesized according to general procedure B from benzhydrazide (0.236 g, 1.73 mmol, 2.0 equiv) and 4,4'-(cyclopent-1-ene-1,2-diyl)bis(5-methylthiophene-2-carbaldehyde) (0.273 g, 0.86 mmol, 1.0 equiv). Product obtained as a pale green powder (0.47 g, 99 %).[8]

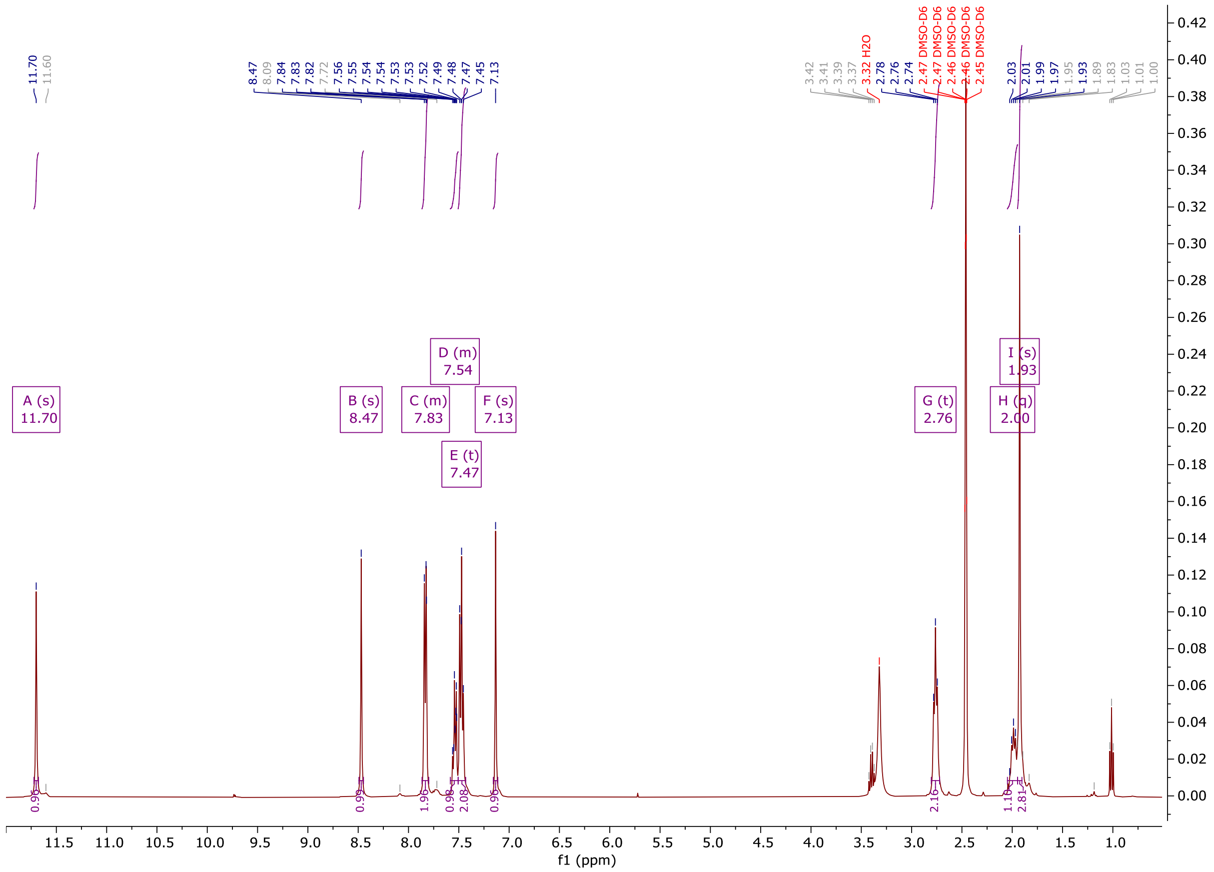

^{1}H NMR (400 MHz, DMSO-d_6, 298 K) δ (ppm) 11.70 (s, 2H), 8.47 (s, 2H), 7.83 (d, J = 6.5 Hz, 4H), 7.57 – 7.52 (m, 2H), 7.50 – 7.45 (m, 4H), 7.13 (s, 2H), 2.76 (t, J = 7.5 Hz, 4H), 2.00 (q, J = 7.5 Hz , 2H), 1.93 (s, 6H)

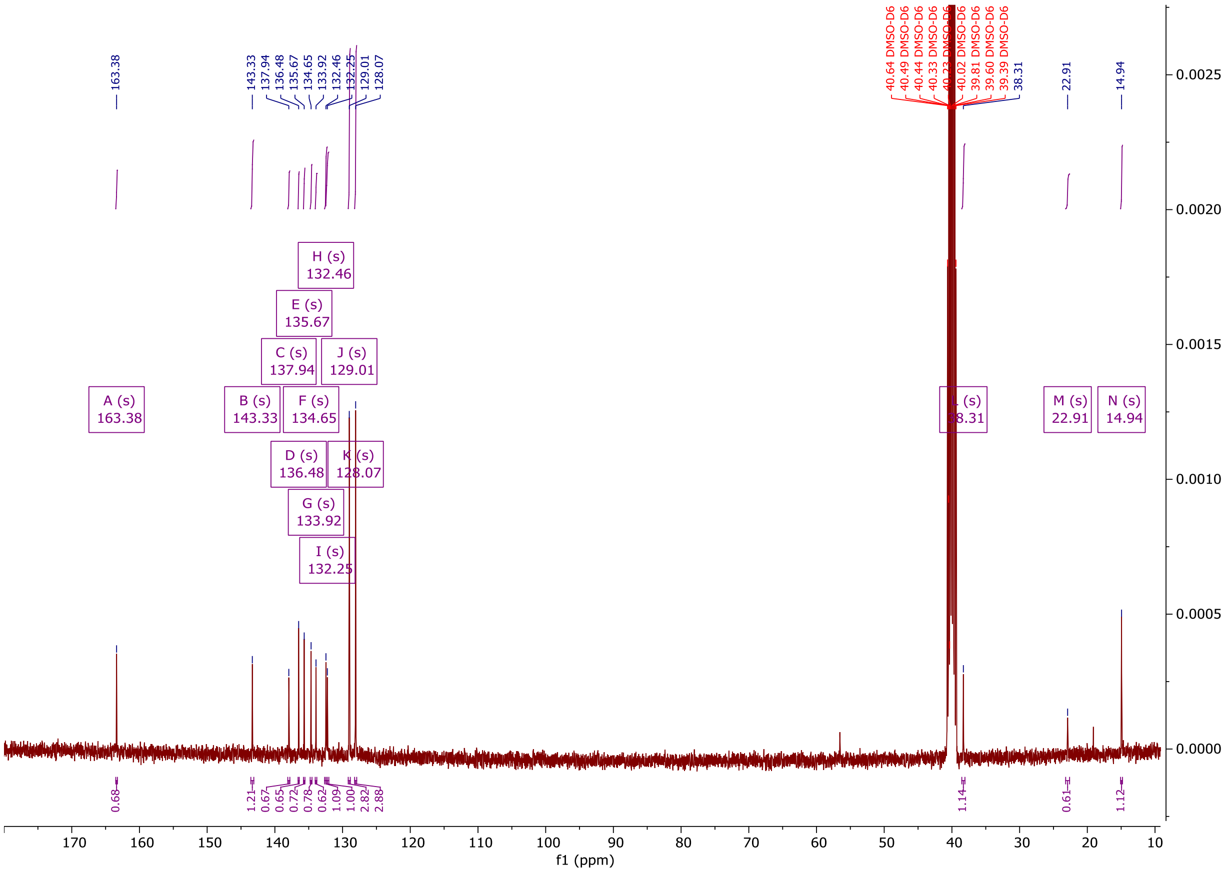

^{13}**C NMR** (101 MHz, DMSO-*d*$_6$, 298 K) δ (ppm) 163.4, 143.4, 138.0, 136.5, 135.7, 134.7, 133.9, 132.5, 132.3, 129.0, 128.1, 38.3, 22.9, 14.9

HRMS (ESI+) m/z [M + Na]$^+$ **:** calculated for [$C_{31}H_{28}N_4O_2S_2$+Na]$^+$ 575.1546, found 575.1547

Melting point: 243 – 245 °C

3 PHOTOSWITCHING

Photoswitching properties of the acylhydrazones were studied via UV-Vis spectroscopy in combination with the source of monochromatic light (Xenon lamp). Solutions of acylhydrazones in acetonitrile (1×10^{-5} M) were irradiated with a chosen wavelength of light based on the absorption maximum while being stirred, and UV-Vis spectra were taken at given time intervals.

3.1 Photoswitching of AH1

The UV-Vis spectrum of **AH1** in acetonitrile (1·10^{-5} M) has shown one strong band at around 317 nm and this wavelength was then chosen for irradiation. The solution was irradiated with 317 nm light and simultaneously UV-Vis spectra were obtained every 5 seconds. As seen in Figure S 1, the intensity of the peak at around 317 nm gradually decreases and regions at 240-250 nm and at 350-400 nm increase in their intensity, indicating the switching from *E*-form to photoswitched-form.

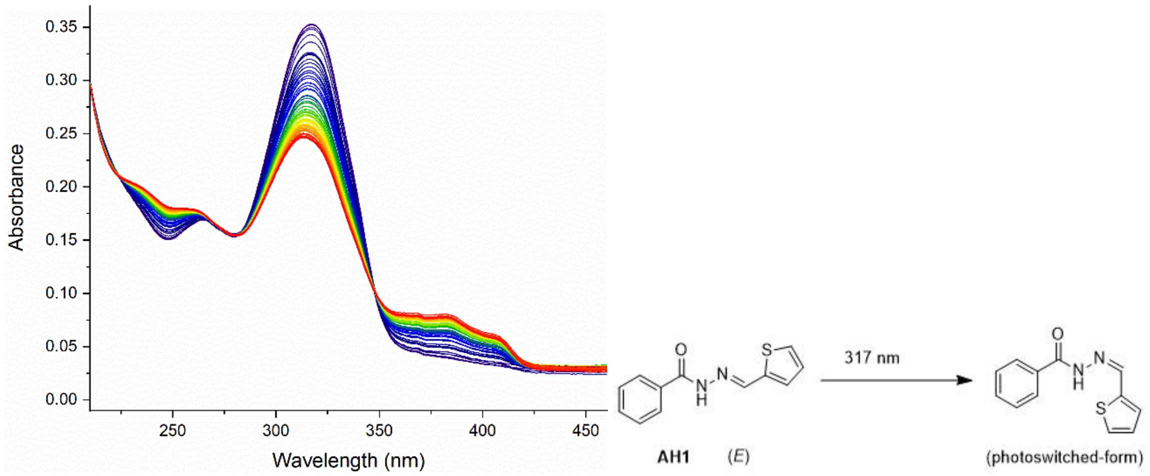

Figure S 1 Photoisomerization of **AH1** from *E*-form to photoswitched-form. Time development of UV-vis traces is color-coded by blue to green to yellow to red gradient.

The irradiation wavelength was set at the most intense peak associated with the photoswitched-form isomer. The solution was irradiated with 385 nm light and simultaneously UV-Vis spectra were recorded every 15 seconds. We have observed reverse changes in the spectra as compared to irradiation with 317 nm, confirming reversible photoswitching of **AH1** from photoswitched-form back to *E*-form (Figure S 2).

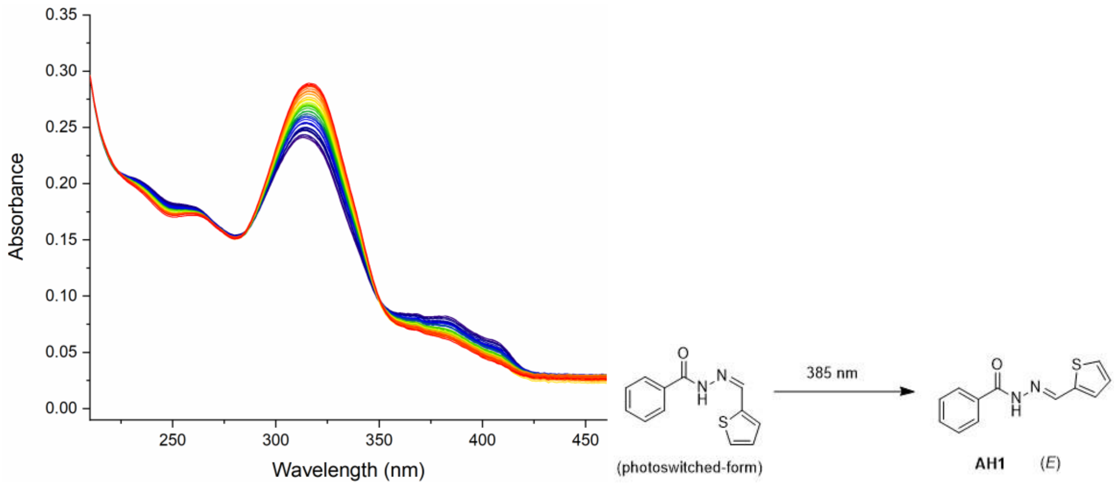

Figure S 2 Photoisomerization of **AH1** from photoswitched-form to *E*-form. Time development of UV-vis traces is color-coded by blue to green to yellow to red gradient.

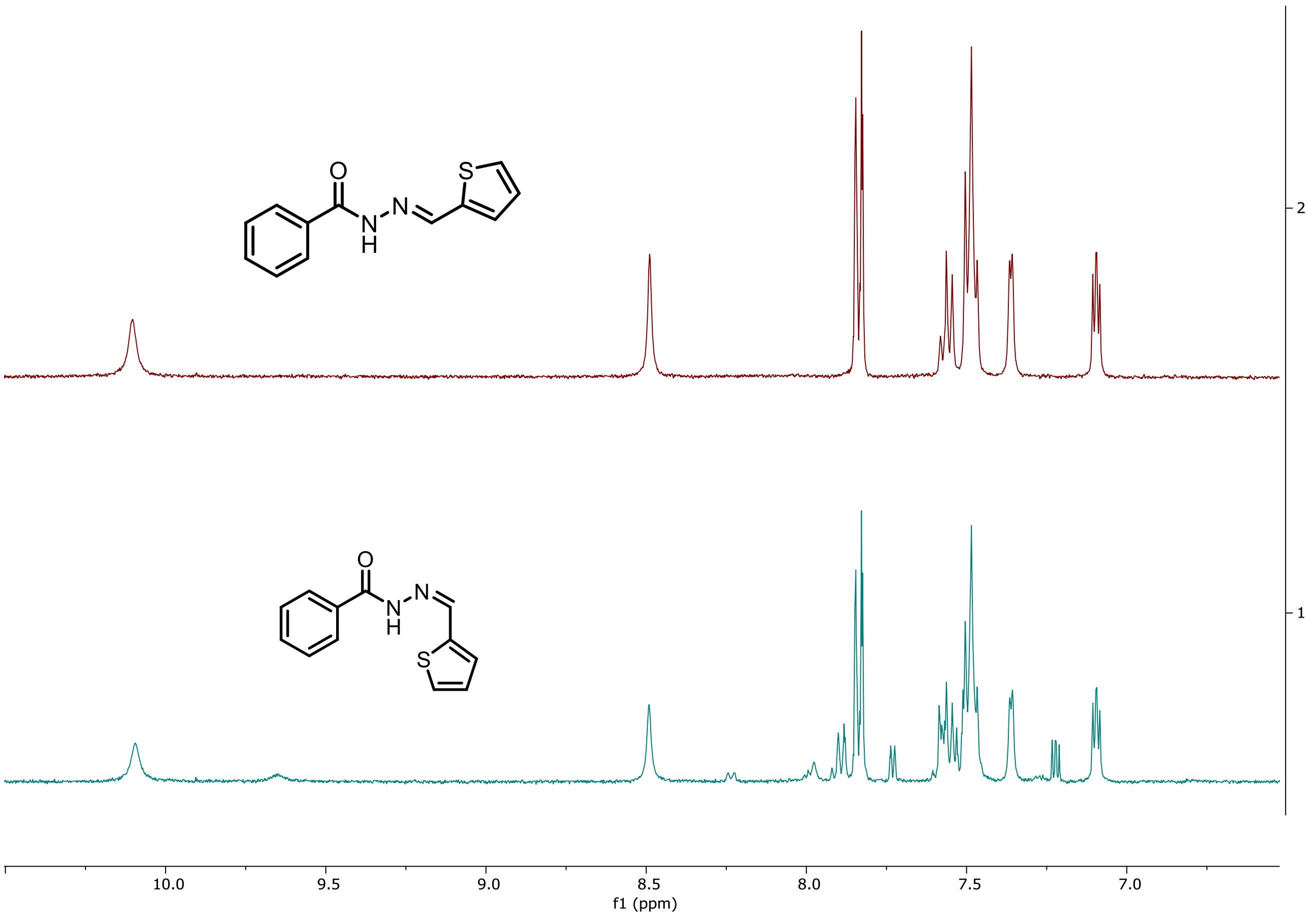

Figure S 3 ^{1}H NMR spectra of non-irradiated AH1 solution (up) and irradiated AH1 solution (down). We can observe new set of triplet at 7.22 and new set of dublets at 7.73 and 7.89 ppm in comparison with the non-irradiated sample.

Photoswitching of **AH1** was also studied by ^{1}H NMR in the presence of internal standard – *t*-BuOH. The solution of **AH1** in deuterated acetonitrile ($1\cdot10^{-3}$ M) with *t*-BuOH (3 µmol) was irradiated by 317 nm light for 3 hours to achieve PSS. The NMR spectra were measured before and after irradiation. We can see that integral intensity of non-irradiation **AH1** is 0.26 compared to *t*-BuOH and joined integral intensity of the *E*-form and photoswitched-form after irradiation is also 0.26 . This makes all of the species observable in the ^{1}H NMR spectrum.

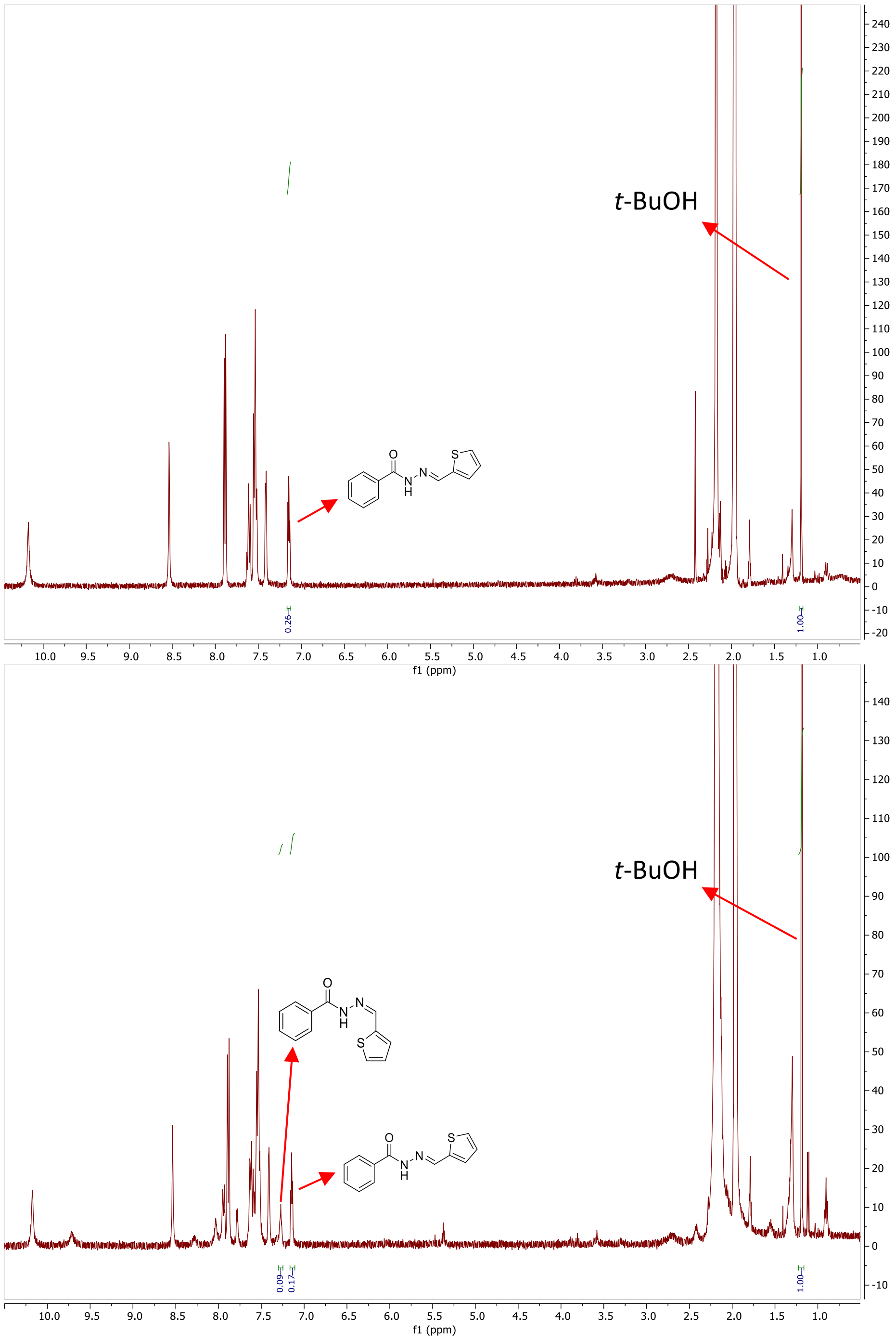

Figure S 4 ^{1}H NMR spectra of non-irradiated solution of **AH1** with *t*-BuOH (up) and irradiated solution of **AH1** with *t*-BuOH (down). We can clearly see that integral intensity of non-irradiated **AH1** matches with the joined integral intensity of **AH1** E-form and photoswitched-form

3.2 Repeated photoswitching of AH1 in solution

We investigated whether it is possible to repeat the photoisomerization multiple times from *E*-form to photoswitched-form and *vice versa*. The solution of **AH1** in acetonitrile (1·10^{-5} M) was irradiated with 317 nm light for 40 minutes and we observed a change in the UV-Vis spectrum associated with isomerization from *E*-form to photoswitched-form. The solution was then irradiated with 380 nm light for 120 minutes and we observed reverse changes in the spectra as compared to irradiation with 317 nm associated with isomerization from photoswitched-form to *E*-form. We repeated photoisomerization 8 times and we observed the same behavior in every cycle. We can clearly confirm that **AH1** undergoes repeated photoisomerization in solution without fatigue or photochemical decomposition (Figure S 5).

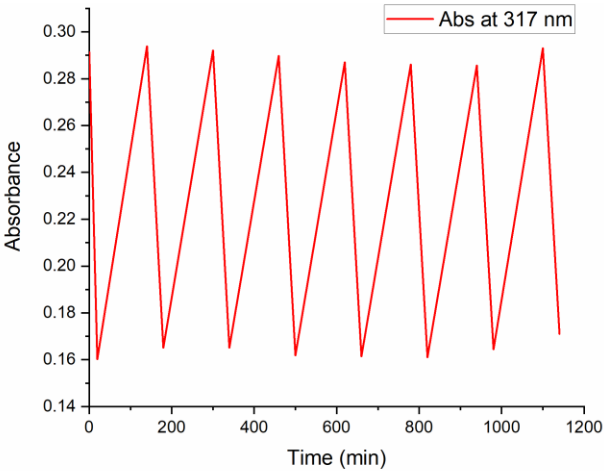

Figure S 5 Absorbance of **AH1** at 317 nm changes periodically as the molecule undergoes repeated photoisomerization cycles.

3.3 Photoswitching of AH2

The UV-Vis spectrum of **AH2** in acetonitrile ($1 \cdot 10^{-5}$ M) has shown one strong band at around 295 nm and this wavelength was then chosen for irradiation. The solution was irradiated with 295 nm light and simultaneously UV-Vis spectra were obtained every 5 seconds. As seen in Figure S 6, the intensity of the peak at around 295 nm gradually decreases, but we did not observe any new set of peaks around the area of 390 - 450 nm. Thus, we can conclude that the 3-thienyl-based acylhydrazones do not behave the same feature as the 2-thienyl-based acylhydrazones.

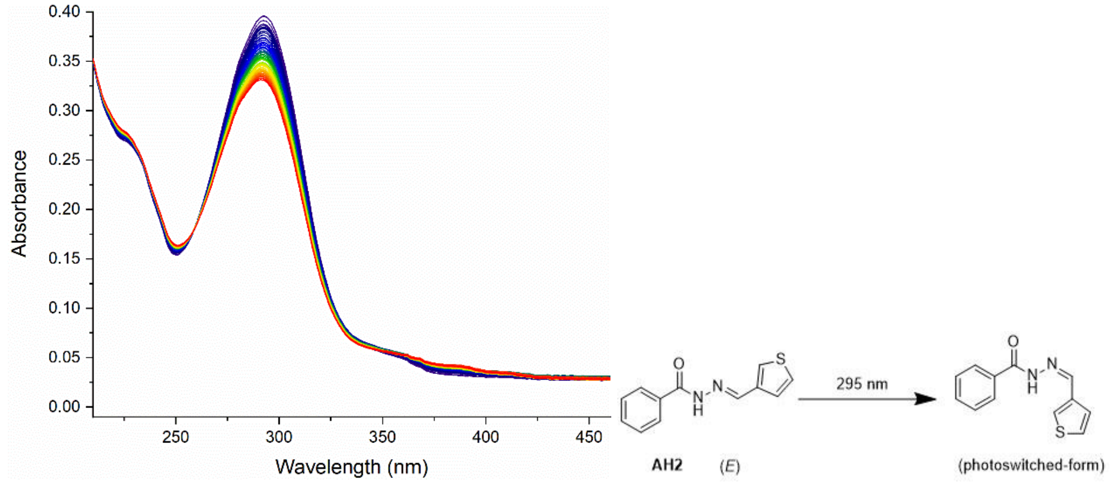

Figure S 6 Photoisomerization of **AH2** from *E*-form to photoswitched-form. Time development of UV-vis traces is color-coded by blue to green to yellow to red gradient.

It was experimentally confirmed that no photoisomerization occurs after irradiation with higher wavelengths such as 385 nm (Figure S 7).

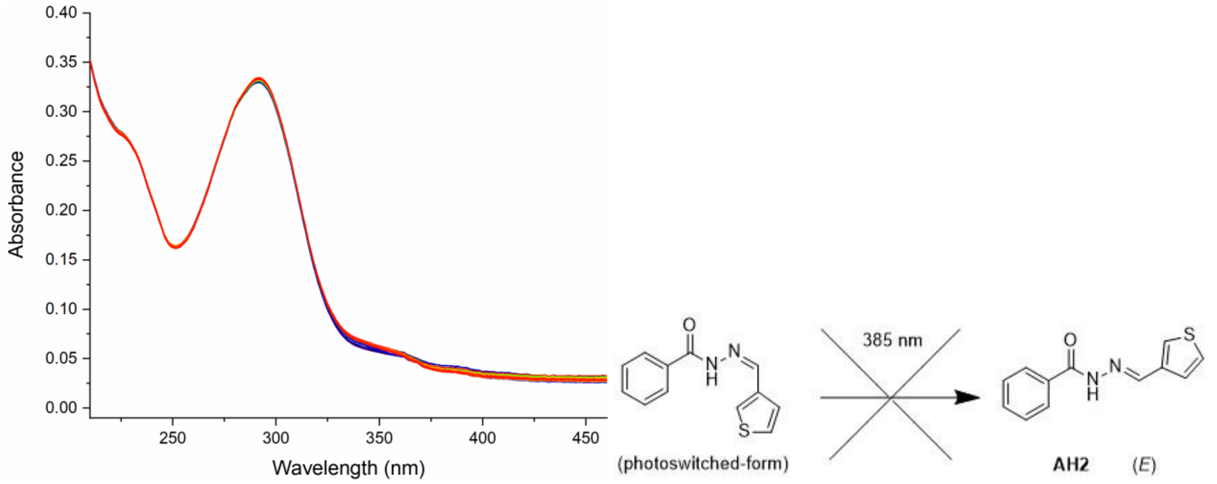

Figure S 7 No photoisomerization after irradiation with 385 nm. Time development of UV-vis traces is color-coded by blue to green to yellow to red gradient.

3.4 Photoswitching of AH3

The UV-Vis spectrum of **AH3** in acetonitrile ($1\cdot10^{-5}$ M) has shown one strong band at around 325 nm and this wavelength was then chosen for irradiation. The solution was irradiated with 325 nm light and simultaneously UV-Vis spectra were obtained every 5 seconds. As seen in Figure S 8, the intensity of the peak at around 325 nm gradually decreases and regions at 250-260 nm and at 355-425 nm increase in intensity, indicating the switching from *E*-form to photoswitched-form.

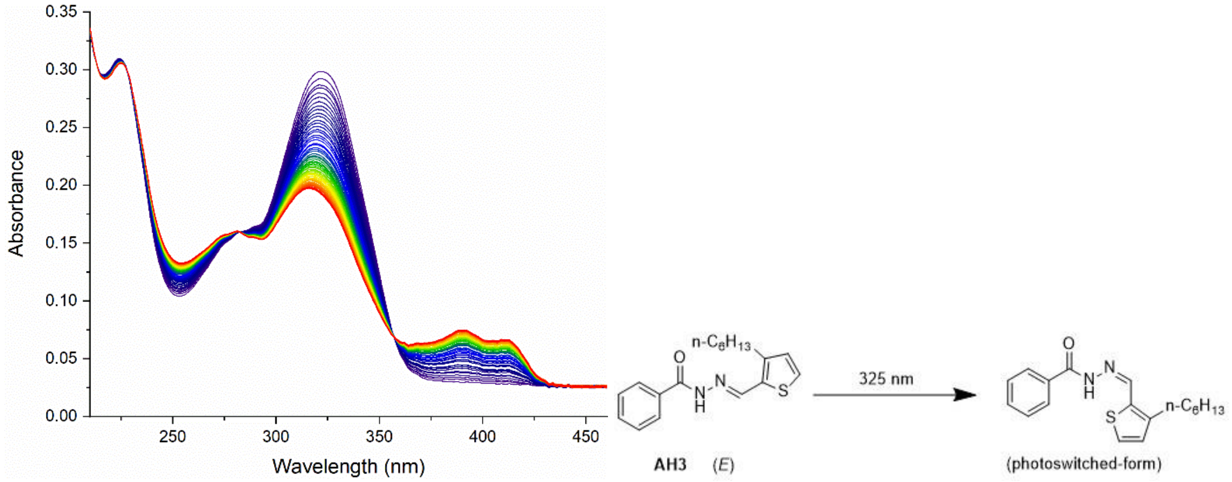

Figure S 8 Photoisomerization of **AH3** from *E*-form to photoswitched-form. Time development of UV-vis traces is color-coded by blue to green to yellow to red gradient.

The irradiation wavelength was set at the most intense peak associated with the photoswitched-form isomer. The solution was irradiated with 390 nm light and simultaneously UV-Vis spectra were obtained every 15 seconds. We have observed reverse changes in the spectra as compared to irradiation with 325 nm, confirming reversible photoswitching of **AH3** from photoswitched-form back to *E*-form (Figure S 9).

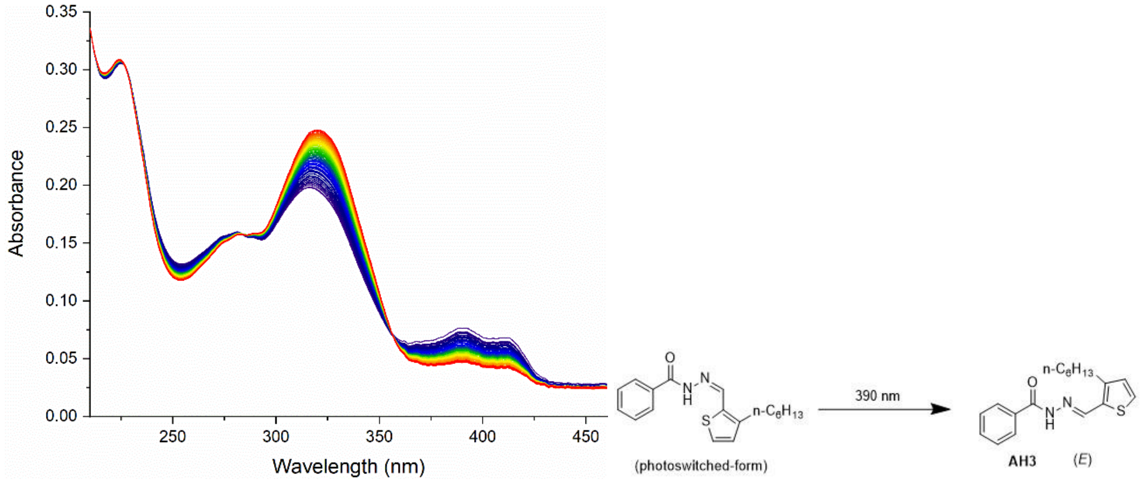

Figure S 9 Photoisomerization of **AH3** from photoswitched-form to *E*-form. Time development of UV-vis traces is color-coded by blue to green to yellow to red gradient.

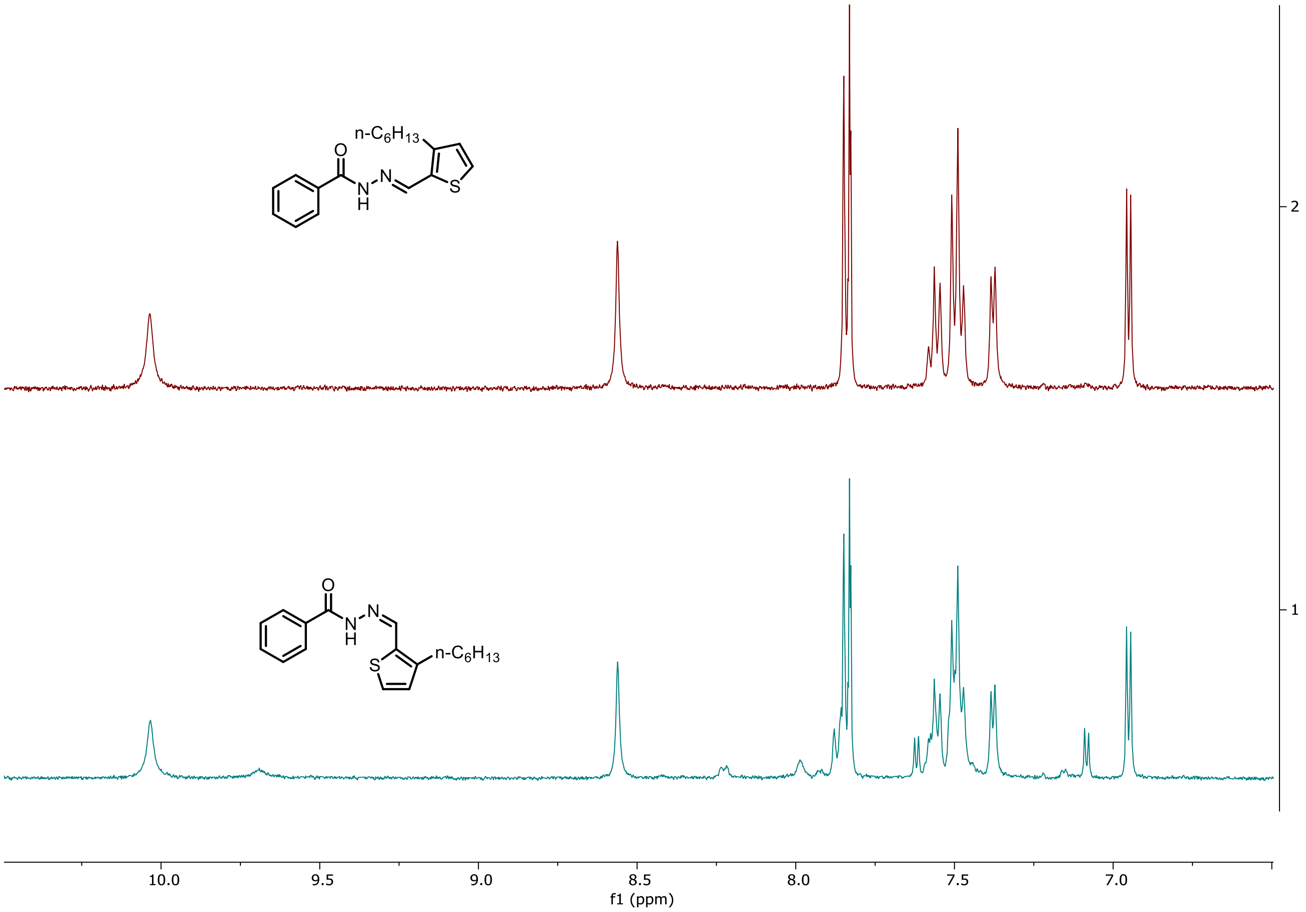

Figure S 10 ^{1}H NMR spectra of non-irradiated **AH3** solution (up) and irradiated **AH3** solution (down). We can observe new set of dublets at 7.08 at 7.62 ppm in comparison with the non-irradiated sample.

3.5 Repeated photoswitching of AH3 in solution

We investigated whether it is possible to repeat the photoisomerization multiple times from *E*-form to photoswitched-form and *vice versa*. The solution of **AH3** in acetonitrile ($1 \cdot 10^{-5}$ M) was irradiated with 325 nm light for 40 minutes and we observed a change in the UV-Vis spectrum associated with isomerization from *E*-form to photoswitched-form. The solution was then irradiated with 390 nm light for 40 minutes and we observed reverse changes in the spectra as compared to irradiation with 325 nm associated with isomerization from photoswitched-form to *E*-form. We repeated photoisomerization 8 times and we observed the same behavior in every cycle. We can clearly confirm that **AH3** undergoes repeated photoisomerization in solution without fatigue or photochemical decomposition (Figure S 11).

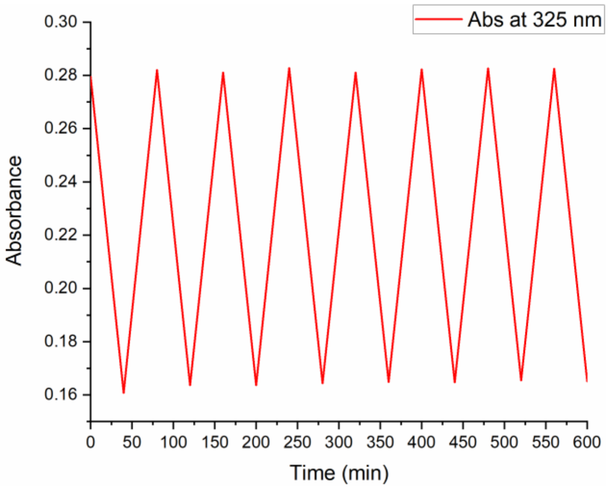

Figure S 11 Absorbance of **AH3** at 325 nm changing periodically as the molecule undergoes repeated photoisomerization cycles.

3.6 Photoswitching of AH4

The UV-Vis spectrum of **AH4** in acetonitrile ($1 \cdot 10^{-5}$ M) has shown one strong band at around 330 nm and this wavelength was then chosen for irradiation. The solution was irradiated with 330 nm light and simultaneously UV-Vis spectra were obtained every 5 seconds. As seen in Figure S 12, the intensity of the peak at around 330 nm gradually decreases and regions at 250–265 nm and at 370 –435 nm increase in intensity, indicating the switching from *E*-form to photoswitched-form.

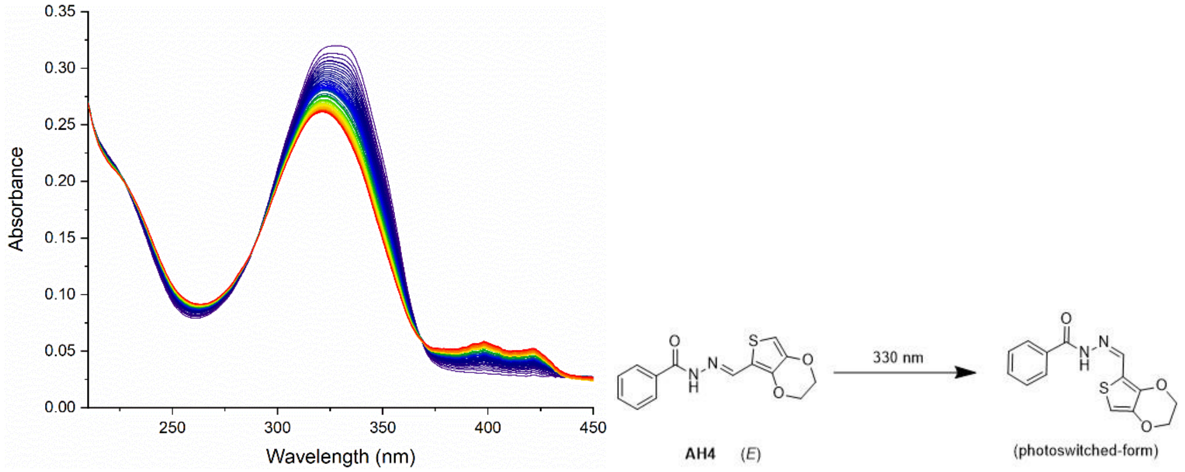

Figure S 12 Photoisomerization of **AH4** from *E*-form to photoswitched-form. Time development of UV-vis traces is color-coded by blue to green to yellow to red gradient.

The irradiation wavelength was set at the most intense peak associated with the photoswitched-form isomer. The solution was irradiated with 400 nm light and simultaneously UV-Vis spectra were obtained every 15 seconds. We have observed reverse changes in the spectra as compared to irradiation with 330 nm, confirming reversible photoswitching of **AH4** from photoswitched-form back to *E*-form (Figure S 13).

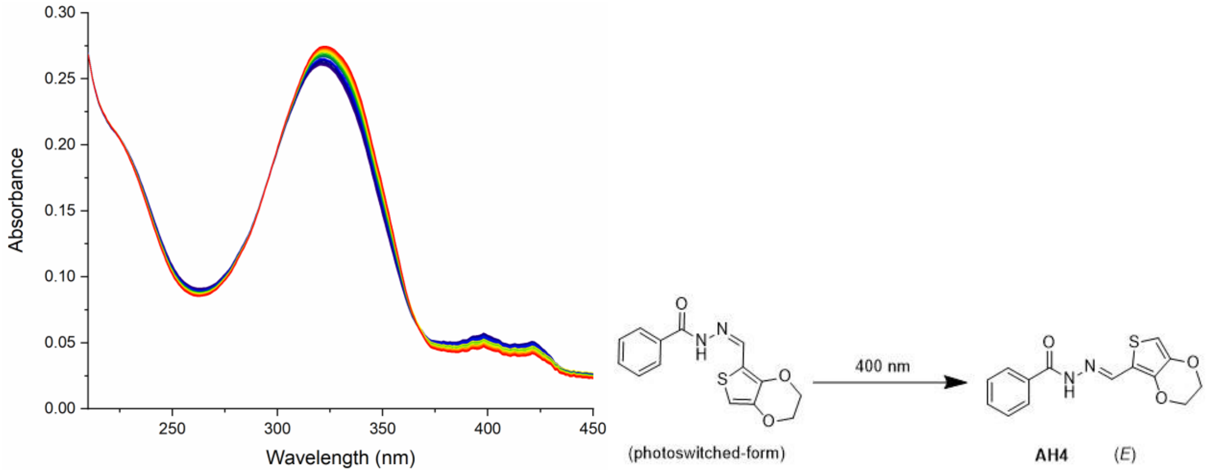

Figure S 13 Photoisomerization of **AH4** from photoswitched-form to *E*-form. Time development of UV-vis traces is color-coded by blue to green to yellow to red gradient.

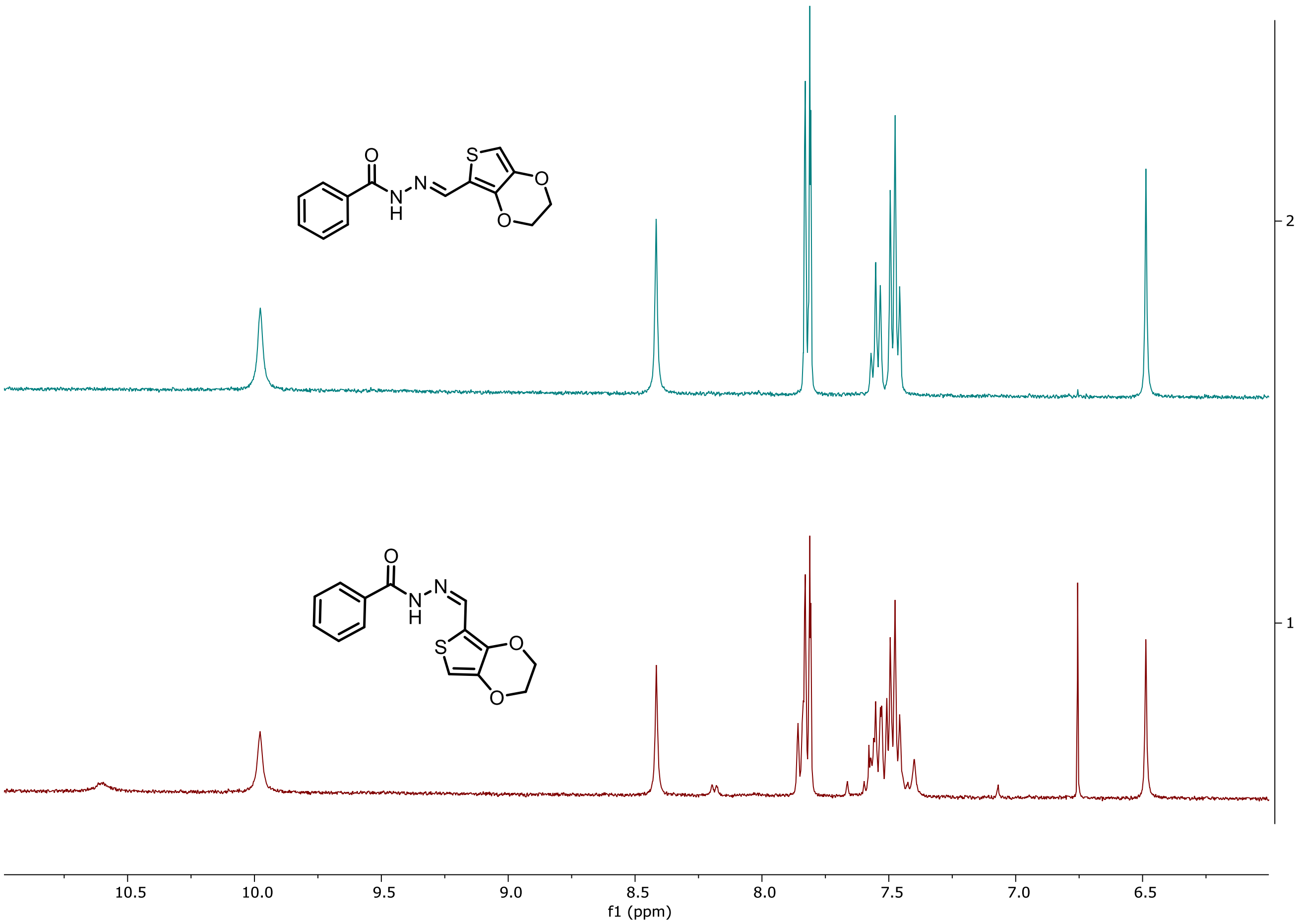

Figure S 14 ^{1}H NMR spectra of non-irradiated **AH4** solution (up) and irradiated **AH4** solution (down). We can observe new set of singlet at 6.75 and a new dublet at 8.18 ppm in comparison with the non-irradiated sample.

3.7 Repeated photoswitching of AH4 in solution

We investigated whether it is possible to repeat the photoisomerization multiple times from *E*-form to photoswitched-form and *vice versa*. The solution of **AH4** in acetonitrile ($1 \cdot 10^{-5}$ M) was irradiated with 330 nm light for 40 minutes and we observed a change in the UV-Vis spectrum associated with isomerization from *E*-form to photoswitched-form. The solution was then irradiated with 400 nm light for 40 minutes and we observed reverse changes in the spectra as compared to irradiation with 330 nm associated with isomerization from photoswitched-form to *E*-form. We repeated photoisomerization 8 times and we observed the same behavior in every cycle. We can clearly confirm that **AH4** undergoes repeated photoisomerization in solution without fatigue or photochemical decomposition (Figure S 15).

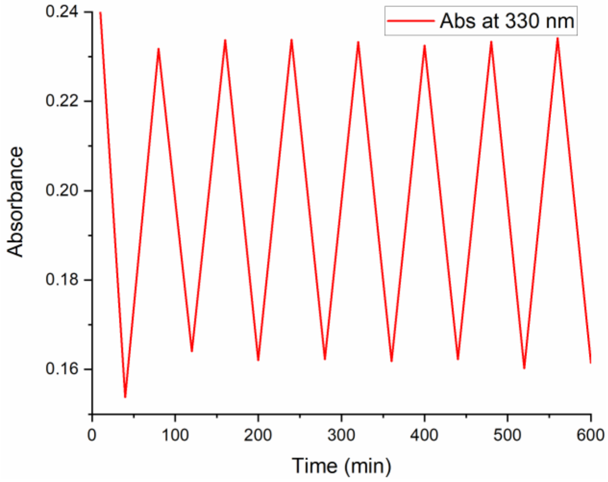

Figure S 15 Absorbance of **AH4** at 330 nm changing periodically as the molecule undergoes repeated photoisomerization cycles.

3.8 Photoswitching of AH5

The UV-Vis spectrum of **AH5** in acetonitrile (1·10^{-5} M) has shown one strong band at around 340 nm and this wavelength was then chosen for irradiation. The solution was irradiated with 340 nm light and simultaneously UV-Vis spectra were obtained every 5 seconds. As seen in Figure S 16, the intensity of the peak at around 340 nm gradually decreases and regions at 250–280 nm and at 400–450 nm increase in intensity, indicating the switching from *E*-form to photoswitched-form.

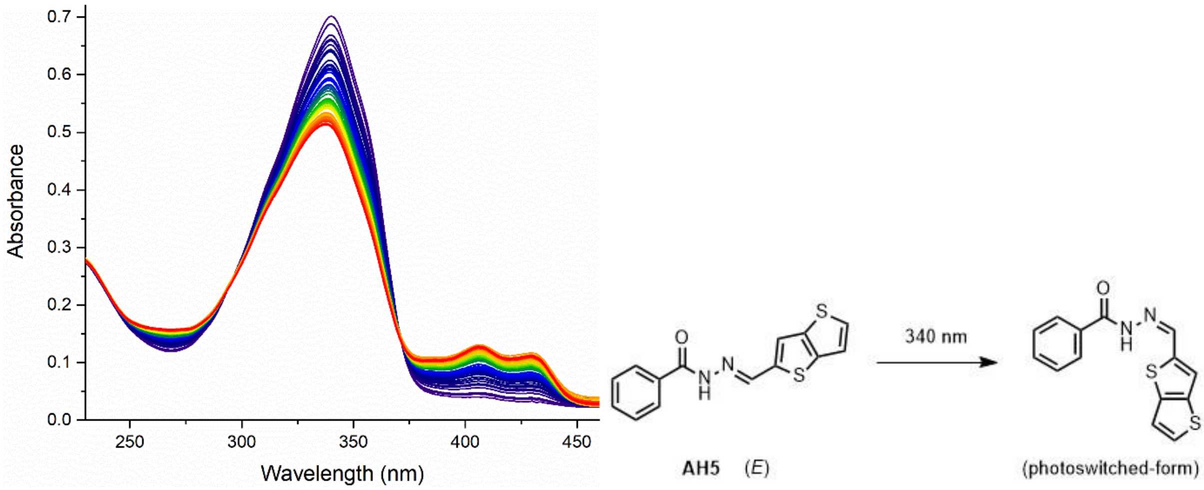

Figure S 16 Photoisomerization of **AH5** from *E*-form to photoswitched-form. Time development of UV-vis traces is color-coded by blue to green to yellow to red gradient.

The irradiation wavelength was set at the most intense peak associated with the photoswitched-form isomer. The solution was irradiated with 405 nm light and simultaneously UV-Vis spectra were obtained every 15 seconds. We have observed reverse changes in the spectra as compared to irradiation with 340 nm, confirming reversible photoswitching of **AH5** from photoswitched-form back to *E*-form (Figure S 17).

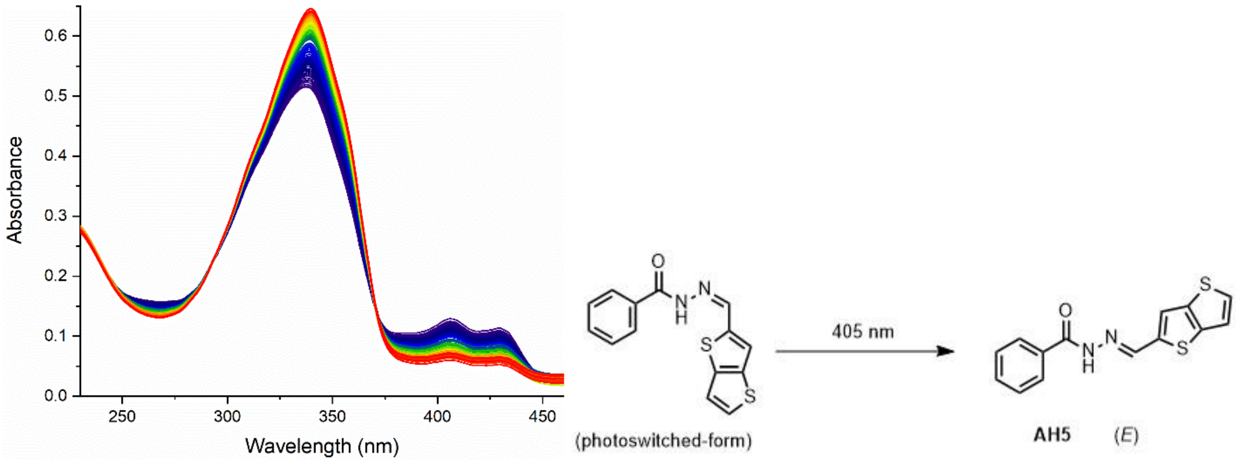

Figure S 17 Photoisomerization of **AH5** from photoswitched-form to *E*-form. Time development of UV-vis traces is color-coded by blue to green to yellow to red gradient.

Photoswitching of **AH5** was also studied by NMR spectroscopy. The solution of **AH5** in deuterated acetonitrile ($1 \cdot 10^{-3}$ M) was irradiated by 340 nm light until the PSS was reached. NMR spectrum shows a new set of signals and the *E*- to photoswitched-form ratio after reaching PSS is 77 to 23.

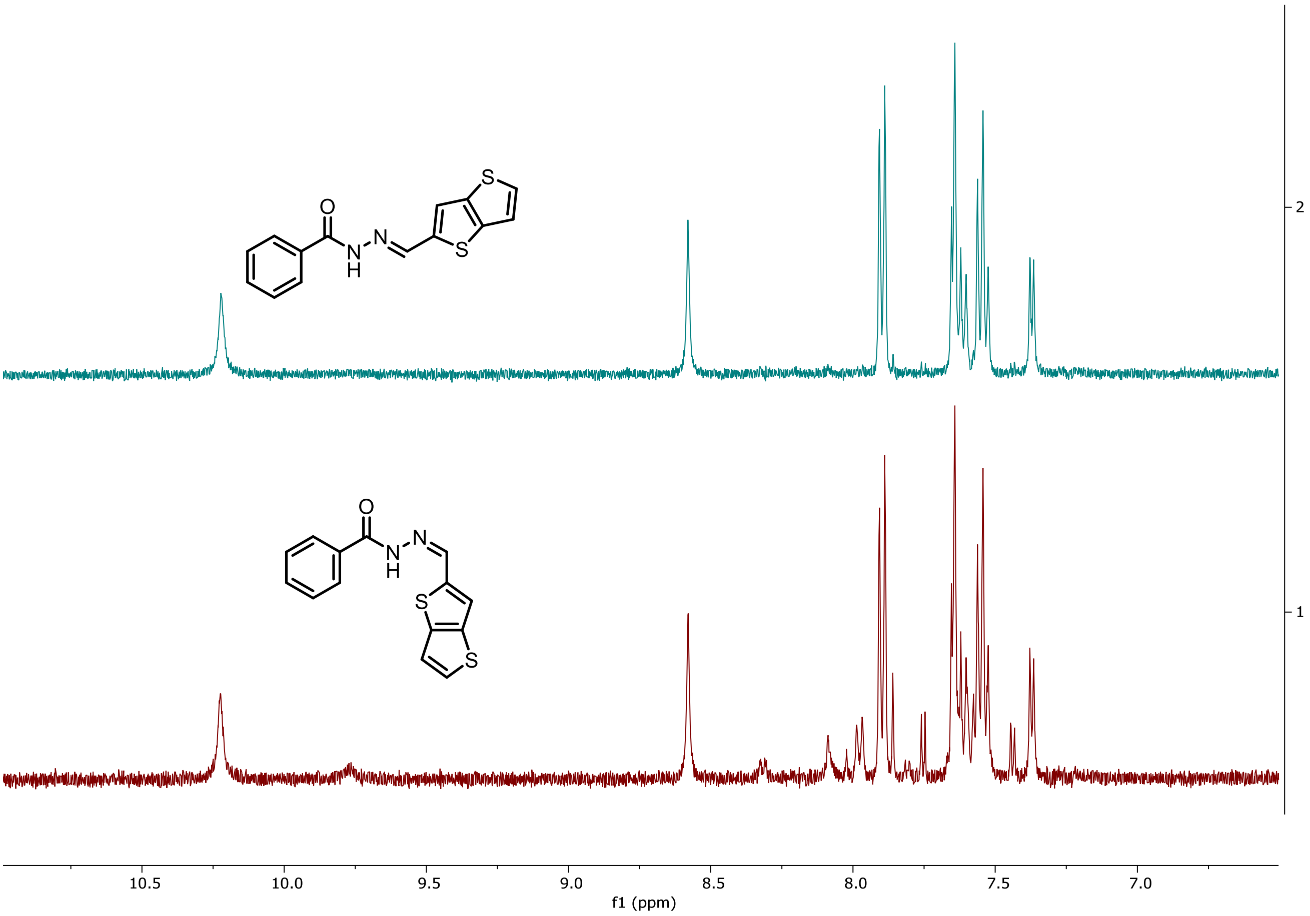

Figure S 18 ^{1}H NMR spectra of non-irradiated **AH5** solution (up) and irradiated **AH5** solution (down). We can observe new set of doublets at 7.44, 7.75 and 7.98 ppm in comparison with the non-irradiated sample.

3.9 Thermal stability of AH5 in solution

We studied the stability of photoswitched-form of **AH5** solution in acetonitrile. The solution was irradiated with 340 nm light to reach PSS and then UV-Vis spectra were acquired over the period of 6 hour. Based on these results (Figure S 19) we calculated the $t_{1/2}$ = 6.42 h, which can be classified as a P-type photoswitch.

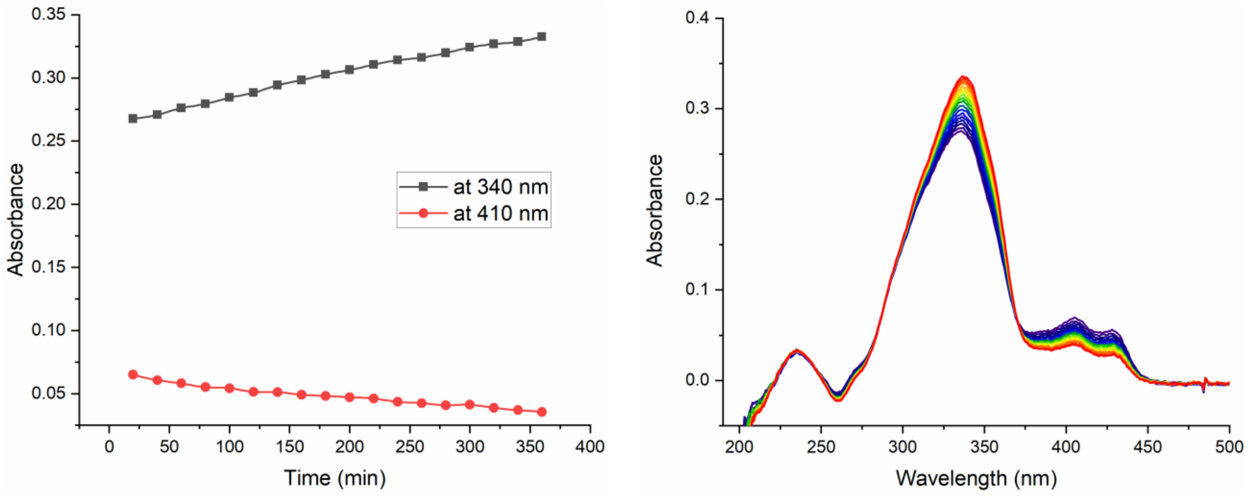

Figure S 19 The change of absorbance at 340 nm and 410 nm over 6 hours.

3.10 Repeated photoswitching of AH5 in solution

We investigated whether it is possible to repeat the photoisomerization multiple times from *E*-form to photoswitched-form and *vice versa*. The solution of **AH5** in acetonitrile ($1\cdot10^{-5}$ M) was irradiated with 340 nm light for 10 minutes and we observed a change in the UV-Vis spectrum associated with isomerization from *E*-form to photoswitched-form. The solution was then irradiated with 405 nm light for 60 minutes and we observed reverse changes in the spectra as compared to irradiation with 340 nm associated with isomerization from photoswitched-form to *E*-form. We repeated photoisomerization 8 times and we observed the same behavior in every cycle. We can clearly confirm that **AH5** undergoes repeated photoisomerization in solution without fatigue or photochemical decomposition (Figure S 20).

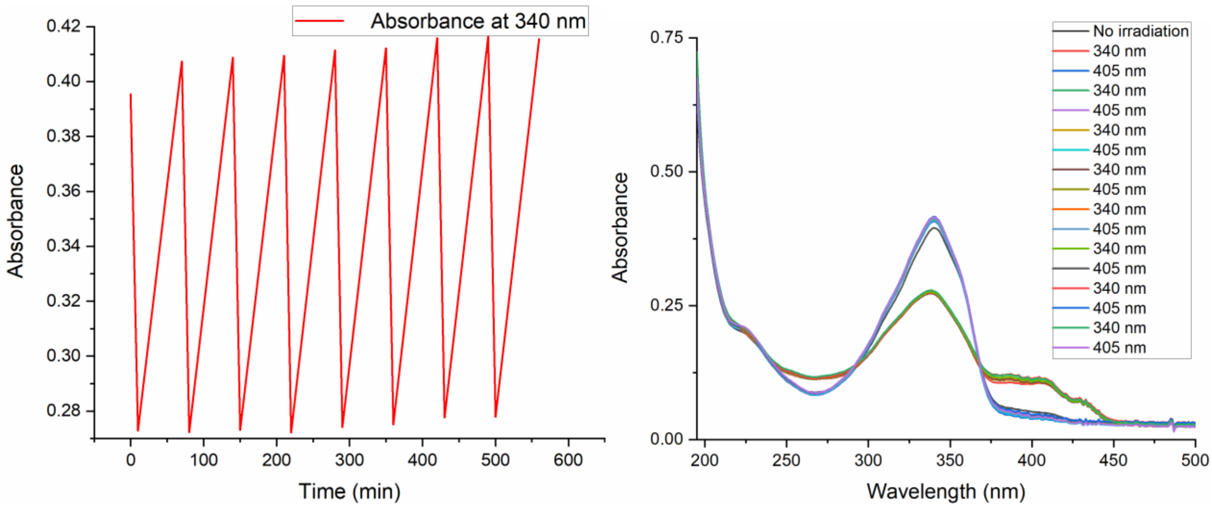

Figure S 20 Absorbance of **AH5** at 340 nm changing periodically as the molecule undergoes repeated photoisomerization cycles.

3.11 Photoswitching of AH6

The UV-Vis spectrum of **AH6** in acetonitrile ($1 \cdot 10^{-5}$ M) has shown one strong band at around 340 nm and this wavelength was then chosen for irradiation. The solution was irradiated with 340 nm light and simultaneously UV-Vis spectra were obtained every 5 seconds. As seen in Figure S 21, the intensity of the peak at around 340 nm gradually decreases and region at 370-430 nm increases in intensity, indicating the switching from *E*-form to photoswitched-form.

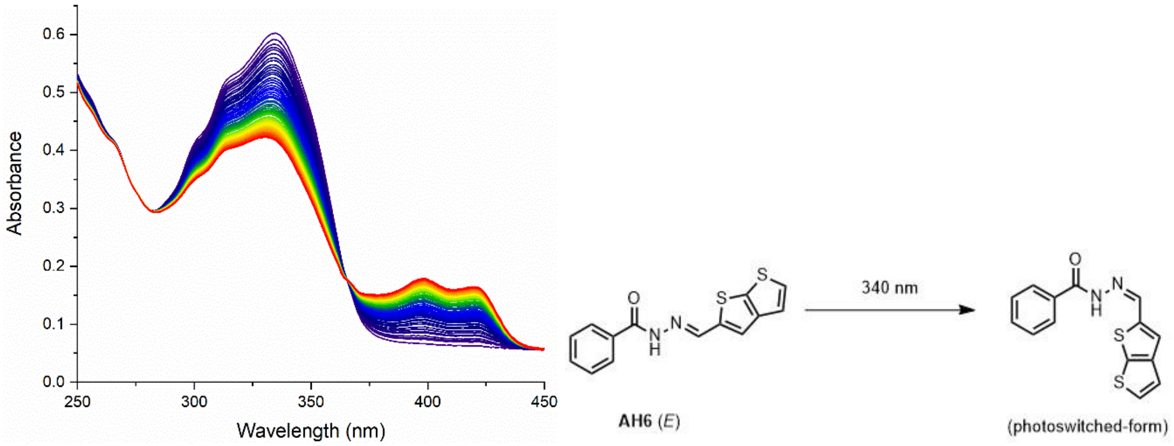

Figure S 21 Photoisomerization of **AH6** from *E*-form to photoswitched-form. Time development of UV-vis traces is color-coded by blue to green to yellow to red gradient. Time development of UV-vis traces is color-coded by blue to green to yellow to red gradient.

The irradiation wavelength was set at the most intense peak associated with the photoswitched-form isomer. The solution was irradiated with 410 nm light and simultaneously UV-Vis spectra were obtained every 15 seconds. We have observed reverse changes in the spectra as compared to irradiation with 340 nm, confirming reversible photoswitching of **AH6** from photoswitched-form back to *E*-form (Figure S 22).

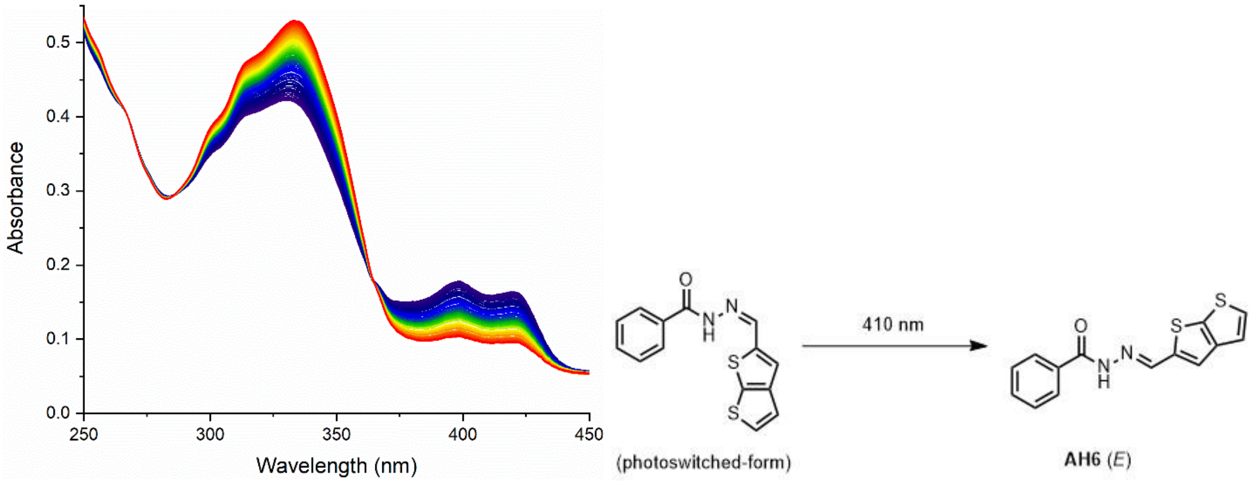

Figure S 22 Photoisomerization of **AH6** from photoswitched-form to *E*-form. Time development of UV-vis traces is color-coded by blue to green to yellow to red gradient.

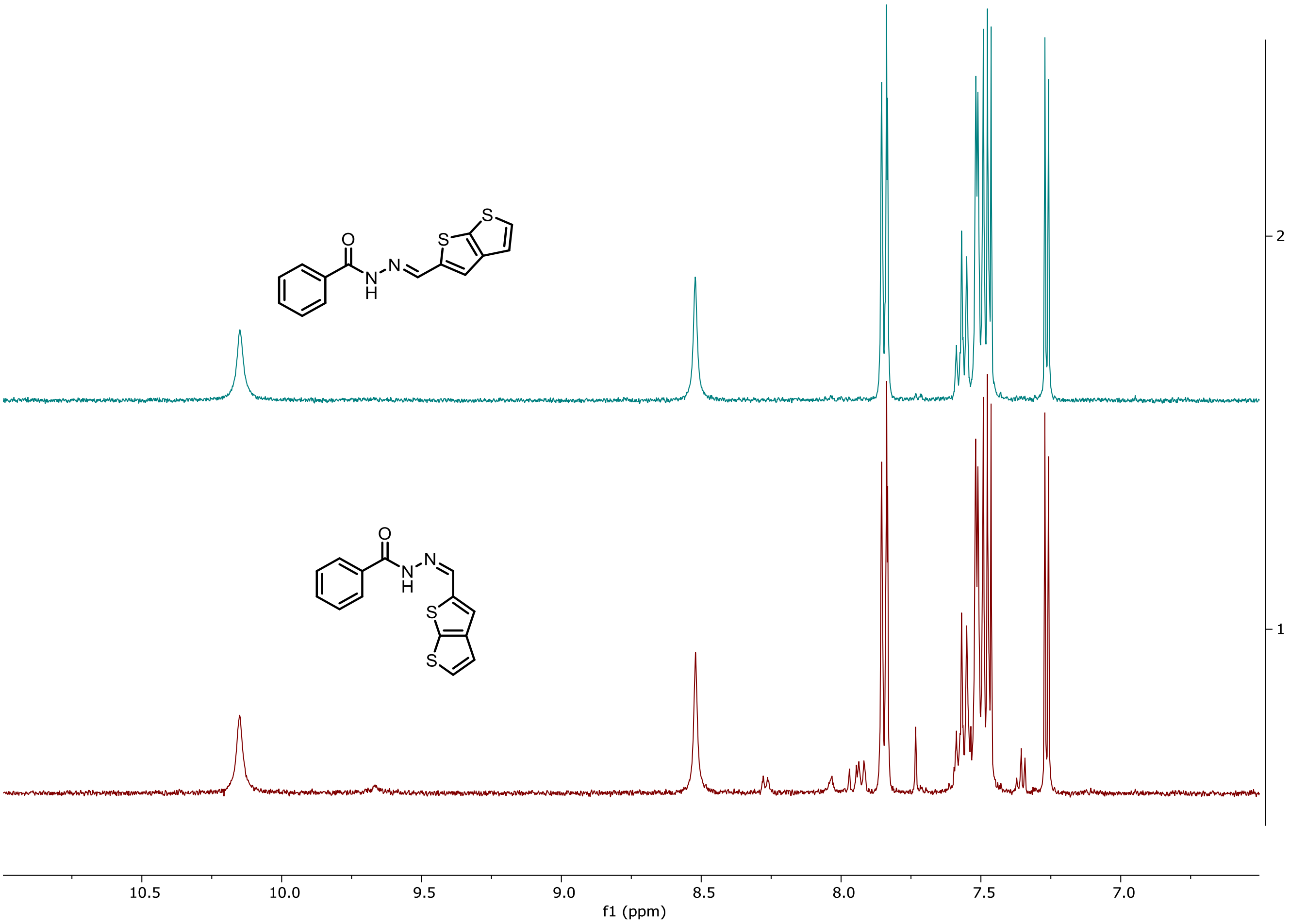

Figure S 23 ^{1}H NMR spectra of non-irradiated **AH6** solution (up) and irradiated **AH6** solution (down). We can observe new set of doublets at 7.35, 7.92 and a singlet at 7.73 ppm in comparison with the non-irradiated sample.

3.12 Repeated photoswitching of AH6 in solution

We investigated whether it is possible to repeat the photoisomerization multiple times from *E*-form to photoswitched-form and *vice versa*. The solution of **AH5** in acetonitrile ($1 \cdot 10^{-5}$ M) was irradiated with 340 nm light for 40 minutes and we observed a change in the UV-Vis spectrum associated with isomerization from *E*-form to photoswitched-form. The solution was then irradiated with 410 nm light for 40 minutes and we observed reverse changes in the spectra as compared to irradiation with 340 nm associated with isomerization from photoswitched-form to *E*-form. We repeated photoisomerization 8 times and we observed the same behavior in every cycle. We can clearly confirm that **AH6** undergoes repeated photoisomerization in solution without fatigue or photochemical decomposition (Figure S 24).

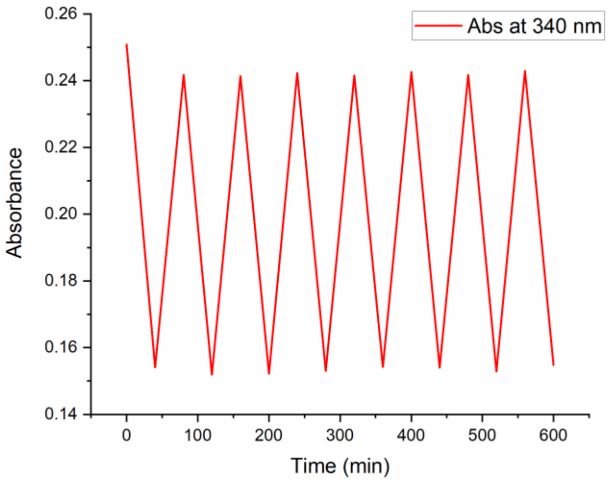

Figure S 24 Absorbance of **AH6** at 340 nm changing periodically as the molecule undergoes repeated photoisomerization cycles.

3.13 Photoswitching of AH7

The UV-Vis spectrum of **AH7** in acetonitrile ($1.5 \cdot 10^{-5}$ M) has shown two strong bands at around 380 nm and this wavelength was then chosen for irradiation. The solution was irradiated with 380 nm light and simultaneously UV-Vis spectra were obtained every 5 seconds. As seen in Figure S 25, the intensity of two peaks at around 380 nm gradually decreases and region at 425–480 nm increase in intensity, indicating the switching from *E*-form to photoswitched-form.

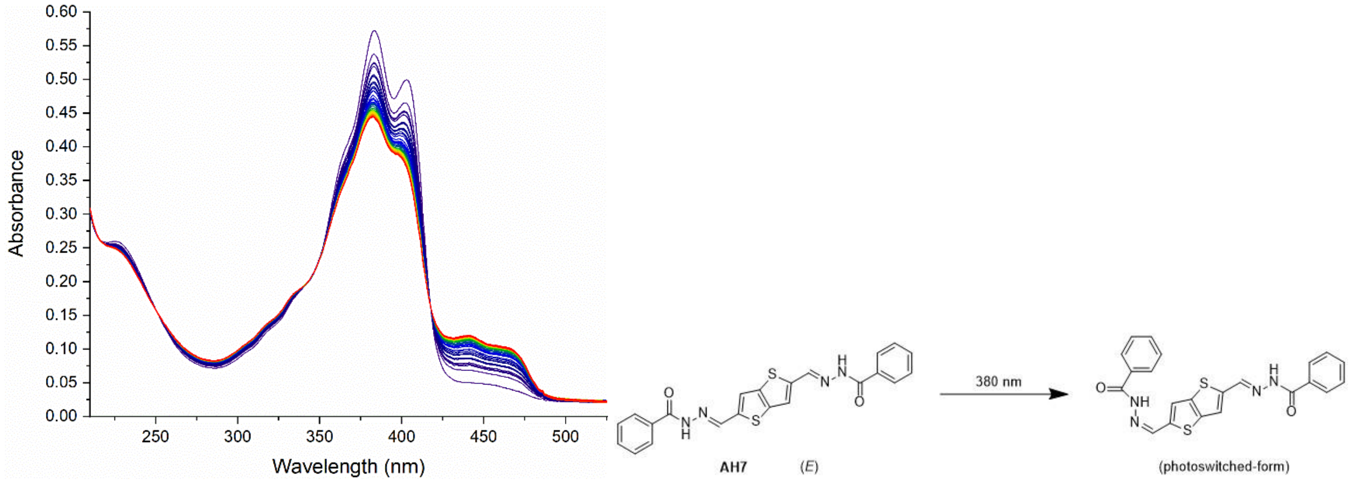

Figure S 25 Photoisomerization of **AH7** from *E*-form to photoswitched-form. Time development of UV-vis traces is color-coded by blue to green to yellow to red gradient.

The irradiation wavelength was set at the most intense peak associated with the photoswitched-form isomer. The solution was irradiated with 442 nm light and simultaneously UV-Vis spectra were obtained every 15 seconds. We have observed reverse changes in the spectra as compared to irradiation with 380 nm, confirming reversible photoswitching of **AH7** from photoswitched-form back to *E*-form (Figure S 26).

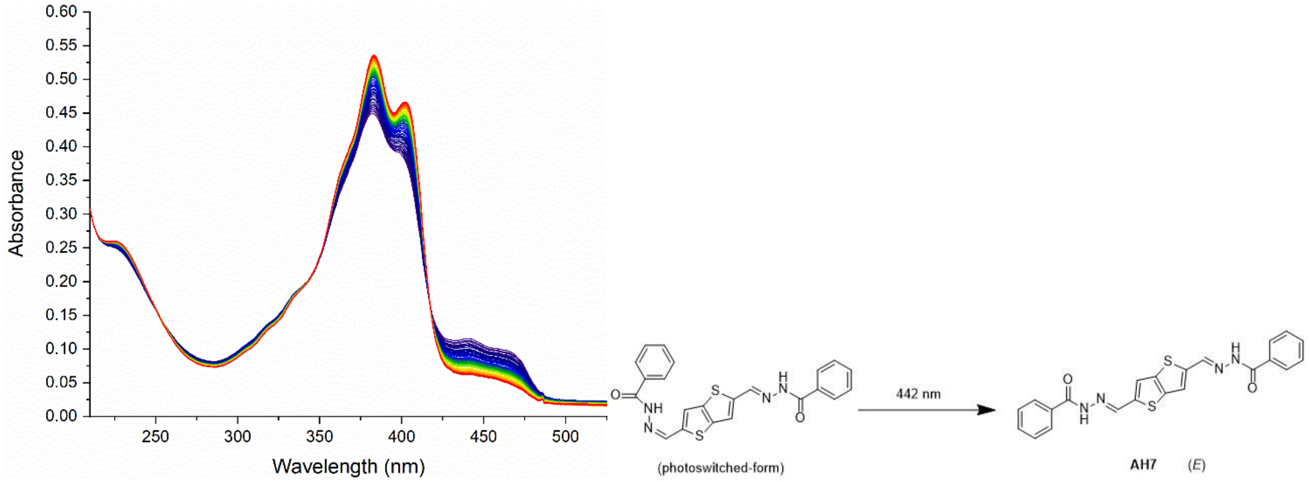

Figure S 26 Photoisomerization of **AH7** from photoswitched-form to *E*-form. Time development of UV-vis traces is color-coded by blue to green to yellow to red gradient.

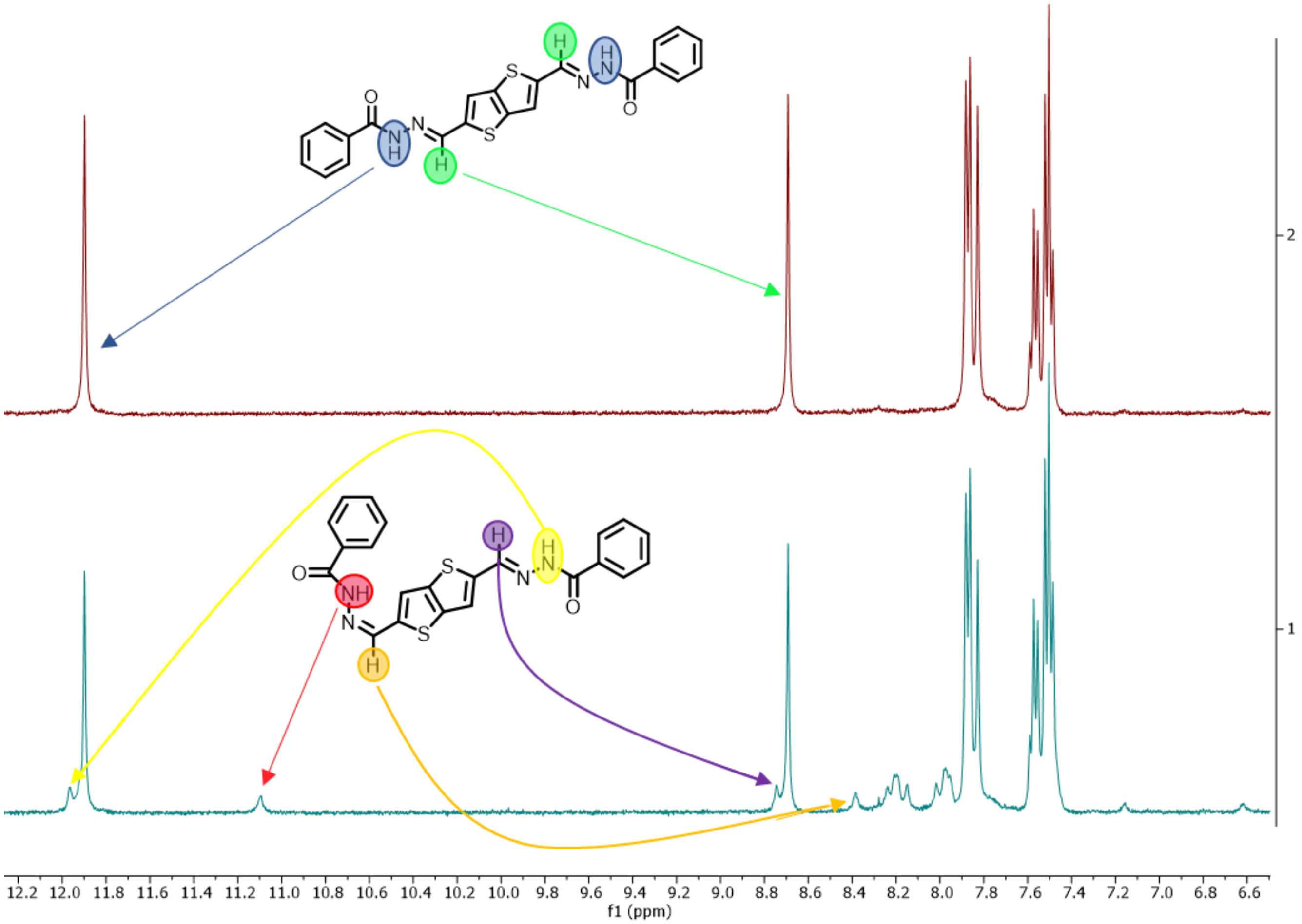

Figure S 27 ^{1}H NMR spectra of non-irradiated **AH7** in solution (up) and irradiated **AH7** in solution (down). We can observe new set of singlets at 11.96, 11.01, 8.74, 8.38 and new multiplets at 8.2 and 7.98 ppm in comparison with the non-irradiated sample suggesting that the photoswitched-form is not symmetric, *i.e.* only one acylhydrazone moiety undergoes photoswitching.

3.14 Repeated photoswitching of AH7 in solution

We investigated whether it is possible to repeat the photoisomerization multiple times from *E*-form to photoswitched-form and *vice versa*. The solution of **AH7** in DMSO ($1{\cdot}10^{-5}$ M) was irradiated with 380 nm light for 40 minutes and we observed a change in the UV-Vis spectrum associated with isomerization from *E*-form to photoswitched-form. The solution was then irradiated with 442 nm light for 120 minutes and we observed reverse changes in the spectra as compared to irradiation with 380 nm associated with isomerization from photoswitched-form to *E*-form. We repeated photoisomerization 8 times and we observed the same behavior in every cycle. We can clearly confirm that **AH9** undergoes repeated photoisomerization in solution without fatigue or photochemical decomposition (Figure S 28).

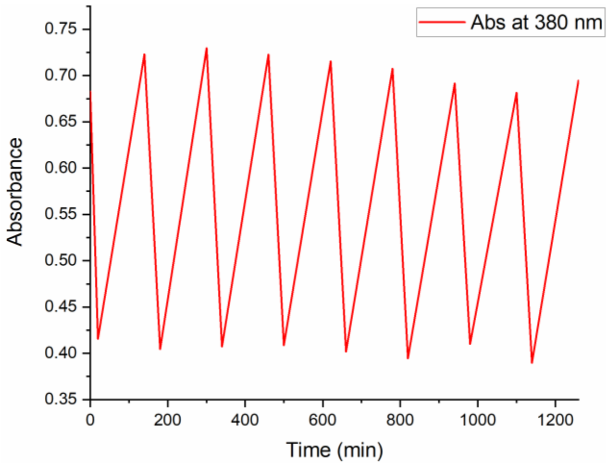

Figure S 28 Absorbance of **AH7** at 380 nm changing periodically as the molecule undergoes repeated photoisomerization cycles.

3.15 Photoswitching of AH8

The UV-Vis spectrum of **AH8** in acetonitrile (5·10^{-5} M) has shown two strong bands at around 320 nm and this wavelength was then chosen for irradiation. The solution was irradiated with 320 nm light and simultaneously UV-Vis spectra were obtained every 5 seconds. As seen in Figure S 29, the intensity of two peaks at around 380 nm gradually decreases and region at 425-480 nm increases in intensity, indicating the switching from *E*-form to photoswitched-form.

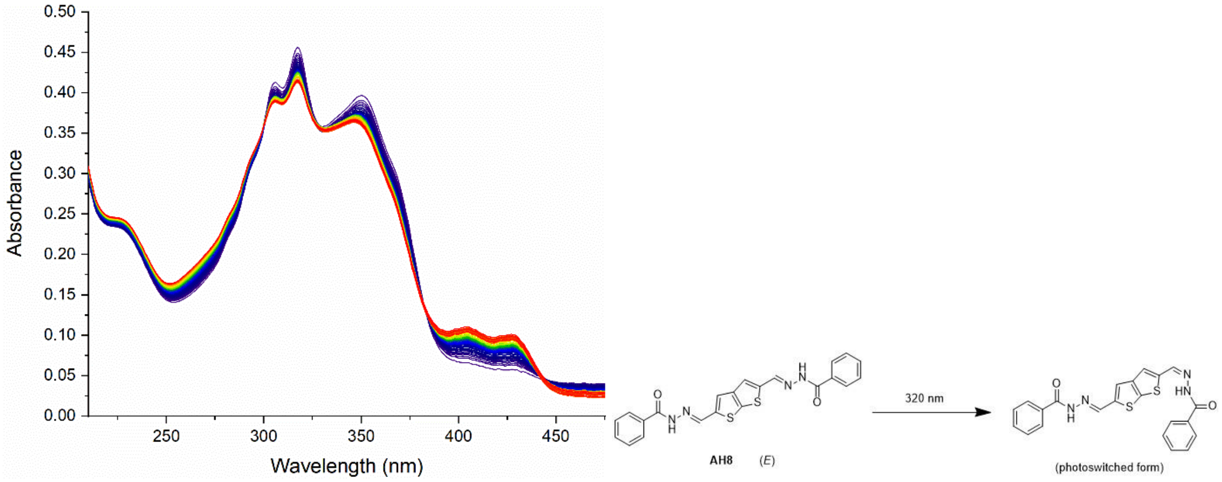

Figure S 29 Photoisomerization of **AH8** from *E*-form to photoswitched-form. Time development of UV-vis traces is color-coded by blue to green to yellow to red gradient.

The irradiation wavelength was set at the most intense peak associated with the photoswitched-form isomer. The solution was irradiated with 405 nm light and simultaneously UV-Vis spectra were obtained every 15 seconds. We have observed reverse changes in the spectra as compared to irradiation with 320 nm, confirming reversible photoswitching of **AH8** from photoswitched-form back to *E*-form (Figure S 30).

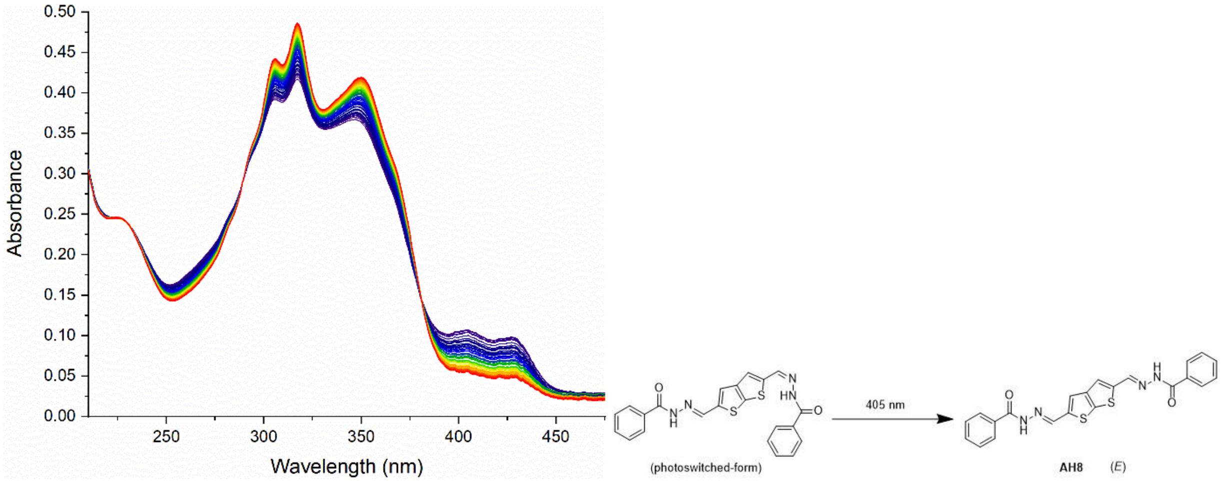

Figure S 30 Photoisomerization of **AH8** from photoswitched-form to *E*-form. Time development of UV-vis traces is color-coded by blue to green to yellow to red gradient.

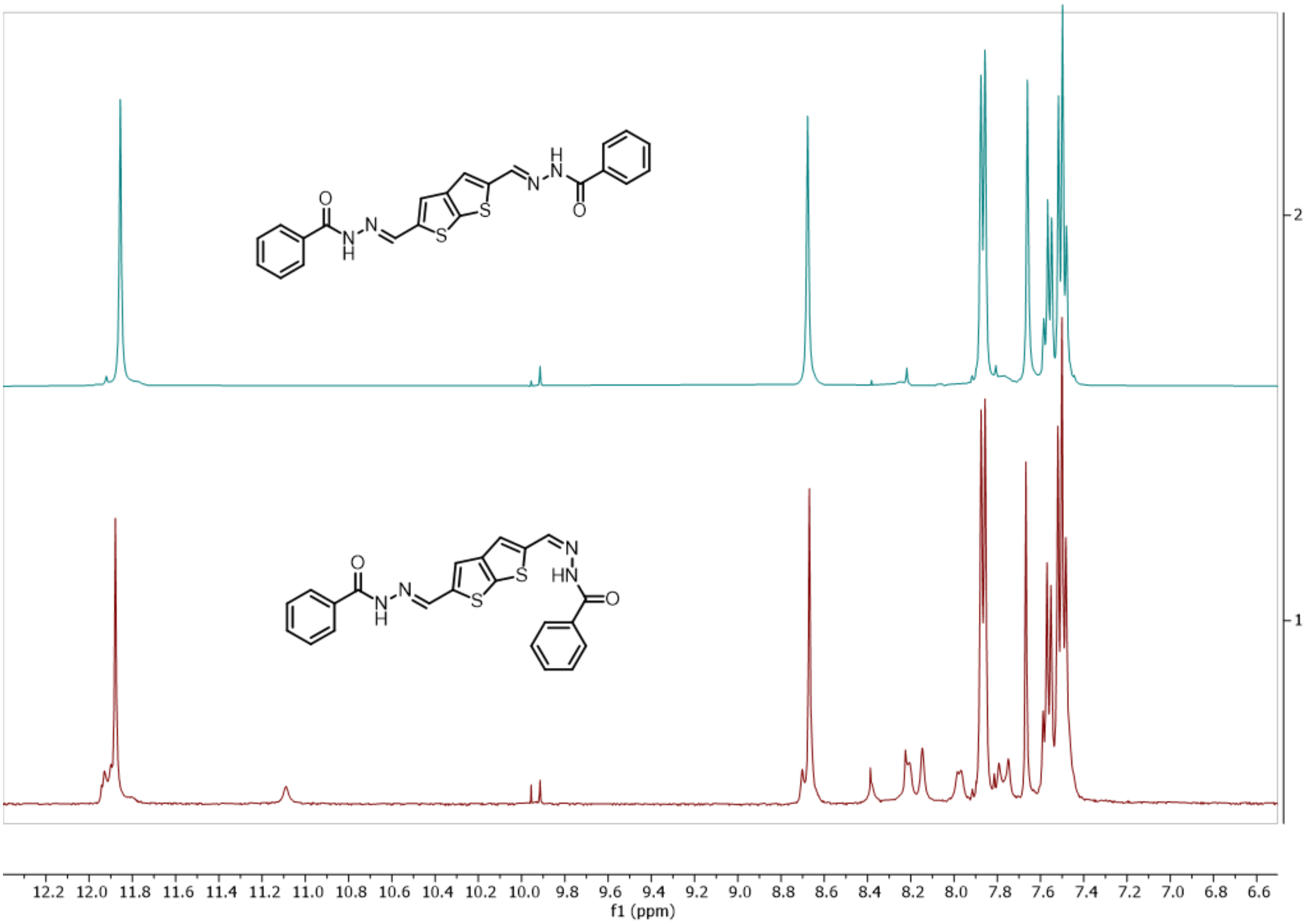

Figure S 31 ^{1}H NMR spectra of non-irradiated **AH8** in solution (up) and irradiated **AH8** in solution (down). We can observe new set of singlets at 11.92, 11.09, 8.70, 8.39 and new multiplets at 8.18 and 7.97 ppm in comparison with the non-irradiated sample suggesting that the photoswitched-form is not symmetric, *i.e.* only one acylhydrazone moiety undergoes photoswitching.

3.16 Repeated photoswitching of AH8 in solution

We investigated whether it is possible to repeat the photoisomerization multiple times from *E*-form to photoswitched-form and *vice versa*. The solution of **AH8** in Acetonitrile ($1\cdot10^{-5}$ M) was irradiated with 320 nm light for 40 minutes and we observed a change in the UV-Vis spectrum associated with isomerization from *E*-form to photoswitched-form. The solution was then irradiated with 405 nm light for 120 minutes and we observed reverse changes in the spectra as compared to irradiation with 320 nm associated with isomerization from photoswitched-form to *E*-form. We repeated photoisomerization 8 times and we observed the same behavior in every cycle. We can clearly confirm that **AH8** undergoes repeated photoisomerization in solution with a small fatigue (Figure S 32). We studied also whether the fatigue would be visible at higher wavelength (Figure S 33) and the fatique was less noticeable at 350 nm.

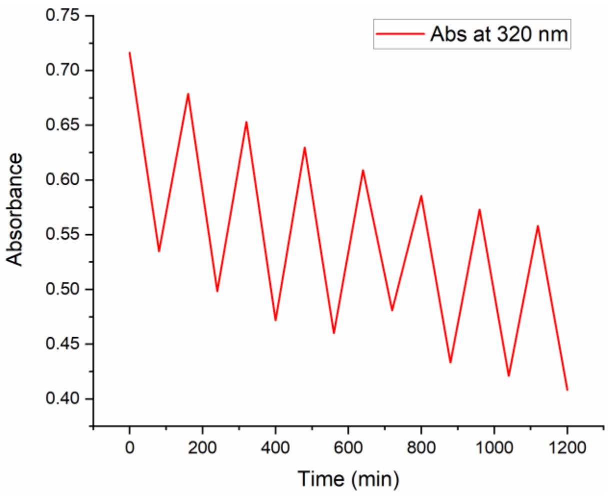

Figure S 32 Absorbance of **AH8** at 320 nm changing periodically as the molecule undergoes repeated photoisomerization cycles.

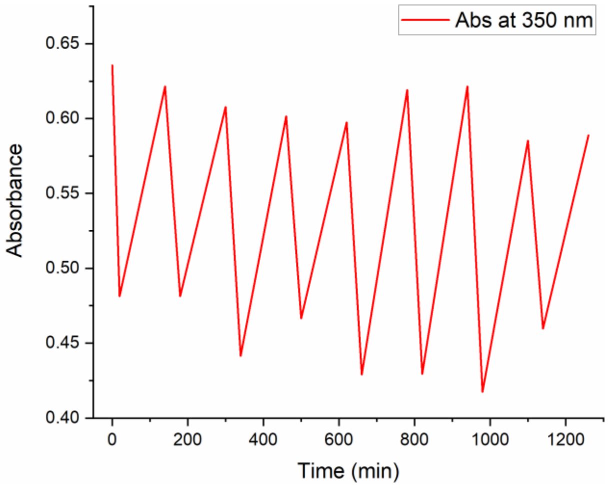

Figure S 33 Absorbance of **AH8** at 350 nm changing periodically as the molecule undergoes repeated photoisomerization cycles.

3.17 Photoswitching of AH9

The UV-Vis spectrum of **AH9** in acetonitrile ($1\cdot10^{-5}$ M) has shown one strong band at around 395 nm and this wavelength was then chosen for irradiation. The solution was irradiated with 395 nm light and simultaneously UV-Vis spectra were obtained every 5 seconds. As seen in Figure S 34, the intensity of the peak at around 395 nm gradually decreases and region at 420-490nm increases in intensity, indicating the switching from *E*-form to photoswitched-form.

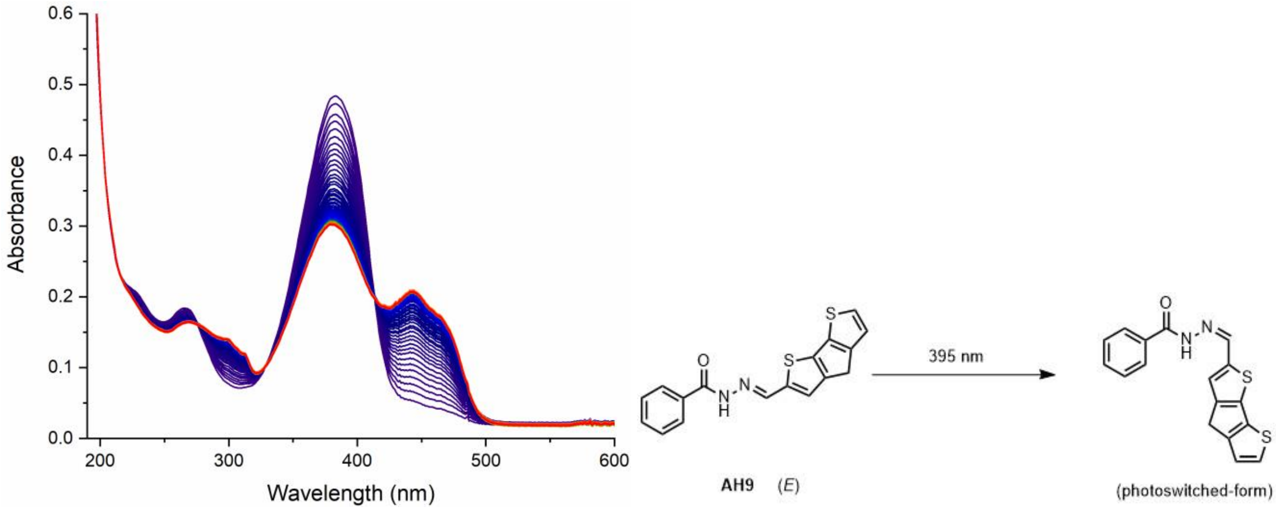

Figure S 34 Photoisomerization of **AH9** from *E*-form to photoswitched-form. Time development of UV-vis traces is color-coded by blue to green to yellow to red gradient.

The irradiation wavelength was set at the most intense peak associated with the photoswitched-form isomer. The solution was irradiated with 445 nm light and simultaneously UV-Vis spectra were obtained every 10 seconds. We have observed reverse changes in the spectra as compared to irradiation with 395 nm, clearly confirming reversible photoswitching of **AH9** from photoswitched-form back to *E*-form (Figure S 35)

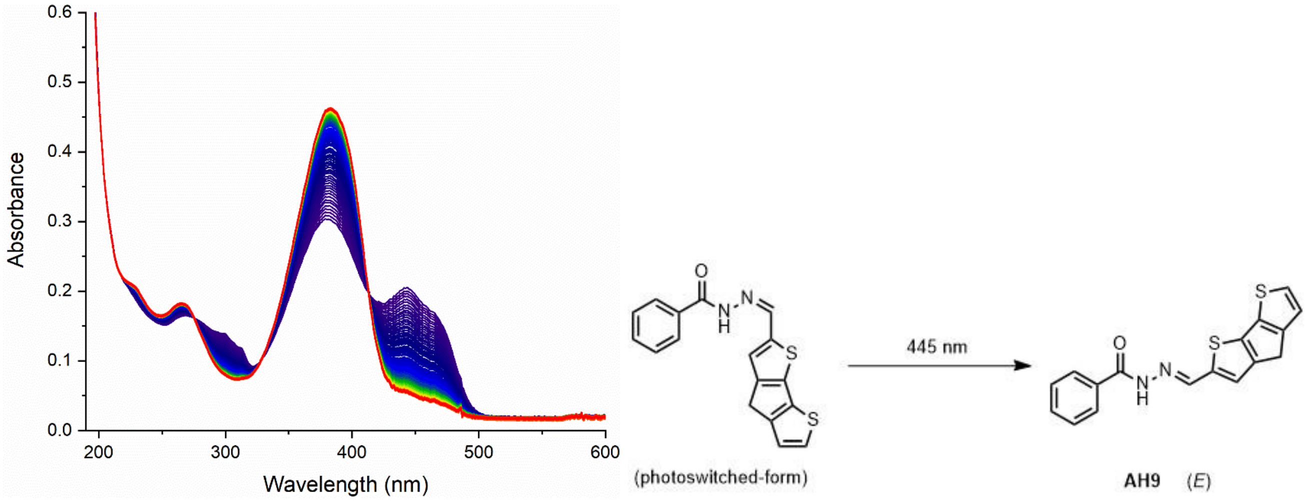

Figure S 35 Photoisomerization of **AH9** from photoswitched-form to *E*-form. Time development of UV-vis traces is color-coded by blue to green to yellow to red gradient.

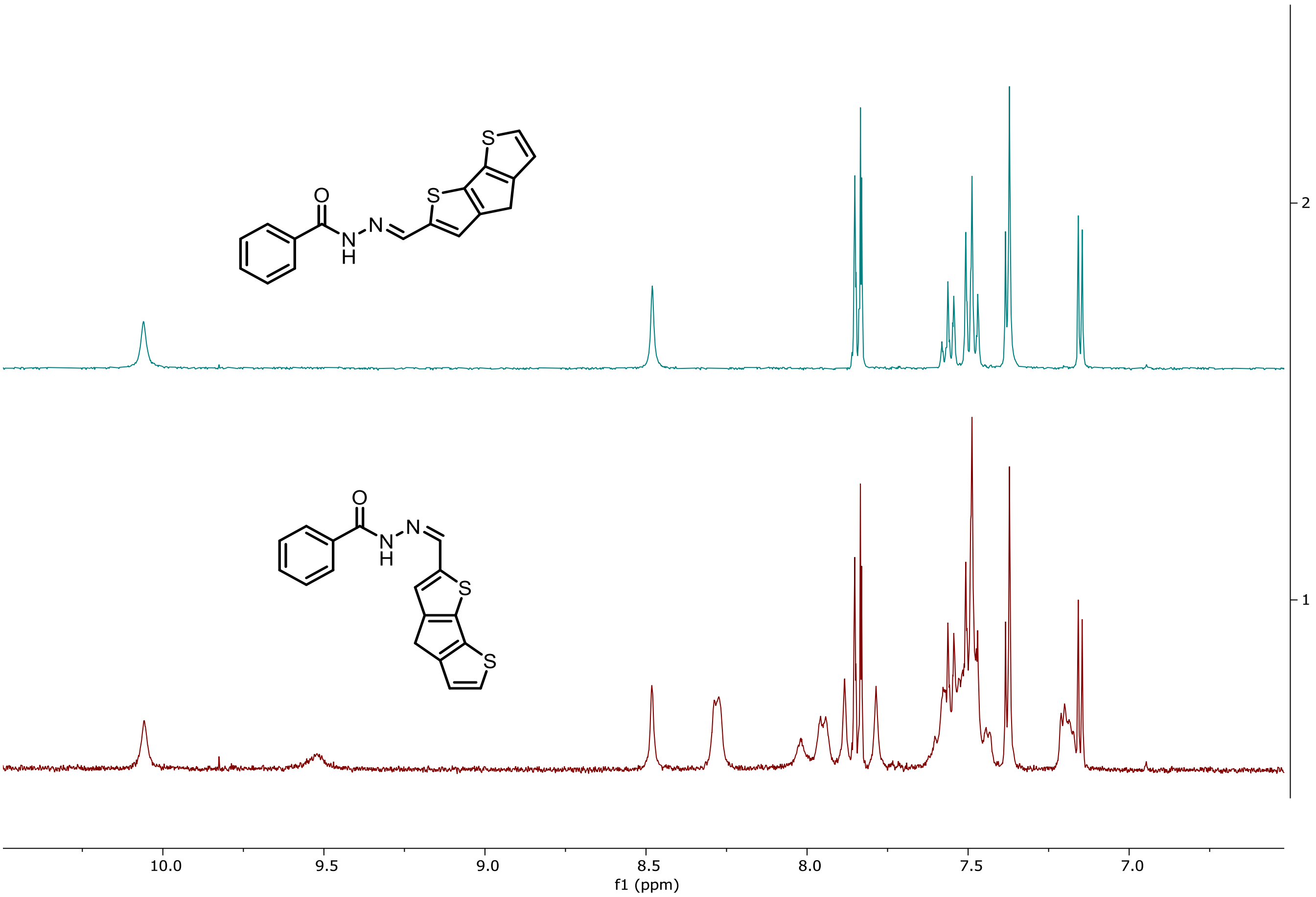

Figure S 36 ^{1}H NMR spectra of non-irradiated **AH9** in solution (up) and irradiated **AH9** in solution (down). We can observe new set of singlets at 7.2, 7.44, 7.79, 7.88, 11.96, 11.01, 8.74, 8.38 and new multiplets at 8.2 and 7.98 ppm in comparison with the non-irradiated.

3.18 Repeated photoswitching of AH9 in solution

We investigated whether it is possible to repeat the photoisomerization multiple times from *E*-form to photoswitched-form and *vice versa*. The solution of **AH9** in Acetonitrile ($1\cdot10^{-5}$ M) was irradiated with 395 nm light for 40 minutes and we observed a change in the UV-Vis spectrum associated with isomerization from *E*-form to photoswitched-form. The solution was then irradiated with 442 nm light for 120 minutes and we observed reverse changes in the spectra as compared to irradiation with 395 nm associated with isomerization from photoswitched-form to *E*-form. We repeated photoisomerization 8 times and we observed the same behavior in every cycle. We can clearly confirm that **AH9** undergoes repeated photoisomerization in solution without fatigue or photochemical decomposition (Figure S 37).

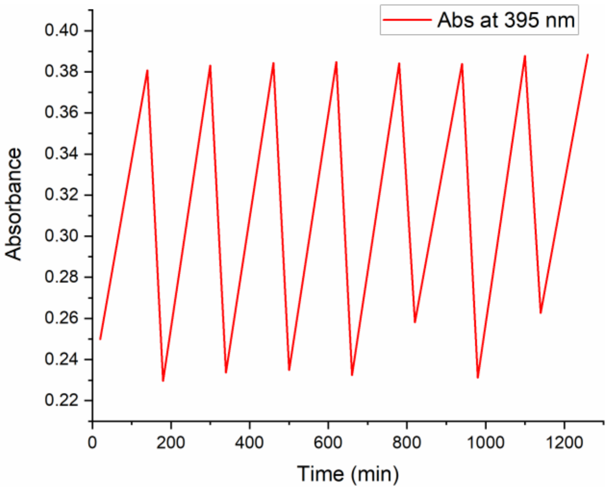

Figure S 37 Absorbance of **AH9** at 395 nm changing periodically as the molecule undergoes repeated photoisomerization cycles.

3.19 Photoswitching of the DAE-2AH1

The UV-Vis spectrum of **DAE-2AH1** in DMF ($1\cdot10^{-5}$ M) has shown one strong band at around 340 nm and this wavelength was then chosen for irradiation. The solution was irradiated with 340 nm light and simultaneously UV-Vis spectra were obtained every 3 seconds. As seen in Figure S 38, the intensity of the peak at around 340 nm gradually decreases and regions at 360-430nm and 485-630 increase in intensity, indicating the switching from *E*-open-form to photoswitched-form at both DAE and AH sites.

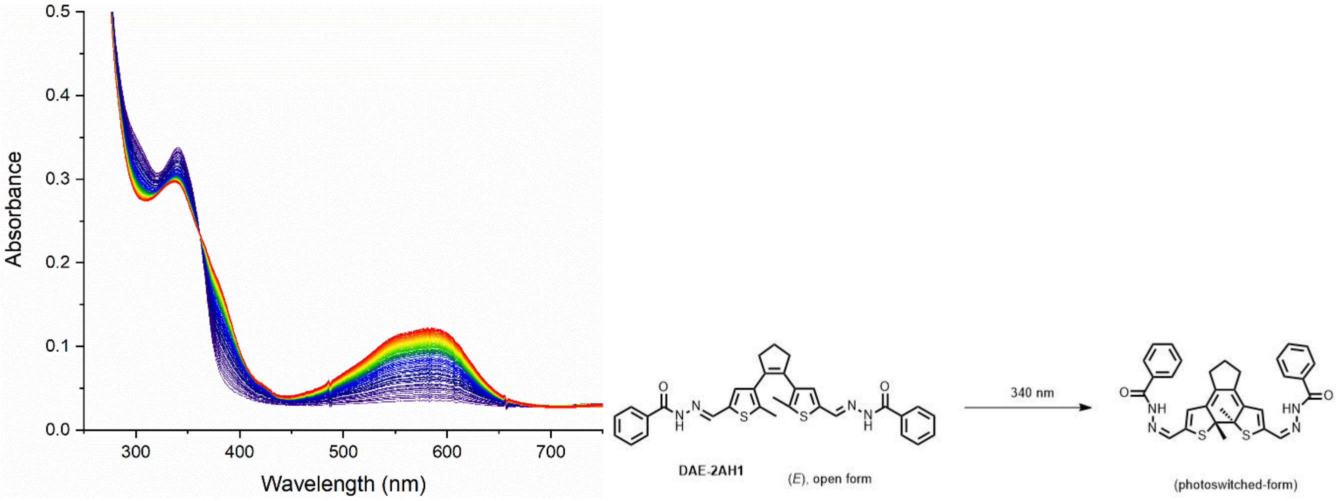

Figure S 38 Photoisomerization of **DAE-2AH1** from (*E*)-open-form to photoswitched-form. Time development of UV-vis traces is color-coded by blue to green to yellow to red gradient.

The irradiation wavelength was set at the most intense peak associated with the DAE cyclization. The solution was irradiated with 575 nm light and simultaneously UV-Vis spectra were obtained every 540 seconds. We have observed reverse changes in the spectra as compared to irradiation with 340 nm, confirming reversible photoswitching of **DAE-2AH1** from the photoswitched-form back to *E*-open-form (Figure S 39).

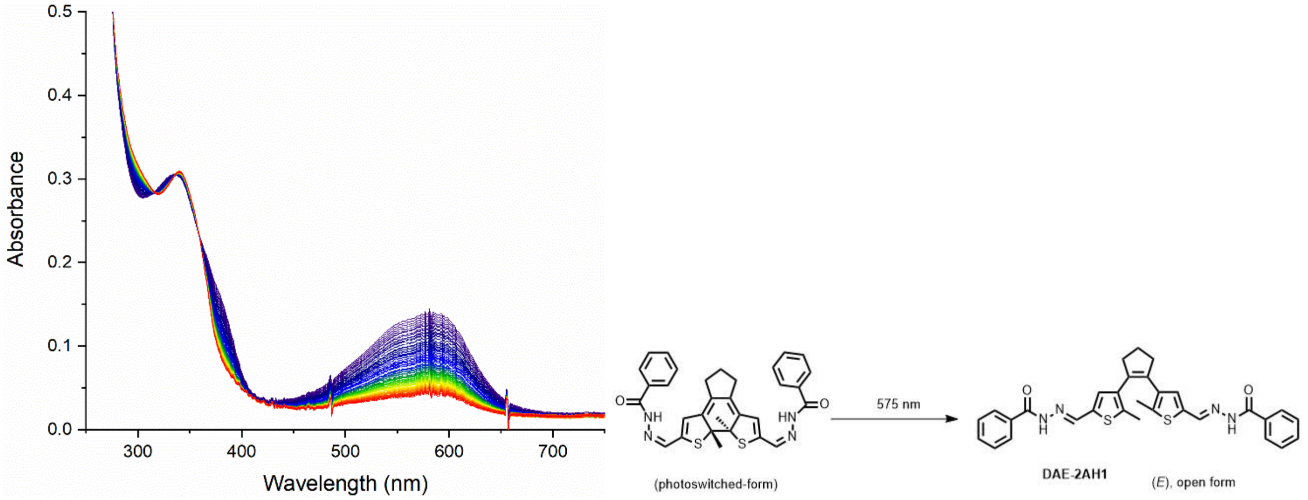

Figure S 39 Photoisomerization of **DAE-2AH1** from photoswitched-form to *E*- open form. Time development of UV-vis traces is color-coded by blue to green to yellow to red gradient.

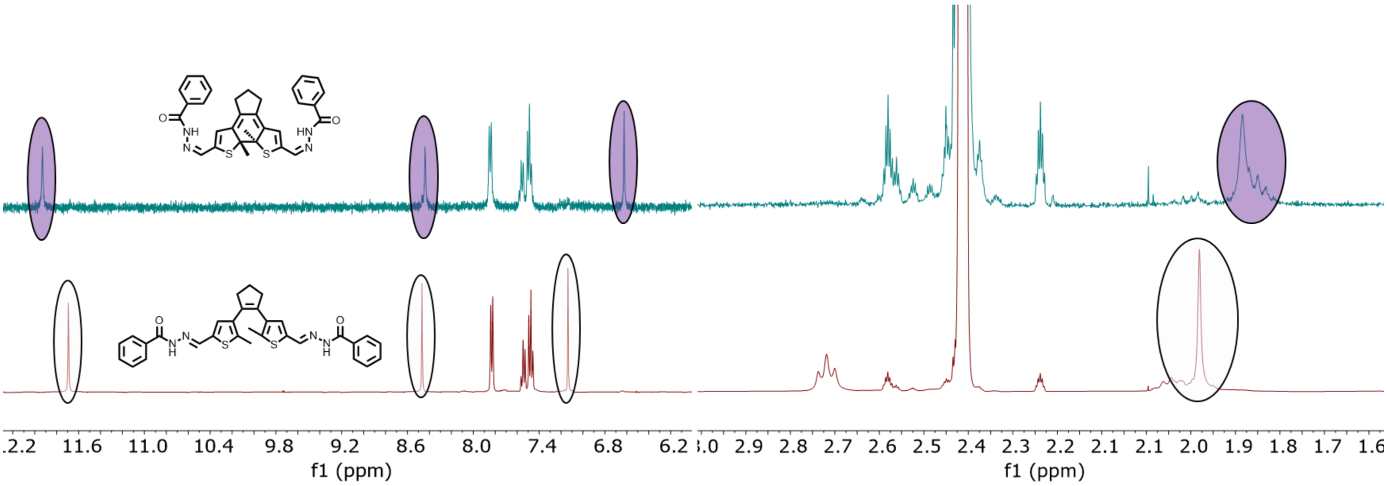

Figure S 40 Photoswitching of DAE-2AH1 observed by NMR. Complete transformation into photoswitched-form was observed.

4 QUANTUM YIELDS

4.1 Actinometry

We determined the intensity of the light at the irradiation wavelength (340 nm) by actinometry using potassium ferrioxalate solution.[9,10] Fresh solutions of potassium ferrioxalate (0.006 M in 0.05 M H_2SO_4) and phenanthroline 0.1 wt% in 0.5 M H_2SO_4/1.6 M sodium acetate were prepared. We prepared two quartz cuvettes, each containing 3 mL of the freshly prepared ferrioxalate solution. One cuvette was kept in dark while the other was irradiated for 60 s. Stirring was provided by a small stirring bar and a magnetic stirrer under the cuvette not interfering with the irradiation path that was from the side of the cuvette. When irradiation was over, we added 0.5 mL of the prepared phenanthroline buffered solution both to the irradiated cuvette and to the reference cuvette kept in the dark, and for both cuvettes the absorbance at 510 nm was recorded.

We calculated the light intensity from the following equation

$$I_0 = \frac{\Delta A^{510nm}}{\Delta t \cdot 1000 \cdot \Phi^{340nm} \cdot \varepsilon^{510nm}} \cdot \frac{3.5\ mL}{3\ mL}$$

where ΔA^{510nm} is the difference in absorbance measured at 510 nm between the irradiated sample and the reference kept in dark (0.215), Δt is the irradiation time (60 s), Φ^{340nm} is the quantum yield of ferrous ion production at 340 nm (1.24), ε^{510nm} is the molar extinction coefficient of the phenanthroline complex at 510 nm (11100 L mol^{-1} cm^{-1}). With this experiment, we calculated the intensity of the light at 340 nm to be 3.04×10^{-10} E s^{-1} cm^{-3}. We also measured the power at the same wavelength using a power meter (Thorlabs: Compact Power and Energy Meter Console, model PM100D, equipped with a Slim Photodiode Power Sensor, UV-Extended Si, 200 - 1100 nm, model S130VC) and compared the power obtained by the two methods after converting to the same units using the equation:

$$P = I_0 \cdot h \cdot N_A \cdot \nu \cdot V$$

where P is the power (in W), I_0 is the intensity of the irradiating light calculated from actinometry (3.03593×10^{-10} E s^{-1} cm^{-3}), *h* is the Plank constant (6.63×10^{-34} J s), N_A is the Avogadro constant (6.022×10^{23} mol^{-1}), ν is the frequency of the light used (8.817×10^{14} s^{-1}), and V is the irradiated volume (3 cm^3). Results of actinometry and power meter were consistent within 5 % uncertainty interval, therefore power meter was used in further studies to measure the photon flux during the photoswitching experiment.

4.2 Quantum yield determination for AH1

Then we calculated the quantum yield of the conversion using the following equation[8]

$$\Phi_{E\to Z}^{317nm} = \frac{dA^{317nm}}{dt} \cdot \frac{1}{1000 \cdot I_0 \cdot \varepsilon_E^{317nm} \cdot (1 - 10^{-A^{317nm}})}$$

where dA^{317nm}/dt is the difference in absorbance over the irradiation time, *i.e.* the rate of absorbance change, considering only the part when the conversion of *E* to *Z* is below 5% (0.00124); I_0 is the intensity of the light source calculated from the actinometry experiment (2.07×10^{-10} E s^{-1} cm^{-3}, 163 μW), ε_E^{317nm} is the molar extinction coefficient of the pure *E* isomer at 317 nm (30647 L mol^{-1} cm^{-1}) and A^{317nm} is the total absorption at 317 nm (0.30647). From this we calculate that Φ (*E*→*Z*) at 317nm is 0.39.

4.3 Quantum yield determination for AH3

Then we calculated the quantum yield of the conversion using the following equation[8]

$$\Phi_{E\to Z}^{325nm} = \frac{dA^{325nm}}{dt} \cdot \frac{1}{1000 \cdot I_0 \cdot \varepsilon_E^{325nm} \cdot (1 - 10^{-A^{325nm}})}$$

where dA^{325nm}/dt is the difference in absorbance over the irradiation time, *i.e.* the rate of absorbance change, considering only the part when the conversion of *E* to *Z* is below 5% (0.00124); I_0 is the intensity of the light source calculated from the actinometry experiment (2.07×10^{-10} E s^{-1} cm^{-3}, 161 μW), ε_E^{325nm} is the molar extinction coefficient of the pure *E* isomer at 325 nm (44492 L mol^{-1} cm^{-1}) and A^{325nm} is the total absorption at 325 nm (0.44492). From this we calculate that Φ (*E*→*Z*) at 317nm is 0.38.

4.4 Quantum yield determination for AH4

Then we calculated the quantum yield of the conversion using the following equation[8]

$$\Phi_{E\to Z}^{330nm} = \frac{dA^{330nm}}{dt} \cdot \frac{1}{1000 \cdot I_0 \cdot \varepsilon_E^{330nm} \cdot (1 - 10^{-A^{330nm}})}$$

where dA^{330nm}/dt is the difference in absorbance over the irradiation time, *i.e.* the rate of absorbance change, considering only the part when the conversion of *E* to *Z* is below 5% (0.00124); I_0 is the intensity of the light source calculated from the actinometry experiment (2.07×10^{-10} E s^{-1} cm^{-3}, 186 µW), ε_E^{330nm} is the molar extinction coefficient of the pure *E* isomer at 330 nm (27668 L mol^{-1} cm^{-1}) and A^{330nm} is the total absorption at 330 nm (0.2767). From this we calculate that Φ (*E*→*Z*) at 330 nm is 0.42.

4.5 Quantum yield determination for AH5

Then we calculated the quantum yield of the conversion using the following equation[8]

$$\Phi_{E\to Z}^{340nm} = \frac{dA^{340nm}}{dt} \cdot \frac{1}{1000 \cdot I_0 \cdot \varepsilon_E^{340nm} \cdot (1 - 10^{-A^{340nm}})}$$

where dA^{340nm}/dt is the difference in absorbance over the irradiation time, *i.e.* the rate of absorbance change, considering only the part when the conversion of *E* to *Z* is below 5% (0.00124); I_0 is the intensity of the light source calculated from the actinometry experiment (2.07×10^{-10} E s^{-1} cm^{-3}, 240 µW), ε_E^{340nm} is the molar extinction coefficient of the pure *E* isomer at 340 nm (33000 L mol^{-1} cm^{-1}) and A^{340nm} is the total absorption at 340 nm (0.3304). From this we calculate that Φ (*E*→*Z*) at 340nm is 0.35.

4.6 Quantum yield determination for AH6

Then we calculated the quantum yield of the conversion using the following equation[8]

$$\Phi_{E\to Z}^{340nm} = \frac{dA^{340nm}}{dt} \cdot \frac{1}{1000 \cdot I_0 \cdot \varepsilon_E^{340nm} \cdot (1 - 10^{-A^{340nm}})}$$

where dA^{340nm}/dt is the difference in absorbance over the irradiation time, *i.e.* the rate of absorbance change, considering only the part when the conversion of *E* to *Z* is below 5% (0.00124); I_0 is the intensity of the light source calculated from the actinometry experiment (2.07×10^{-10} E s^{-1} cm^{-3}, 178 µW), ε_E^{340nm} is the molar extinction coefficient of the pure *E* isomer at 340 nm (25369 L mol^{-1} cm^{-1}) and A^{340nm} is the total absorption at 340 nm (0.2537). From this we calculate that Φ (*E*→*Z*) at 340nm is 0.58.

4.7 Quantum yield determination for AH7

Then we calculated the quantum yield of the conversion using the following equation[8]

$$\Phi_{E\to Z}^{380nm} = \frac{dA^{380nm}}{dt} \cdot \frac{1}{1000 \cdot I_0 \cdot \varepsilon_E^{380nm} \cdot (1 - 10^{-A^{380nm}})}$$

where dA^{380nm}/dt is the difference in absorbance over the irradiation time, *i.e.* the rate of absorbance change, considering only the part when the conversion of *E* to *Z* is below 5% (0.00124); I_0 is the intensity of the light source calculated from the actinometry experiment (2.07×10^{-10} E s^{-1} cm^{-3}, 222 µW), ε_E^{380nm} is the molar extinction coefficient of the pure *E* isomer at 380 nm (68856 L mol^{-1} cm^{-1}) and A^{380nm} is the total absorption at 380 nm (0.6886). From this we calculate that Φ (*E*→*Z*) at 380nm is 0.45.

4.8 Quantum yield determination for AH8

Then we calculated the quantum yield of the conversion using the following equation[8]

$$\Phi_{E\to Z}^{320nm} = \frac{dA^{320nm}}{dt} \cdot \frac{1}{1000 \cdot I_0 \cdot \varepsilon_E^{320nm} \cdot (1 - 10^{-A^{320nm}})}$$

where dA^{320nm}/dt is the difference in absorbance over the irradiation time, *i.e.* the rate of absorbance change, considering only the part when the conversion of *E* to *Z* is below 5% (0.00124); I_0 is the intensity of the light source calculated from the actinometry experiment (2.07 x 10^{-10} E s^{-1} cm^{-3}, 163 µW), ε_E^{320nm} is the molar extinction coefficient of the pure *E* isomer at 320 nm (69493 L mol^{-1} cm^{-1}) and A^{320nm} is the total absorption at 320 nm (0.6949). From this we calculate that Φ (*E*→*Z*) at 320nm is 0.28.

4.9 Quantum yield determination for AH9

Then we calculated the quantum yield of the conversion using the following equation[8]

$$\Phi_{E\to Z}^{395nm} = \frac{dA^{395nm}}{dt} \cdot \frac{1}{1000 \cdot I_0 \cdot \varepsilon_E^{395nm} \cdot (1 - 10^{-A^{395nm}})}$$

where dA^{395nm}/dt is the difference in absorbance over the irradiation time, *i.e.* the rate of absorbance change, considering only the part when the conversion of *E* to *Z* is below 5% (0.00124); I_0 is the intensity of the light source calculated from the actinometry experiment (2.07 x 10^{-10} E s^{-1} cm^{-3}, 244 µW), ε_E^{395nm} is the molar extinction coefficient of the pure *E* isomer at 395 nm (37282 L mol^{-1} cm^{-1}) and A^{395nm} is the total absorption at 395 nm (0.3728). From this we calculate that Φ (*E*→*Z*) at 395nm is 0.51.

5 SOLID STATE PHOTOSWITCHING

Photoswitching in solution proceeds by S_0-S_1 transition followed by relaxation by bond rotation. The excited states are often susceptible to concentration quenching and therefore it is challenging to achieve photoswitching in solid state. Acylhydrazones (10 mg) were dissolved in acetonitrile (3 mL) with the help of ultrasound and heating. To find out if photoswitching is possible also in the solid state, a solution of **AH**s was drop-casted on quartz, dried and the sample was studied using UV-Vis spectroscopy in combination with the source of monochromatic light (Xenon lamp).

5.1 Solid state photoswitching of AH1

We have observed very similar changes in the UV-Vis spectra as in the previous experiment in solution: appearance of a new absorbance feature at 375–450 nm upon irradiation at 330 nm and decrease of the absorbance in this region upon irradiation at 395 nm. Therefore, we conclude that the photoswitching is feasible also in the solid state (Figure S 41).

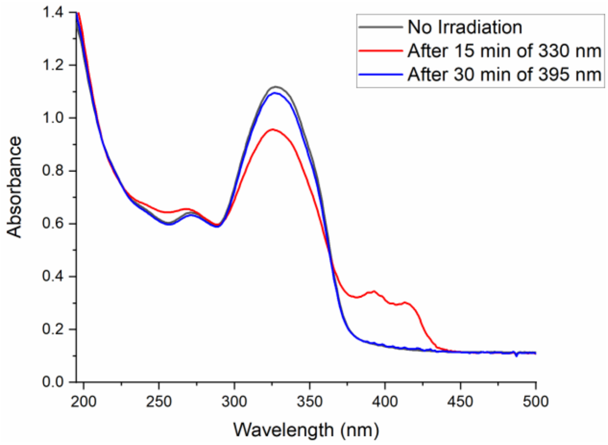

Figure S 41 Solid state photoswitching of pure **AH1**

5.2 Solid state photoswitching of AH3

We have observed very similar changes in the UV-Vis spectra as in the previous experiment in solution: appearance of a new absorbance feature at 350–450 nm upon irradiation at 335 nm and decrease of the absorbance in this region upon irradiation at 400 nm. Therefore, we conclude that the photoswitching is feasible also in the solid state (Figure S 42).

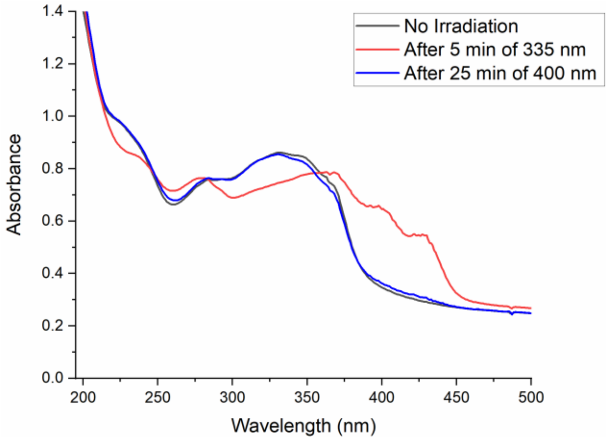

Figure S 42 Solid state photoswitching of pure **AH3**

5.3 Solid state photoswitching of AH4

We have observed very similar changes in the UV-Vis spectra as in the previous experiment in solution: appearance of a new absorbance feature at 380–450 nm upon irradiation at 335 nm and decrease of the absorbance in this region upon irradiation at 410 nm. Therefore, we conclude that the photoswitching is feasible also in the solid state (Figure S 43).

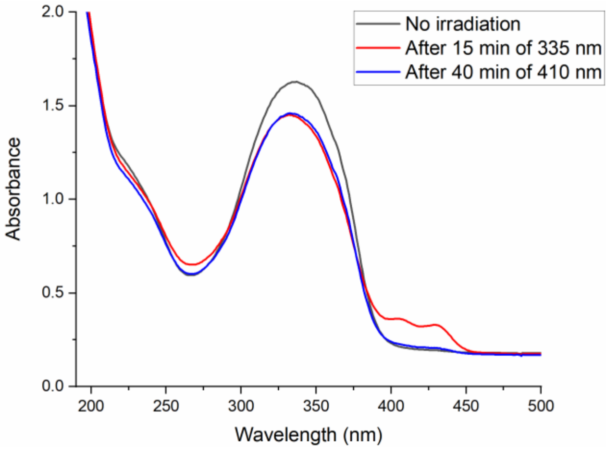

Figure S 43 Solid state photoswitching of pure **AH4**

5.4 Solid state photoswitching of AH5

We have observed very similar changes in the UV-Vis spectra as in the previous experiment in solution: appearance of a new absorbance feature at 400–450 nm upon irradiation at 355 nm and decrease of the absorbance in this region upon irradiation at 430 nm. Therefore, we conclude that the photoswitching is feasible also in the solid state (Figure S 44).

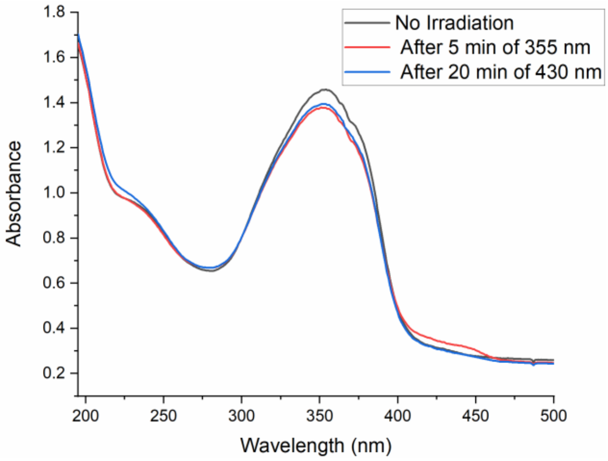

Figure S 44 Solid state photoswitching of pure **AH5**

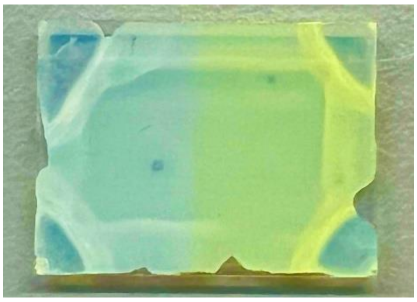

Figure S 45 Photo of solid sample of **AH5** on Quarz, left side is not irradiated while the right side was irradiated with 365 nm light for 5 minutes

5.5 Solid state photoswitching of AH6

We have observed very similar changes in the UV-Vis spectra as in the previous experiment in solution: appearance of a new absorbance feature at 400–450 nm upon irradiation at 350 nm and decrease of the absorbance in this region upon irradiation at 415 nm. Therefore, we conclude that the photoswitching is feasible also in the solid state (Figure S 46).

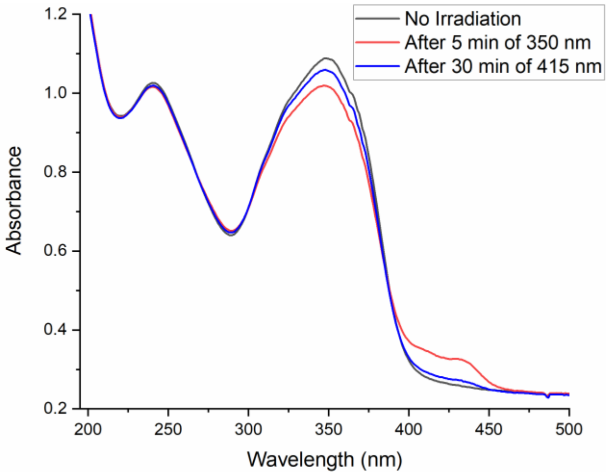

Figure S 46 Solid state photoswitching of pure **AH6**

6 PHOTOSWITCHING OF AHS IN PMMA MATRIX

However, measurement of pure films is challenging due to extremely high optical density, light scattering effects, nonhomogeneous film morphology and weak adhesion of the film to the substrate. Instead the polymer matrix of poly(methyl methacrylate) (PMMA) is more convenient. Photoswitching in PMMA matrix was then studied via UV-Vis spectroscopy in combination with the source of monochromatic light (Xenon lamp). Acylhydrazone (5-10 mg) and PMMA (105 mg) were dissolved in acetone (2-3 mL) with the help of ultrasound bath and heating. The prepared solution was then spin-coated onto the surface of the quartz glass using spin-coater (1000 rpm for 5 seconds followed by 3000 rpm for 60 seconds).

We have observed very similar changes in the UV-Vis spectra as in the previous experiment: appearance of a new absorbance feature at 350–400 nm upon irradiation at 295 nm and decrease of the absorbance in this region upon irradiation at 375 nm. Therefore, we conclude that the photoswitching is feasible also in the PMMA matrix (Figure S 47).

6.1 Photoswitching of AH1 in PMMA matrix

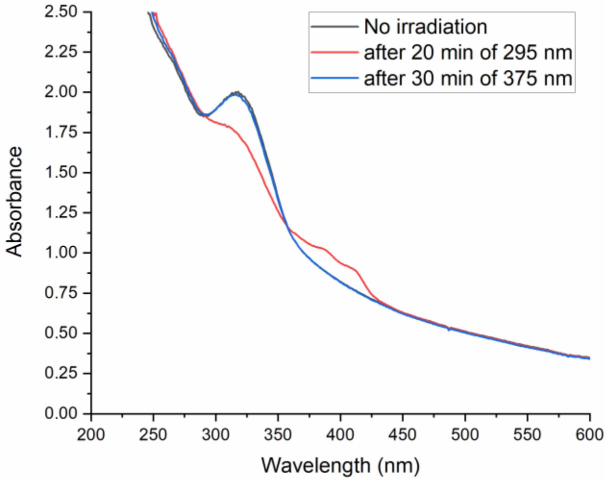

Figure S 47 Photoswitching of **AH1** in the PMMA matrix.

6.2 Photoswitching of AH3 in PMMA matrix

We have observed very similar changes in the UV-Vis spectra as in the previous experiment with: appearance of a new absorbance feature at 355–425 nm upon irradiation at 325 nm and decrease of the absorbance in this region upon irradiation at 395 nm. Therefore, we conclude that the photoswitching is feasible also in the PMMA matrix (Figure S 48).

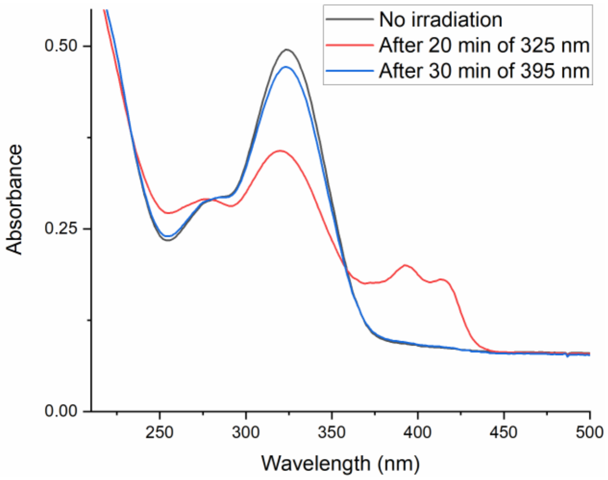

Figure S 48 Photoswitching of **AH3** in the PMMA matrix.

6.3 Photoswitching of AH4 in PMMA matrix

We have observed very similar changes in the UV-Vis spectra as in the previous experiment: appearance of a new absorbance feature at 365-440 nm upon irradiation at 330 nm and decrease of the absorbance in this region upon irradiation at 400 nm. Therefore, we conclude that the photoswitching is feasible also in the PMMA matrix (Figure S 49).

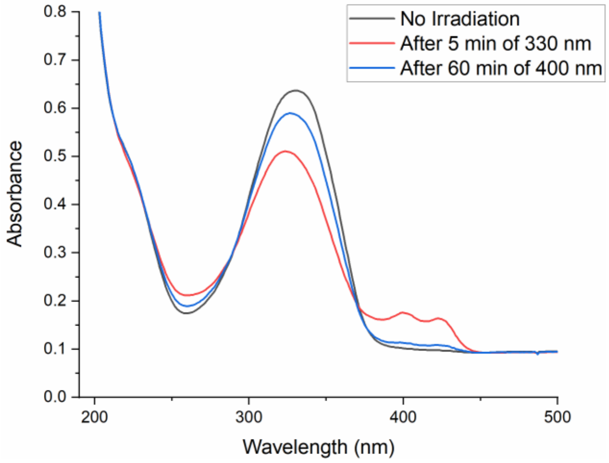

Figure S 49 Photoswitching of **AH4** in the PMMA matrix.

6.4 Photoswitching of AH5 in PMMA matrix

We have observed very similar changes in the UV-Vis spectra as in the previous experiment: appearance of a new absorbance feature at 400–450 nm upon irradiation at 340 nm, decrease of the absorbance in this region upon irradiation at 410 nm. Therefore, we conclude that the photoswitching is feasible also in the PMMA matrix (Figure S 50).

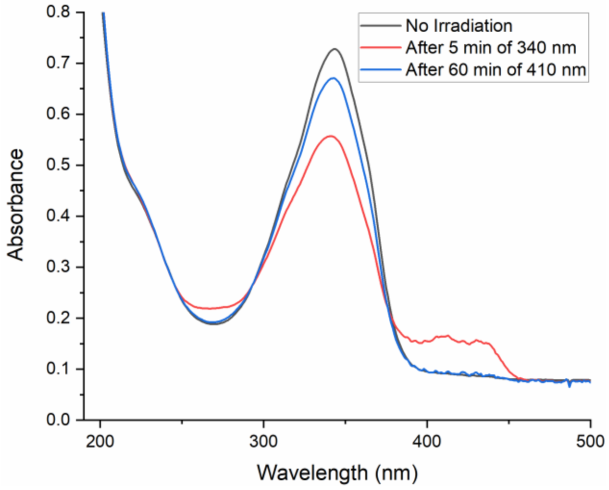

Figure S 50 Photoswitching of **AH5** in the PMMA matrix

The spectra after irradiation to PSS showed only a negligible change over 4 hour (around 4%-7%); thus, it was confirmed that the photoswitched-form is stable in the dark. Hence **AH5** is a P-type in the solid state (Figure S 51).

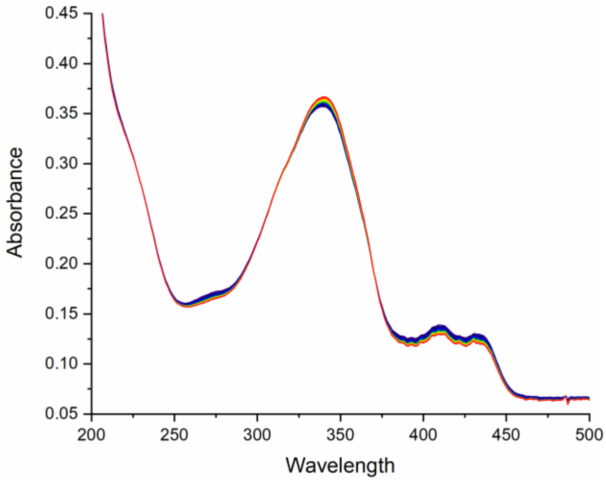

Figure S 51 Thermal stability of irradiated **AH5** in PMMA matrix recorded over 4H.

6.5 Photoswitching of AH6 in PMMA matrix

We have observed very similar changes in the UV-Vis spectra as in the previous experiment: appearance of a new absorbance feature at 370–440 nm upon irradiation at 340 nm and decrease of the absorbance in this region upon irradiation at 410 nm. Therefore, we conclude that photoswitching is also feasible in the PMMA matrix (Figure S 52).

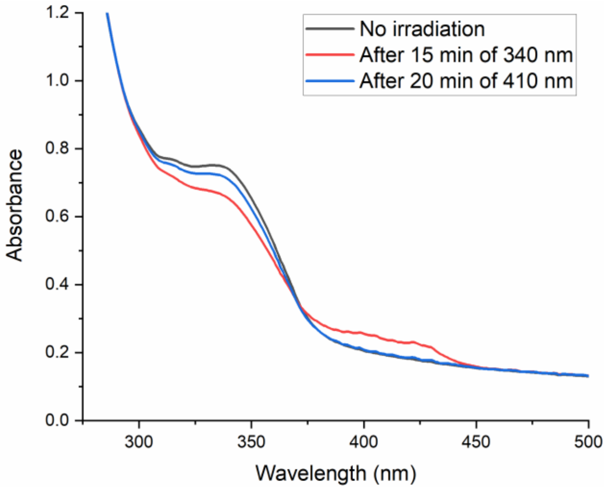

Figure S 52 Photoswitching of **AH6** in the PMMA matrix.

6.6 Photoswitching of AH9 in PMMA matrix

We have observed very similar changes in the UV-Vis spectra as in the previous experiment: appearance of a new absorbance feature at 425-480 nm upon irradiation at 385 nm and decrease of the absorbance in this region upon irradiation at 460 nm. Therefore, we conclude that photoswitching is also feasible in the PMMA matrix (Figure S 53).

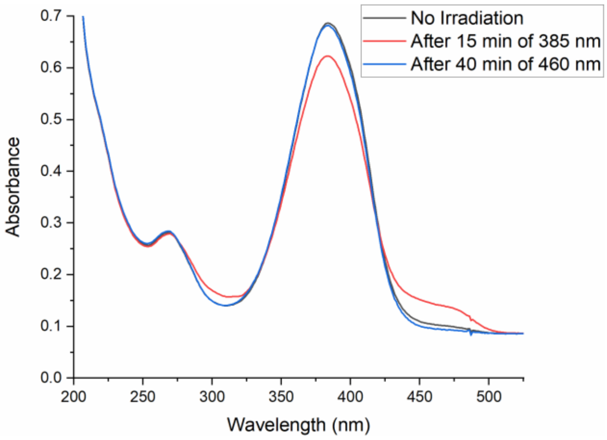

Figure S 53 Photoswitching of **AH9** in the PMMA matrix.

7 ELECTROCHEMISTRY

7.1 Cyclic voltammetry

The cyclic voltammetry was performed in dry acetonitrile solution with 0.1 M tetrabutylammonium hexafluorophosphate electrolyte. The setup had a Pt working and counter electrodes and an Ag/AgCl reference electrode. The Ag/AgCl reference electrode was prepared by first cleaning the Ag wire with nitric acid then keeping it overnight in HCl to passivate the Ag as AgCl. The pseudoreference was calibrated to the Fc/Fc^+ redox couple set to 0.4 V. All electrodes were inserted directly into the studied solution with no separation. Measurements were made using a PalmSens4 potentiostat with PSTrace software at scan rate 50 mV/s; no significant change was observed when the rate was increase to 100 mV/s. The solution was not stirred while running the cyclic voltammetry.

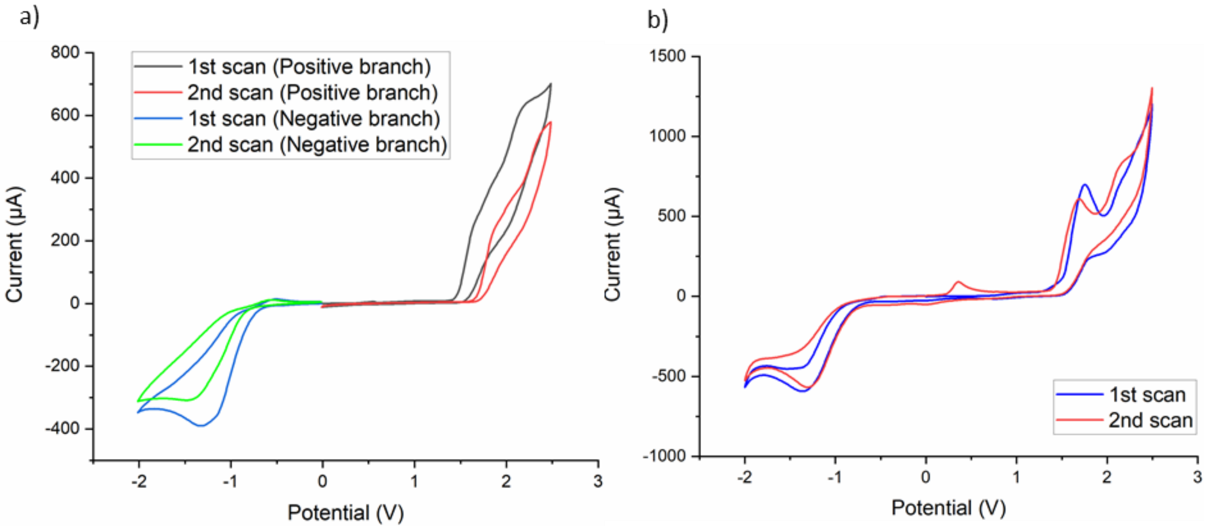

Figure S 54 a) Cyclic voltammograms performed in a solution ($2.5 \cdot 10^{(-3)}$) of **AH1** at scan rate 50 mV/s. Oxidation and reduction branches were performed as independent experiments. Voltammograms were calibrated on Fc/Fc+=0.4 V. b) CV of irradiated form of **AH1** in a solution ($2 \cdot 10^{(-3)}$).

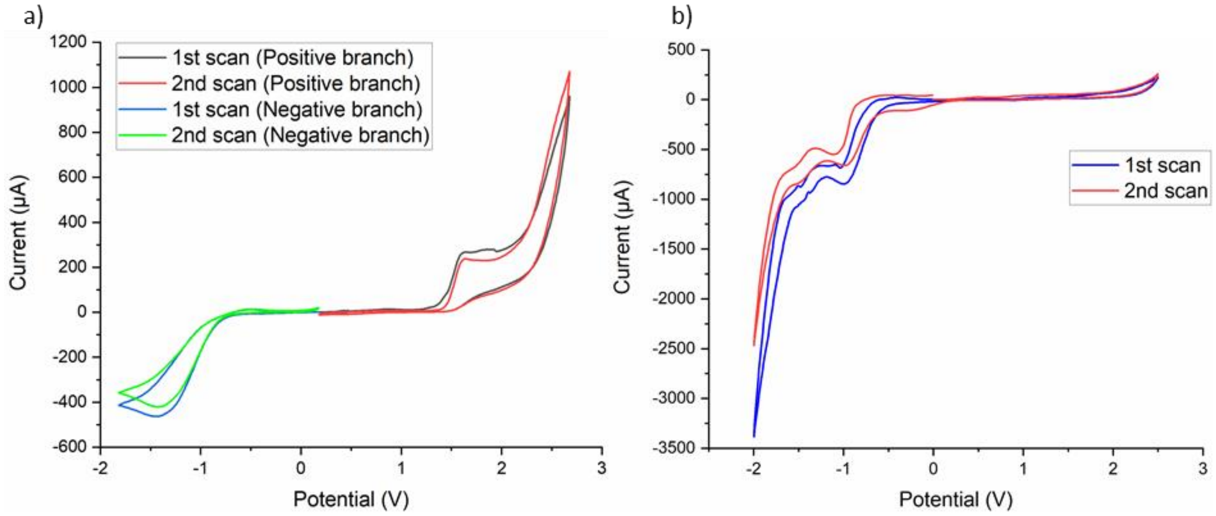

Figure S 55 a) Cyclic voltammograms performed in a solution (2.5·10$^{(-3)}$) of **AH2** at scan rate 50 mV/s. Oxidation and reduction branches were performed as independent experiments. Voltammograms were calibrated on Fc/Fc+=0.4 V. b) CV of irradiated form of **AH2** in a solution (1·10$^{(-3)}$).

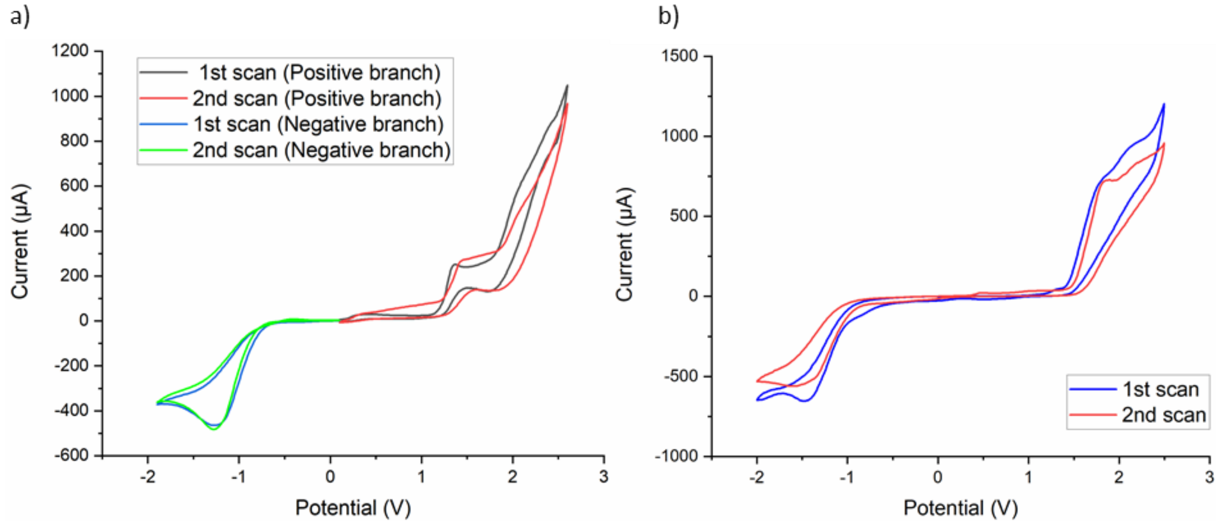

Figure S 56 a) Cyclic voltammograms performed in a solution (2.5·10$^{(-3)}$) of **AH3** at scan rate 50 mV/s. Oxidation and reduction branches were performed as independent experiments. Voltammograms were calibrated on Fc/Fc+=0.4 V. b) CV of irradiated form of **AH3** in a solution (1.5·10$^{(-3)}$).

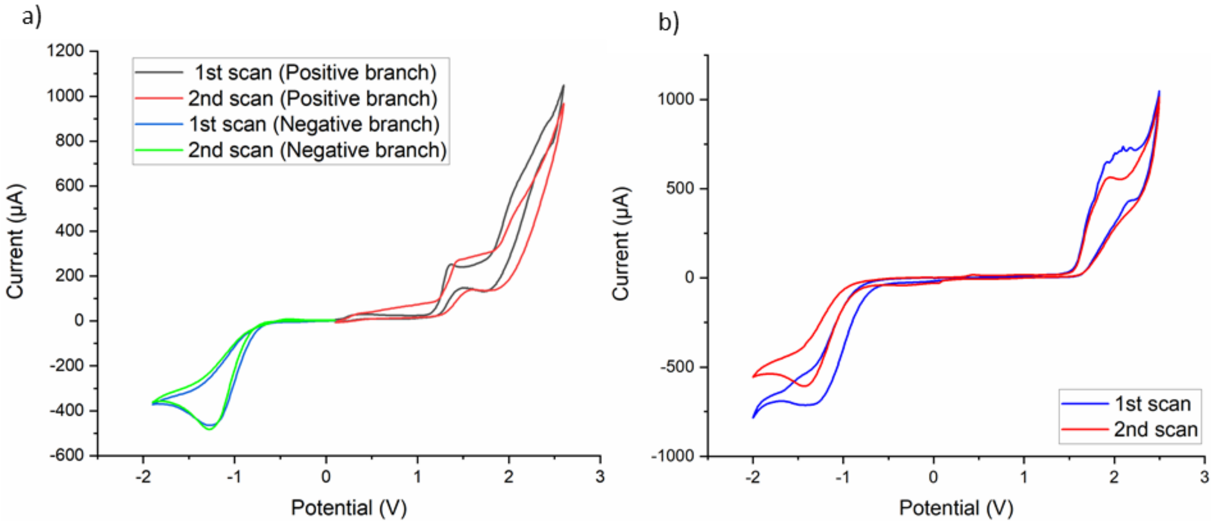

Figure S 57 a) Cyclic voltammograms performed in a solution (2.5·10$^{(-3)}$) of **AH4** at scan rate 50 mV/s. Oxidation and reduction branches were performed as independent experiments. Voltammograms were calibrated on Fc/Fc+=0.4 V. b) CV of irradiated form of **AH4** in a solution (2·10$^{(-3)}$).

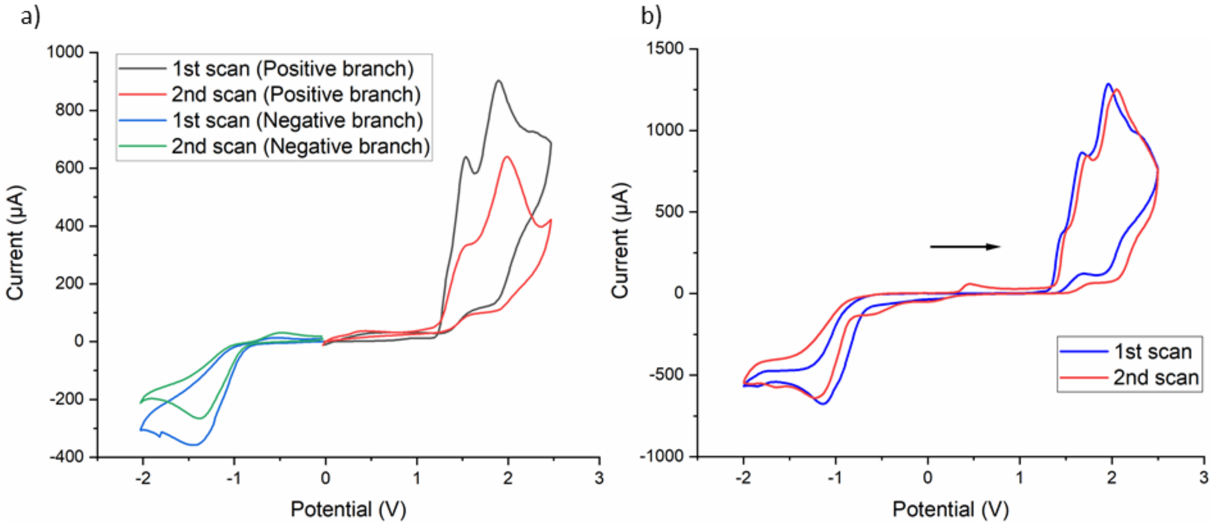

Figure S 58 a) Cyclic voltammograms performed in a solution (2.5·10$^{(-3)}$) of **AH5** at scan rate 50 mV/s. Oxidation and reduction branches were performed as independent experiments. Voltammograms were calibrated on Fc/Fc+=0.4 V. b) CV of irradiated form of **AH5** in a solution (2·10$^{(-3)}$).

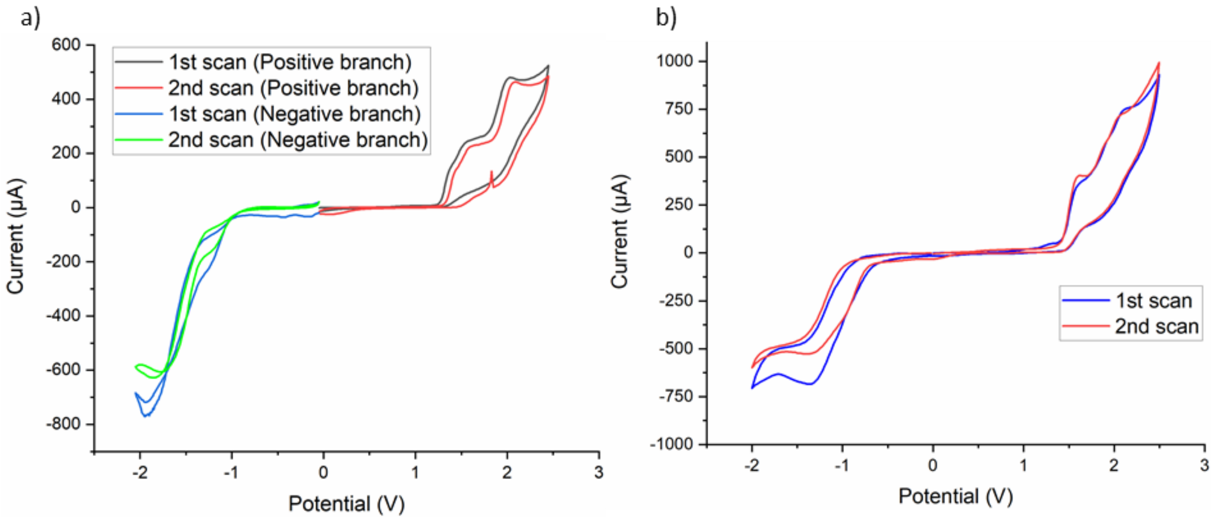

Figure S 59 a) Cyclic voltammograms performed in a solution ($2.5\cdot10^{(-3)}$) of **AH6** at scan rate 50 mV/s. Oxidation and reduction branches were performed as independent experiments. Voltammograms were calibrated on Fc/Fc+=0.4 V. b) CV of irradiated form of **AH6** in a solution ($2\cdot10^{(-3)}$).

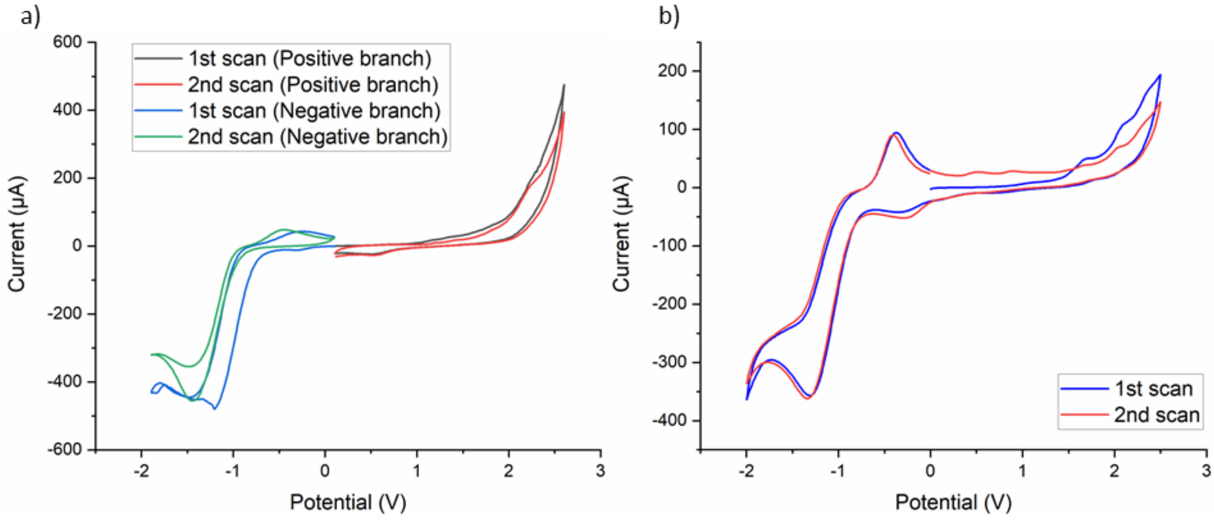

Figure S 60 a) Cyclic voltammograms performed in a solution ($1.5\cdot10^{(-5)}$) of **AH7** at scan rate 50 mV/s. Oxidation and reduction branches were performed as independent experiments. Voltammograms were calibrated on Fc/Fc+=0.4 V. b) CV of irradiated form of **AH7** in a solution ($1.5\cdot10^{(-5)}$).

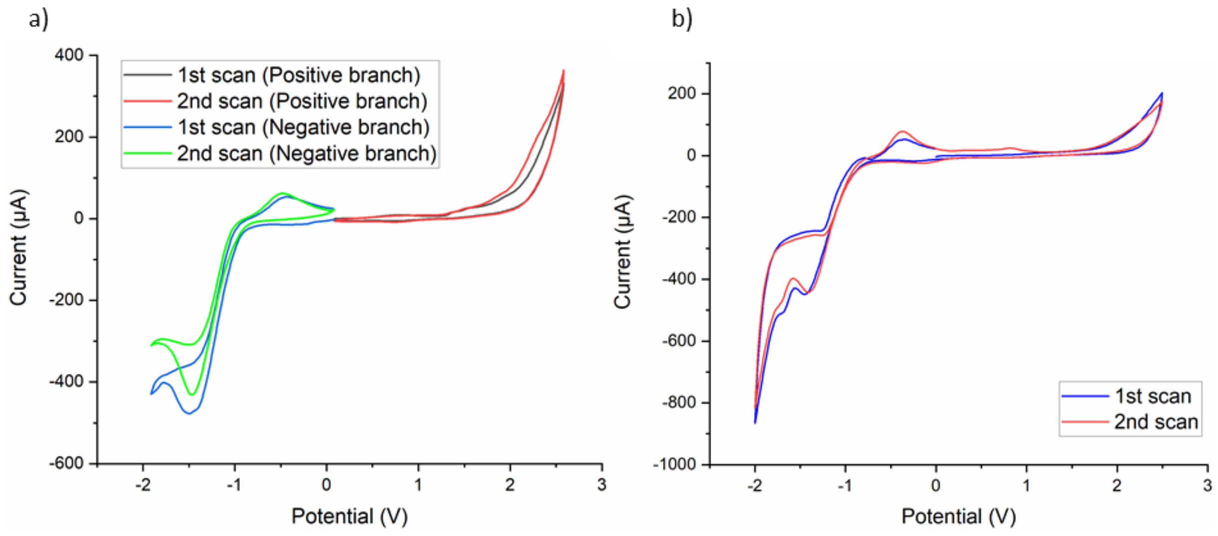

Figure S 61 a) Cyclic voltammograms performed in a solution ($1.5\cdot10^{(-5)}$) of **AH8** at scan rate 50 mV/s. Oxidation and reduction branches were performed as independent experiments. Voltammograms were calibrated on Fc/Fc+=0.4 V. b) CV of irradiated form of **AH8** in a solution ($1.5\cdot10^{(-5)}$).

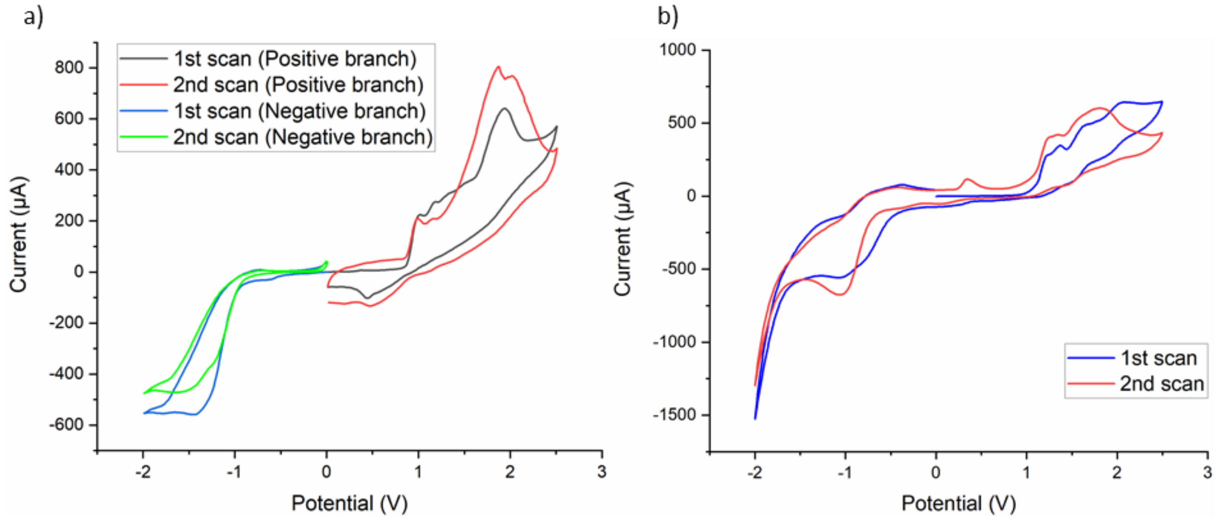

Figure S 62 a) Cyclic voltammograms performed in a solution ($2.5\cdot10^{(-3)}$) of **AH9** at scan rate 50 mV/s. Oxidation and reduction branches were performed as independent experiments. Voltammograms were calibrated on Fc/Fc+=0.4 V. b) CV of irradiated form of **AH9** in a solution ($2\cdot10^{(-3)}$).

7.2 Electroswitching

The solution of **AHs** ($1\cdot10^{-3}$ M in the case of **AH1-6** and **AH9** vs $1\cdot10^{-5}$ M in the case of **AH7-8**) in dry acetonitrile with 0.1 M tetrabutylammonium hexafluorophosphate electrolyte was irradiated with UV light (wavelength is specific for each **AH,** described in the Figures) to isomerize to the photoswitched-form. The formation of the photoswitched-form was confirmed by UV-Vis spectroscopy. After achieving the PSS, we performed a cyclic voltammetry sweep to oxidative potential at 50 mV/s. We observed a dramatic and instantaneous change in the UV-Vis spectrum indicating complete reversal of the photoswitched-form back to the *E*-form after the CV cycle (0

V→2.5 V→(-2.0 V)→0 V) (see below for each **AH**). This experiment shows that it is possible to induce isomerization from photoswitched-form to *E*-form using an electrochemical stimulus. Thus, **AHs** act as “electroswitches”.

7.2.1 Electroswitching of AH1

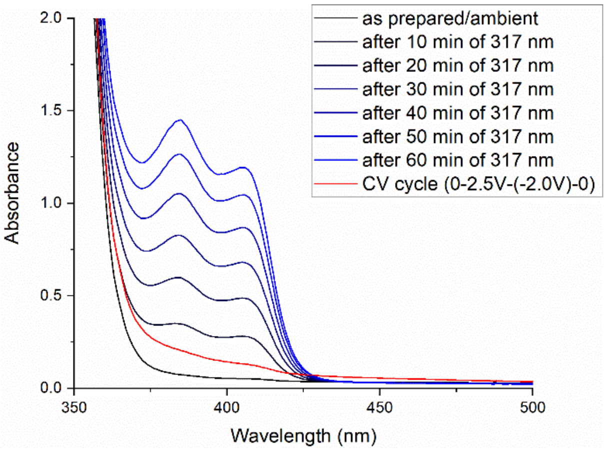

Figure S 63 UV-Vis spectra of the photoisomerization **AH1** and spectrum after cyclic voltammetry in the potential sweep (0-2.5V-(-2.0V)-0). We have observed a dramatic and instantaneous change in the UV-Vis spectrum after the potential was applied indicating applied indicating a complete reversal to the *E*-form.

7.2.2 Electroswitching of AH2

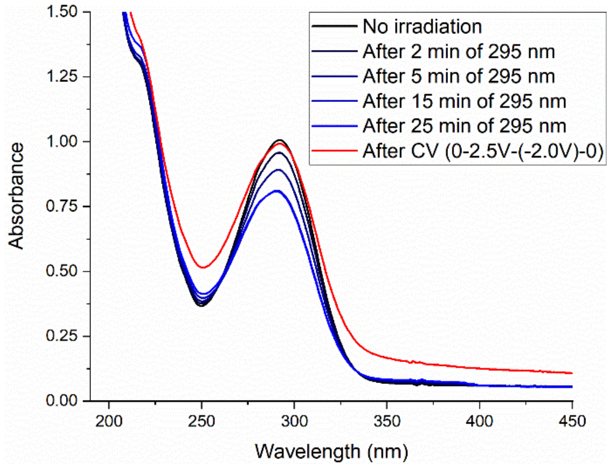

Figure S 64 UV-Vis spectra of the photoisomerization **AH2** and spectrum after cyclic voltammetry in the potential sweep (0-2.5V-(-2.0V)-0). We have observed no change in the UV-Vis spectrum after the potential was applied.

7.2.3 *Electroswitching of AH3*

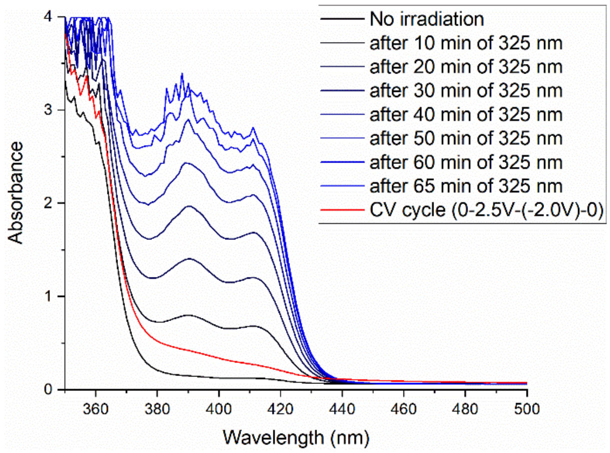

Figure S 65 UV-Vis spectra of the photoisomerization **AH3** and spectrum after cyclic voltammetry in the potential sweep (0-2.5V-(-2.0V)-0). We have observed a dramatic and instantaneous change in the UV-Vis spectrum after the potential was applied indicating a complete reversal to the *E*-form.

7.2.4 *Electroswitching of AH4*

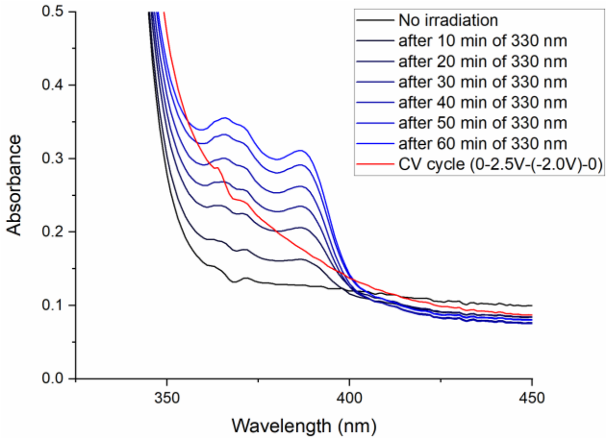

Figure S 66 UV-Vis spectra of the photoisomerization **AH4** after cyclic voltammetry in the potential sweep (0-2.5V-(-2.0V)-0). We have observed a dramatic and instantaneous change in the UV-Vis spectrum after the potential was applied indicating a complete reversal to the *E*-form.

7.2.5 Electroswitching of AH5

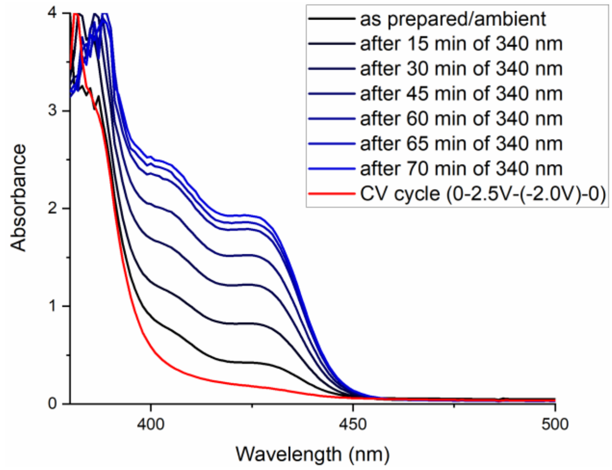

Figure S 67 UV-Vis spectra of the photoisomerization of **AH5** and spectrum after cyclic voltammetry in the potential sweep (0-2.5V-(-2.0V)-0). We have observed a dramatic and instantaneous change in the UV-Vis spectrum after the positive potential was applied indicating a complete reversal to the *E*-form.

7.2.6 Control experiment after electroswitching

A control experiment was carried out in order to investigate whether the applied CV can cause any damage to the molecule. A solution of **AH5** ($2.5 \cdot 10^{(-3)}$ M) in deuterated Acetonitrile was prepared with $LiClO_4$ electrolyte (0.1 M). The solution was then irradiated by 340 nm to achieve the PSS state and then 2 cycles of CV were applied (0-2.5V-(-2.0V)-0). The UV-Vis spectra show a dramatic and instantaneous change in the UV-Vis spectrum after the potential was applied indicating a complete reversal to the *E*-form (Figure S 68). The NMR spectra show that after CV we lose all of the signals that are associated with a photoswitched-form and only a negligible amount of this form is converted back to aldehyde. Integral intensity revealed that only the photoswitched-form was transformed back to aldehyde after CV.

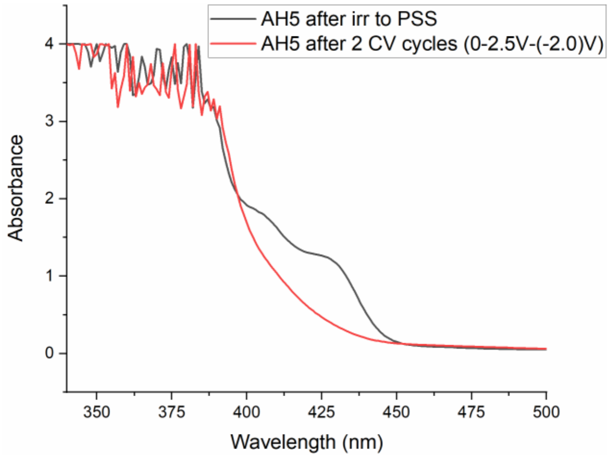

Figure S 68 UV-Vis spectra of the photoisomerization of **AH5** and spectrum after cyclic voltammetry in both positive and negative potential sweep (0-2.5V-(-2.0V)-0). We have observed a dramatic and instantaneous change in the UV-Vis spectrum after the positive potential was applied indicating a complete reversal to the *E*-form.

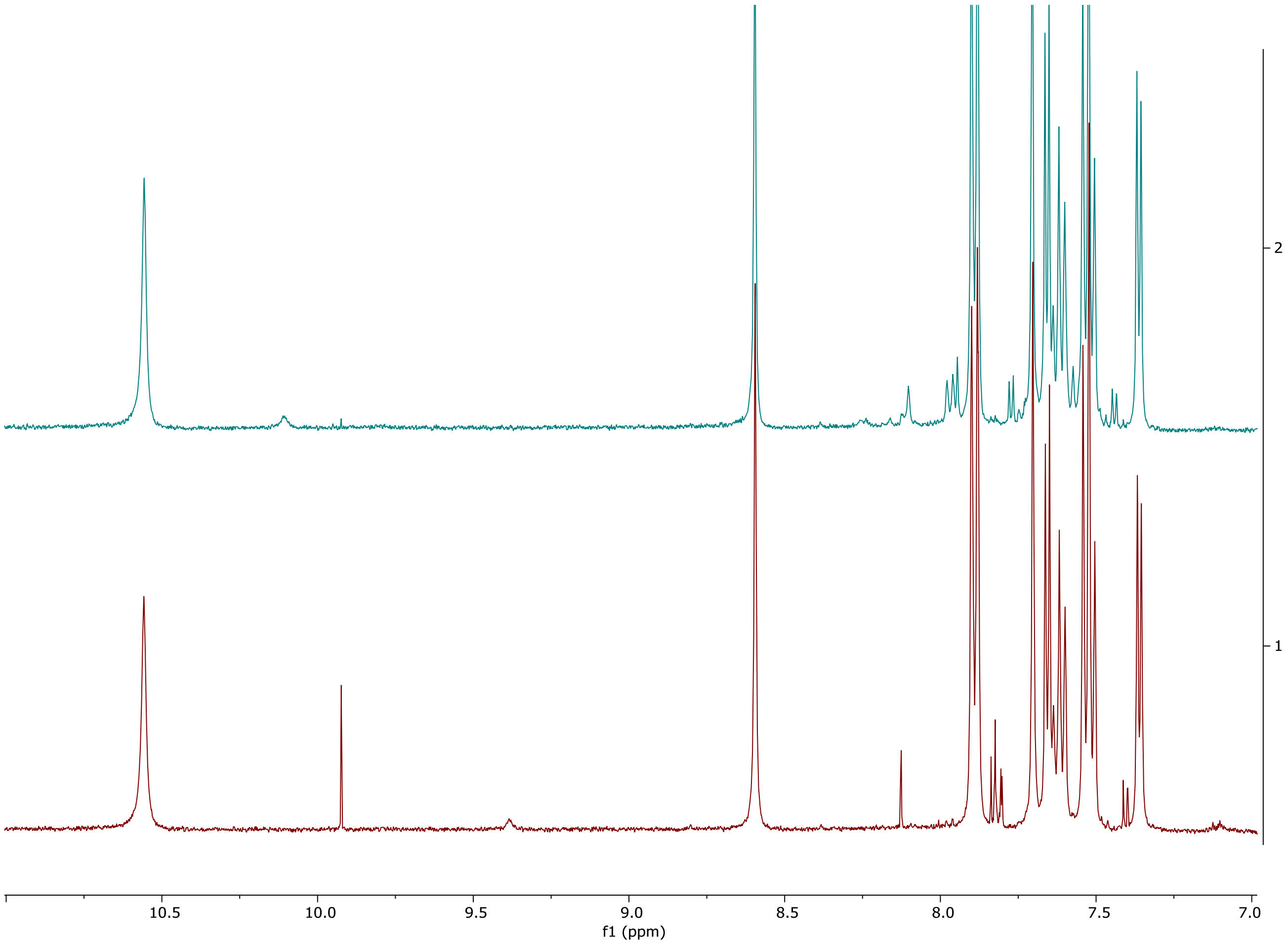

Figure S 69 NMR spectra of **AH5** solution after irradiation to PSS before applying cyclic voltammetry (upper trace) and of **AH5** solution after applying Cyclic voltammetry (bottom trace).

7.2.7 Electroswitching of AH6

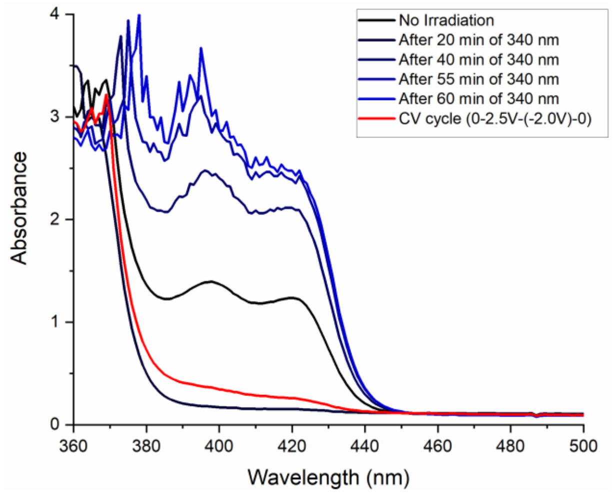

Figure S 70 UV-Vis spectra of the photoisomerization of **AH6** and spectrum after cyclic voltammetry in the potential sweep (0-2.5V-(-2.0V)-0). We have observed a dramatic and instantaneous change in the UV-Vis spectrum after the potential was applied indicating a complete reversal to the *E*-form.

7.2.8 *Electroswitching of AH7*

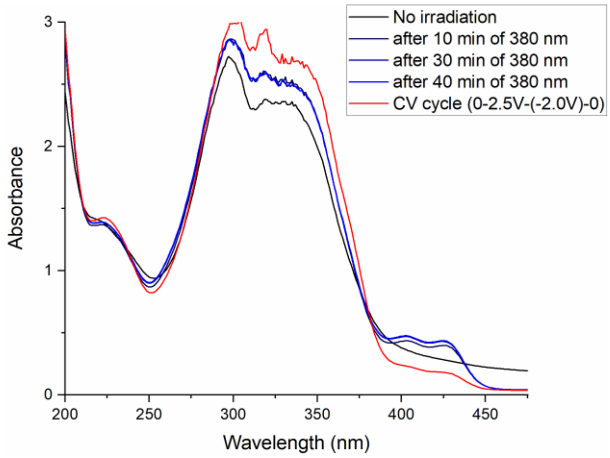

Figure S 71 UV-Vis spectra of the photoisomerization of **AH7** and spectrum after cyclic voltammetry in the potential sweep (0-2.5V-(-2.0V)-0). We have observed a dramatic and instantaneous change in the UV-Vis spectrum after the potential was applied indicating a complete reversal to the *E*-form.

7.2.9 *Electroswitching of AH8*

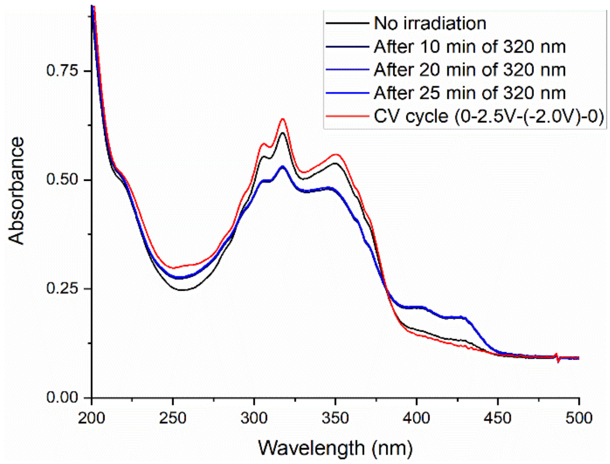

Figure S 72 UV-Vis spectra of the photoisomerization of **AH8** and spectrum after cyclic voltammetry in the potential sweep (0-2.5V-(-2.0V)-0). We have observed a dramatic and instantaneous change in the UV-Vis spectrum after the potential was applied indicating a complete reversal to the *E*-form.

7.2.10 *Electroswitching of AH9*

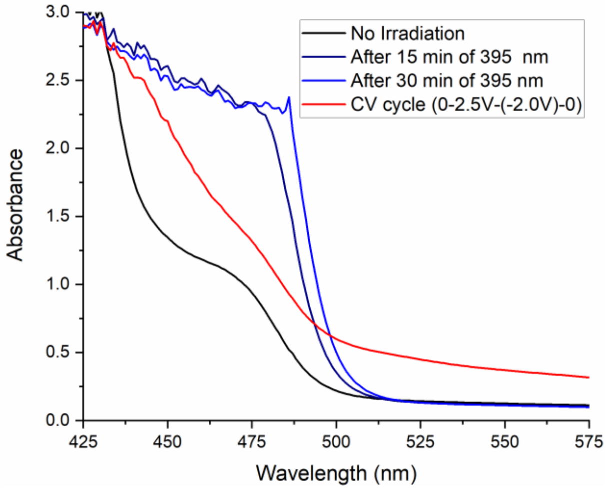

Figure S 73 UV-Vis spectra of the photoisomerization of **AH9** and spectrum after cyclic voltammetry in the potential sweep (0-2.5V-(-2.0V)-0). We have observed a dramatic and instantaneous change in the UV-Vis spectrum after the potential was applied indicating a complete reversal to the *E*-form.

8 FLUORESCENCE

Solution of **AH1** in acetonitrile (10 µM) was excited by 250 nm excitation wavelength with excitation slit set to 10 nm and emission slit to 10 nm, at scan rate 240 nm/min, data interval 2 nm, averaging time 0.5 s, with excitation filter 295-1100 nm and PMT voltage set to high.

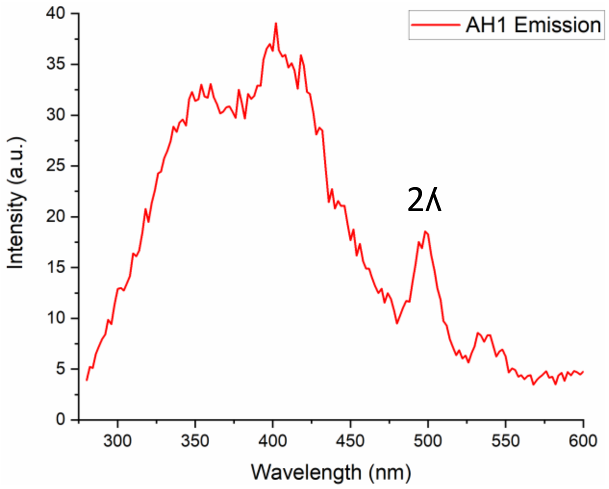

Figure S 74 Fluorescence Emission spectrum of **AH1** solution (c = 10 µM). Signal at 500 nm is 2λ artefact.

9 CALCULATIONS

9.1 Methods

The ground-state equilibrium geometries of AH1 and AH2 were obtained using DFT, employing a ωB97X[11] functional and TZVP basis set.[12,13] The S1 minima were optimized at the state-averaged complete active space self-consistent-field (SA-CASSCF) level. The active space was constructed from 14 electrons in 10 orbitals CAS(14,10). In these calculations, three singlet states (S0, S1, and S2) were considered in the state-averaging procedure. All vertical excitation energies were calculated using the Complete Active Space Second Order Perturbation Theory (CASPT2) method, with the zero-order wavefunction obtained with SA-CASSCF(14,10), in state-averaged calculations which included S0-S3 and T1-T3 states. In the calculations at the geometry of the S1 minima, the spin-orbit coupling matrix elements between the singlet and triplet states were determined. In all calculations, the effect of solvent (acetonitrile) was considered via the conductor-like polarizable continuum model (CPCM).[14] All calculations were performed using Orca program package, version 5.0.4.[15,16]

9.2 Ground state optimization and conformations

For both systems, two possible conformers as shown in Figure S 75 were considered, differing in the δ(S-C(5)-CH-N) dihedral angle of about 0° (**AH1*s-cis*** and **AH2*s-cis***) and 180° (**AH1*s-trans*** and **AH2*s-trans***). The energy differences between **AH1*s-cis*** and ***AH1s-trans***, as well as **AH2*s-cis*** and **AH2*s-trans*** are less than 1.5 kcal/mol, suggesting the possibility of coexistence of both conformers in the solvent. **AH1** exhibits a higher stability by 1.28 kcal/mol in the ***s-cis*** configuration, whereas **AH2** is 1.48 kcal/mol more stable in the ***s-trans*** configuration.

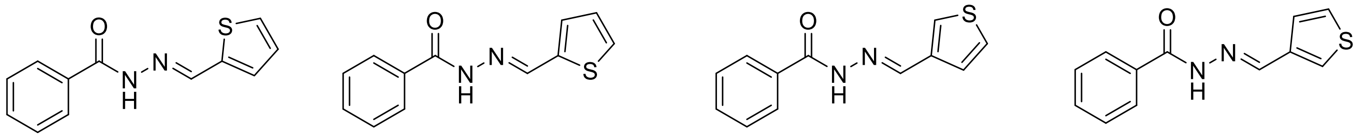

AH1*s-cis* **AH1*s-trans*** **AH2*s-cis*** **AH2*s-trans***

Figure S 75 Definition of considered conformation geometries of *E* isomers of **AH1** and **AH2** used in calculations. *Z* isomers are rotated by 180° around the C=N bond. The *Z* forms of **AH1** are less stable than E forms by 4.75 and 3.55 kcal/mol for s-trans and s-cis conformations, respectively. In the case of **AH2**, the energy *E*/*Z* differences are smaller, of 1.11 and 1.93 kcal/mol for s-trans and s-cis, respectively.

9.3 Vertical excitations and excited states optimizations

The calculated vertical excitation spectra for all systems are reported in Table S 1 and Table S 2, respectively. The singlet excited states (S_1 – S_3) of **AH1*s-cis*** and **AH1*s-trans*** result from the transitions within π-systems. The transition energies for the individual excited states of both systems (Table S 1) are almost identical, differing by less than 0.1 eV. According to the results, the peak at around 317 nm observed experimentally can be interpreted by the state resulting from π→π* transition mostly localized on the (N-CH) bond, while the peak at around 240-250 nm is due to the π(6m)→π*(N-CH), or π(5m)→π*(N-CH), transitions. The first excited states of the photoswitched conformations, both *s-cis* and *s-trans*, exhibit a shift towards shorter wavelengths, approximately 10 nm. However, only the *s-trans* conformation is anticipated to be detected in absorption spectra. According to the calculated oscillator states, only the second excited state of the (*Z*)-s-cis is predicted to contribute to the broad peak around 250 nm.

The calculated excited states of **AH2** (Table S 2) show slightly larger differences in the transition energies between ***s-cis*** and ***s-trans***, reaching up to 0.4 eV. Nevertheless, the characteristics of the transitions are consistent. The calculations predict the S_1 state in the region around 4 eV (300 nm), in agreement with the experimentally observed peak around 295 nm. The band of a smaller intensity at around 250 nm can be interpreted by the excited state calculated at around 5.01 and 5.46 eV for **AH2*s-trans*** and **AH2s-cis**, respectively. All discussed states are characterized by the transitions resulting from the excitations from π-systems of the phenyl ring to π-orbitals delocalized over the whole system (**AH2*s-trans***) or localized on the same ring (**AH2*s-cis***).

The above-described results of the absorption spectra are in very good agreement with the experiment, justifying the reliability of the method for further excited state calculations. Importantly, the calculations do not predict the existence of the band at 350-400 nm observed in the spectra of **AH1**.

To explain the spectroscopic observation, Kasha's rule was considered, according to which the system relaxes on an ultrafast time scale from the generated excited state to the lowest S1 excited state. Thus, subsequent investigations involved the identification of S1 minima aiming to reveal a potential evolution on the potential energy surface. For both systems, three possible S1 minima (**AH1_(*radiative1, radiative2*, *switching*)** and **AH2_(*radiative1, radiative2*, *switching*)**) were located. Table S 3 reports on the two selected dihedral angles used to characterize their structure. The values of dihedral angle Θ, indicating the mutual orientation of the 5-membered and 6-membered rings, show variable deviations of the rings from the ground-state optimized structures, in which both rings lie in the same plane. The dihedral angles Ω, describing the torsion around the N-CH bond, show a smaller flexibility. The deviations from either 0° or 180°, the values defining the planarity of the bond, are not larger than 40°, except **AH1_*switching***, where the Ω is equal to 95°. This parameter is very likely an important factor that influences the excited state behavior of these systems.

Table S 1 Vertical excitation spectra of AH1 calculated at the CASPT2/CASSCF(14,10)/TZVP level, [a]**AH1*s-trans***, **(*Z*)-AH1*s-cis***, and **AH1*s-trans*** are by 1.28, 3.55, and 4.75 kcal/mol less stable than **AH1s-cis** respectively, [b]oscillator strength

	AH1*s-cis*				**AH1*s-trans***[a]			
		ΔE(eV)	λ(nm)	f_{osc}[b]		ΔE(eV)	λ(nm)	f_{osc}[b]
S_1	π(N-CH)→π*(N-CH)	4.009	309	0.06	π(6m)→π*(6m)	3.996	310	0.00
S_2	π(deloc)→π*(deloc)	4.100	302	0.81	π(N-CH)→π*(N-CH)	4.096	303	0.77
S_3	π(6m)→π*(N-CH)	4.971	249	0.11	π(5m)→π*(N-CH)	4.930	251	0.18
	(*Z*)-AH1s-cis[a]				**(*Z*)-AH1*s-trans***[a]			
S_1	π(N-CH)→π*(N-CH)	4.177	297	0.03	π(6m)→π*(6m)	4.145	299	0.50
S_2	π(deloc)→π*(deloc)	5.065	245	0.21	π(N-CH)→π*(N-CH)	4.721	263	0.00
S_3	π(6m)→π*(N-CH)	5.342	232	0.03	π(5m)→π*(N-CH)	5.258	236	0.05

Table S 2 Vertical excitation spectra of AH2 calculated at the CASPT2/CASSCF(14,10)/ TZVP level, [a]**AH2*s-cis***, **(*Z*)-AH2*s-cis***, and **(*Z*)-AH2*s-trans*** are by 1.48, 1.93, and 1.11 kcal/mol less stable than **AH1*s-cis*** respectively, [b]oscillator strength

	AH2*s-cis*[a]				**AH2*s-trans***			
		ΔE(eV)	λ(nm)	f_{osc}[b]		ΔE(eV)	λ(nm)	f_{osc}[b]
S_1	π(6m)→π*(6m)	4.147	299	0.03	π(6m)→π*(deloc)	3.96	313	0.00
S_2	π(6m)→π*(6m)	5.011	247	0.01	π(6m)→π*(deloc)	5.464	227	0.01
S_3	n→π*(N-CH)	5.687	218	0.30	n→π*(deloc)	5.836	212	0.13
	(*Z*)-AH1s-cis[a]				**(*Z*)-AH1s-trans**[a]			
S_1	π(6m)→π*(6m)	4.186	296	0.00	π(6m)→π*(deloc)	4.226	293	0.02

S_2	π(6m)→π*(6m)	4.501	275	0.51	π(6m)→π*(deloc)	4.672	265	0.44
S_3	n→π*(N-CH)	5.525	274	0.10	n→π*(deloc)	5.073	244	0.21

Table S 3 Selected dihedral angles (in deg) of S1 minima optimized at the CASSCF(14,10)/TZVP level. [a]the dihedral angle between 5-membered and 6-membered rings, [b]the torsion angle between (N-CH) bond.

	AH1_*radiative2*	**AH1_*radiative1***	**AH1_*switching***	**AH2_*radiative1***	**AH2_*radiative2***	**AH2_*switching***
Θ[a]	117.4	91.0	67.4	27.5	-85.9	180.0
Ω[b]	169.0	173.6	95.4	-31.6	162.6	7.4

Table S 4 and Table S 5 provide details on the excited state minima of **AH1** and **AH2**, respectively. To propose a plausible evolution of the systems from S_1 minima, the information includes the relative energies and characteristic transitions of S_0, S_1, and T_1 states at the geometries corresponding to S_1 minima. The energies relative to S_0 energies of the more stable ground-state structures, i.e., **AH1*s-cis*** and **AH2*s-trans***, respectively, are considered. **AH1_*radiative2*** and **AH1_*radiative1*** minima show analog behavior; the lowest singlet state (S_0) has a closed-shell electronic configuration, and it is located on the potential energy surface only slightly above the S_0 of **AH1*s-cis*** of the ground-state geometry. The subsequent states are T_1 states, resulting from the transition within the π orbitals primarily localized around the N-CH bond. These states are followed by S_1 states, which are about 1.0 – 1.5 eV higher in energy and have similar characters of transitions. The character of the **AH1_*switching*** differs significantly. At this geometry, the T_1 state is the most energetically stable, followed closely by the open-shell singlet state (the energy difference is 0.15 eV). The closed-shell singlet state is predicted to be approximately 1.0 eV higher in energy compared to the open-shell singlet state. This scenario suggests a potential decay of the S_1 state to a relatively stable T_1, supported also by non-negligible elements of spin-orbit coupling, as shown in Table S 4. Also, in this case, the electronic transitions include π orbitals localized primarily on the N-CH bond. Contrary to **AH1**, all S_1 minima identified for **AH2** (Table S 5) reveal a closed-shell character of their lowest electronic state.

Table S 4 Characterization of the relaxed S1 minima of **AH1** optimized at the CASSCF(14,10)/TZVP level. The energies were calculated at the CASPT2/CASSCF(14,10)/TZVP level, [a]The relative energies are related to the S_0 energies of **AH1*s-cis***, [b]closed-shell electronic structure, [c]the spin-orbit coupling, the values show the largest non-zero elements of the spin-orbit coupling matrix.

	AH1_*radiative2*		**AH1_*radiative1***		**AH1_*switching***	
		ΔE(eV) [a]		ΔE(eV) [a]		ΔE(eV) [a]
S_0	cs[b]	0.115	cs	0.376	π(N)→π*(N-CH)	2.528
S_1	π(N-CH)→π*(N-CH)	3.391	π,n(N)→π*(N-CH)	3.996	cs	3.590
T_1	π(N-CH)→π*(N-CH)	1.934	π(N)→π*(N-CH)	2.922	π(N)→π*(N-CH)	2.377
SOC[c]		< 5		S0→T1:10		S0→T1:22
				S1→T1:18		S1→T1: 8

Table S 5 Characterization of the S1 minima of **AH2** optimized at the CASSCF(14,10)/TZVP level. The energiesa were calculated at the CASPT2/CASSCF(14,10)/TZVP level, [a]The relative energies are related to the S_0 energies of ***AH2s-trans***, [b]closed-shell electronic structure, [c]the spin-orbit coupling, the values show the largest non-zero elements of the spin-orbit coupling matrix.

	AH2_radiative2		***AH2_radiative1***		***AH2_switching***	
		ΔE(eV) [a]		ΔE(eV) [a]		ΔE(eV) [a]
S_0	cs	0.029	cs	0.796	cs	0.445
S_1	π(6m)→π*(deloc)	3.891	n→π*(N-CH)	4.099	π(5m)→π*(deloc)	3.510
T_1	π(N-CH)→π*(deloc)	3.412	π(N+5m)→π*(N-CH)	2.818	π(5m)→π*(deloc)	3.570
SOC[c]		S0→T1<5		S0→T1:8		S0→T1<5
		S1→T1:25		S1→T1:18		S1→T1:18

After the decay of ***AH1_switching***, the system undergoes additional relaxation to the T_1 minimum. Calculations indicate the existence of two possible T_1 minima, situated energetically 0.46 and 0.53 eV below T_1 at ***AH1_switching*** geometry. The vertical excitation energies to T_2 from these states were calculated as 3.04 eV and 3.33 eV, providing the interpretation of the band at 350-400 nm observed in **AH1** spectra.

9.4 Energy scan at dihedral angles in the triplet ground state

We have calculated energies of the triplet state of **AH1** associated with different dihedral angles between the C(5)-CH-N-NH and N-CH-C(5)-S. We conclude that the triplet state is most favored at around 90° dihedral angle between the C(5)-CH-N-NH as at this angle the triplet state of the molecule reaches energy minimum (Figure S 76). However, rather small energy difference was calculated for angles in the range of 90-180°, indicating a conformational flexibility. The dihedral N-CH-C(5)-S angle shows steeper energy gradients and having two clear minima at coplanar geometries (Figure S 77).

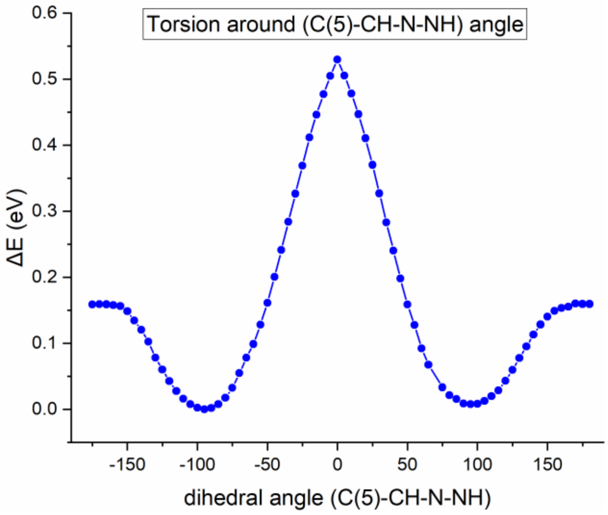

Figure S 76 Energies associated with different dihedral angle of the bonds C(5)-CH-N-NH.

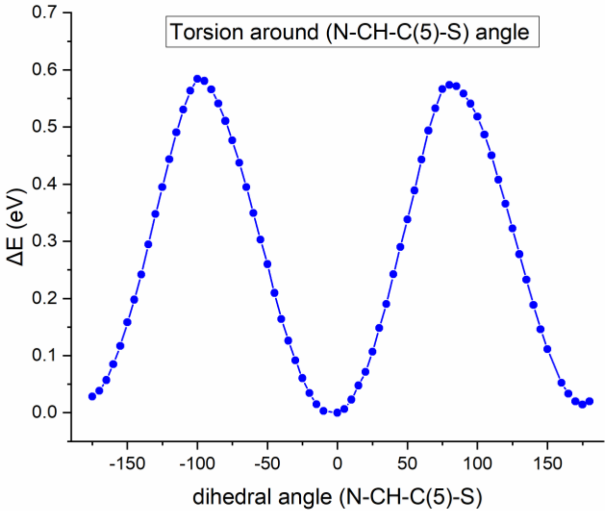

Figure S 77 Energies associated with different dihedral angle of the bonds: N-CH-C(5)-S.

10 ELECTRON PARAMAGNETIC RESONANCE (EPR)

10.1 Experimental

All the EPR spectra were acquired on Bruker EMXplus 10/12 CW (continuous wave) spectrometer equipped with a Premium-X-band microwave bridge. The g_{iso} value of radicals was determined using a built-in spectrometer frequency counter and an ER-036TM NMR-Teslameter (Bruker). All g −values were determined with the precision of ± 0.0002. Irradiated samples in the form of powder or molecular film in PMMA matrix were inserted into the quartz tube (i.d. 4 mm) to record the EPR spectra. In such case, sample weights range from 5 mg to 19 mg. Prior to measurement, all samples were flushed with N_2 and kept under inert atmosphere. In order to compare the EPR intensities, the latter were normalized per 1 mg of sample (see also below).

Room-temperature *in situ* irradiation of the reaction mixture including the spin trapping agent PBN (*N*-tert-Butyl-α-phenylnitrone in the total concentration of 0.045 mol/dm^3) used a home-made setup of a 365 nm commercially available LED. PBN (for ESR spectroscopy, crystalline, assay ≥ 99.5% HPLC) was supplied by Sigma-Aldrich. All solutions were irradiated continuously through the grid of a rectangular ER 4102ST cavity (Bruker) at room temperature in a flat cell (ER 165FCVT-Q, Bruker). Prior to each irradiation, a blank experiment by LED-off-state was performed in order to exclude any EPR signal from the sample before light treatment. The *in situ* irradiation of the acylhydrazone molecular film was performed in the above-described flat cell. One end of the molecular film was laminated between the two pieces of Docuseal foil in order to provide free manipulation and positioning within the flat part and to irradiate the "active" (non-laminated) area of the molecular film, directly inside the EPR probe head. Prior to irradiation, both, the molecular film as well as the flat cell were intensively flushed with N_2. Afterwards, the entire system (cell + film) was assembled and tightly closed under Ar atmosphere within a glove-box in order to exclude air influence during the irradiation. Upon transfer from the glove-box to an EPR spectrometer the above-described system was covered by Al foil. All in situ EPR irradiation experiments were performed within the rectangular EPR probe head and with minimal influence of additional light sources outside of the EPR spectrometer.

10.2 EPR spectra of *in situ* reaction between AH5 and PBN spin trapping agent in acetonitrile

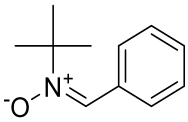

Figure S 78 Structure of Spin Trapping Agent (PBN).

10.2.1 Before Irradiation

AH5 was dissolved in CH_3CN at concentration c = 10 mM and PBN spin trap was added in total concentration of c = 45 mM. The sample was kept in dark and the EPR measured (Figure S 79) shows no signal of the reaction mixture before irradiation, thus meaning the non-irradiated **AH5** does not have unpaired electron density.

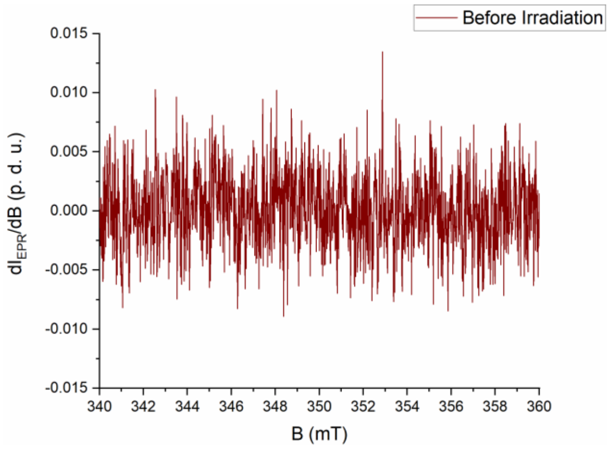

Figure S 79 EPR spectral sweeps recorded before the irradiation (‘dark’ mode). No signal was observed.

10.2.2 Continuous Irradiation

Upon continuous irradiation the reaction mixture gives typical signal of reaction between the PBN spin trap and photoswitched-form of **AH5**. EPR spectrum shows characteristic hyperfine splitting for PBN transient radical adduct with A (1 × ^{14}N) = 1.35 mT and A (1 × ^{1}H) = 0.22 mT. The g-value is centered at 2.0065. This confirms that the unpaired electron density is associated only with photoswitched-form of **AH5**.

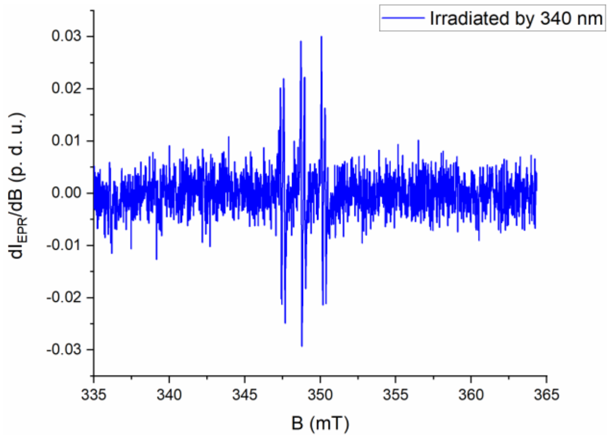

Figure S 80 EPR spectral sweeps recorded upon continuous irradiation. Spectrum shows typical signal centered at *g* = 2.0065 for reaction between the photoswitched-from of **AH5** and PBN spin trap.

11 ACYLHYDRAZONES AS CATALYSTS

11.1 AH5 as a catalyst

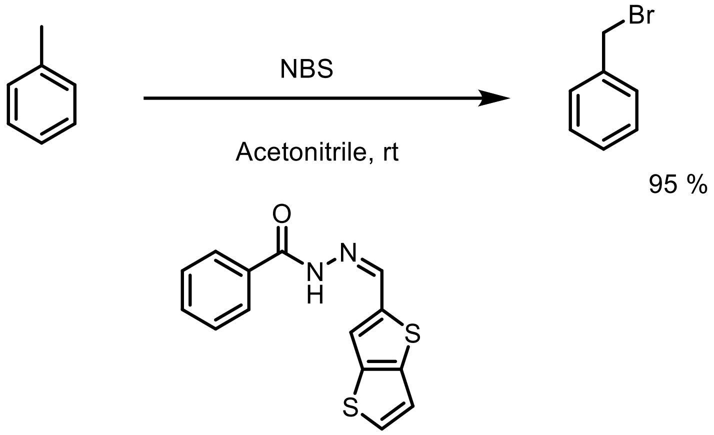

Figure S 81 Radical bromination exploiting photoswitched-form of **AH5** as a catalyst.

Procedure: **AH5** (0.01 mmol) was dissolved in ACN (5 mL) and the solution was irradiated by 340 nm light for 1 hour. After the irradiation has finished, NBS (0.2 mmol) and toluene (0.2 mmol) were added to the solution. The reaction mixture was stirred at rt for 3 hours and analyzed *via* HPLC. Then the solvent was evaporated and resulting mixture was analyzed by ^{1}H NMR.

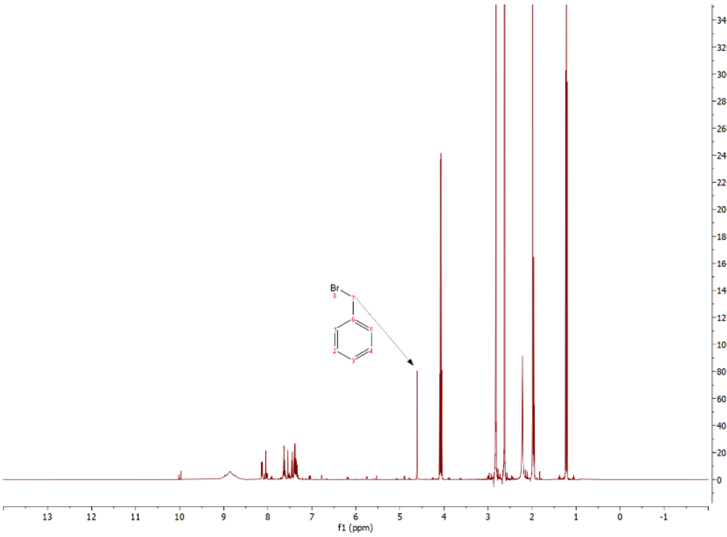

Figure S 82 ^{1}H NMR of resulting mixture after 3H.

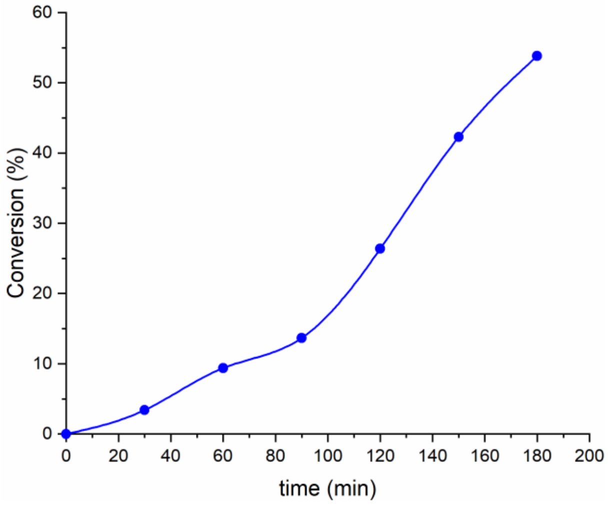

Figure S 83 The conversion of the reaction over 3 hours.

The reaction was also performed with non-irradiated **AH5** and it did not lead to the same conversion as with irradiated catalyst.

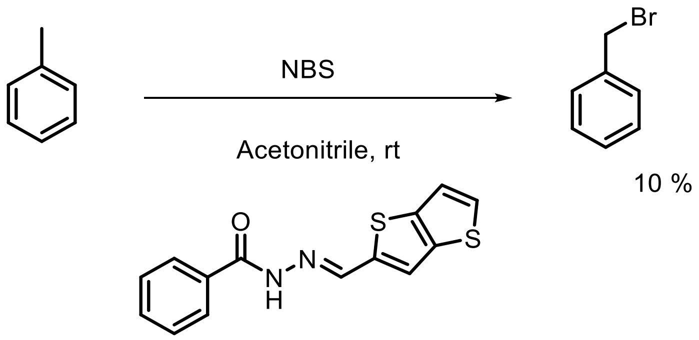

Figure S 84 Radical bromination using non-irradiated **AH5** as a catalyst.

11.2 AH2 as a catalyst

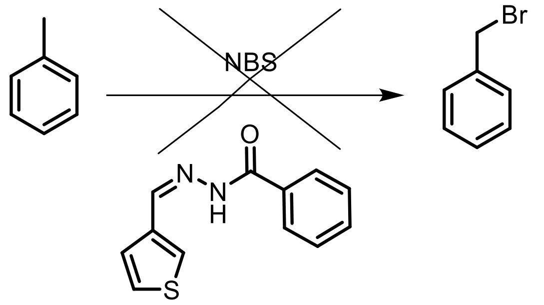

Figure S 85 Radical bromination exploiting photoswitched-form of **AH2** as a catalyst.

Procedure: **AH2** (0.01 mmol) was dissolved in ACN (5 mL) and the solution was irradiated by 295 nm light for 1 hour. After the irradiation has finished, NBS (0.2 mmol) and toluene (0.2 mmol) were added to the solution. The reaction mixture was stirred at rt for 3 hours and analyzed by HPLC. Then the solvent was evaporated and the resulting mixture was analyzed by ^{1}H NMR. *Z*-form of **AH2** did not produce the desired product.

11.3 DAE-2AH1 as a catalyst

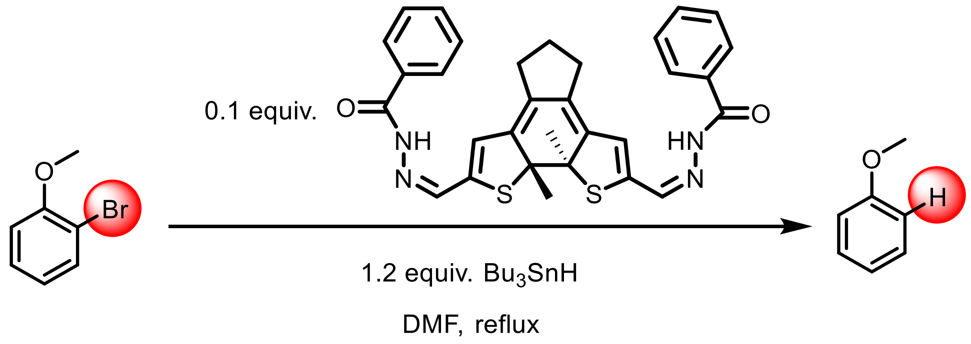

Figure S 86 Radical dehalogenation of 2-bromoanisole exploiting photoswitched-form of **DA-2AH1** as a catalyst

Procedure: **DAE-2AH1** (0.01 mmol) was dissolved in dry DMF (2 mL) and irradiated with 340 nm light for 2H to reach the complete conversion to photoswitched-form. Irradiated **DAE-2AH1** was then added to the evacuated flask filled with Ar containing 2-bromoanisole (0.1 mmol) and Tributylstannane (0.12 mmol). The reaction mixture was then heated to 65 °C for 13 hours and analyzed by HPLC and ^{1}H NMR.

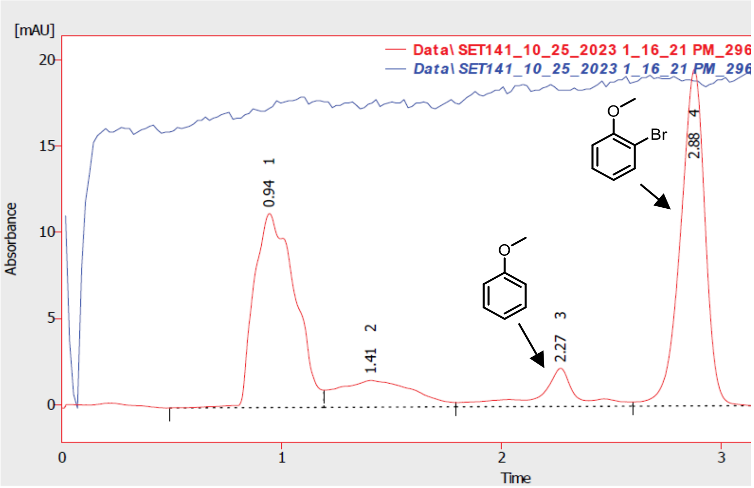

Figure S 87 HPLC chromatograph of resulting reaction mixture after night. We achieved a conversion of 15 %.

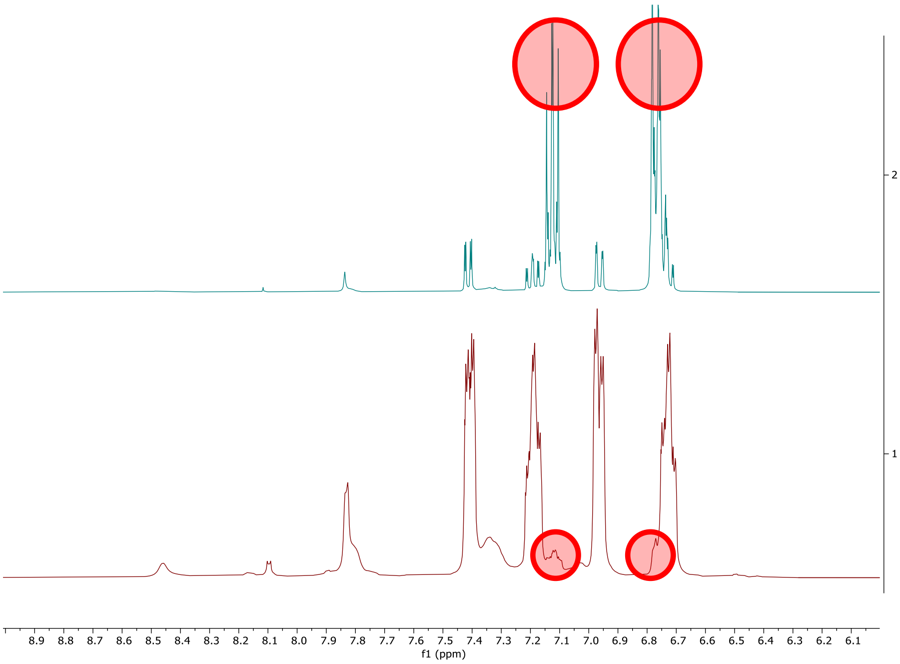

Figure S 88 ^{1}H NMR of the reaction mixture (down) and ^{1}H NMR of the reaction mixture with added anisole as a product (up). The highlighted peaks in the spectrum bellow have higher intensity in the upper spectrum clearly confirming the presence of the product in the reaction mixture.

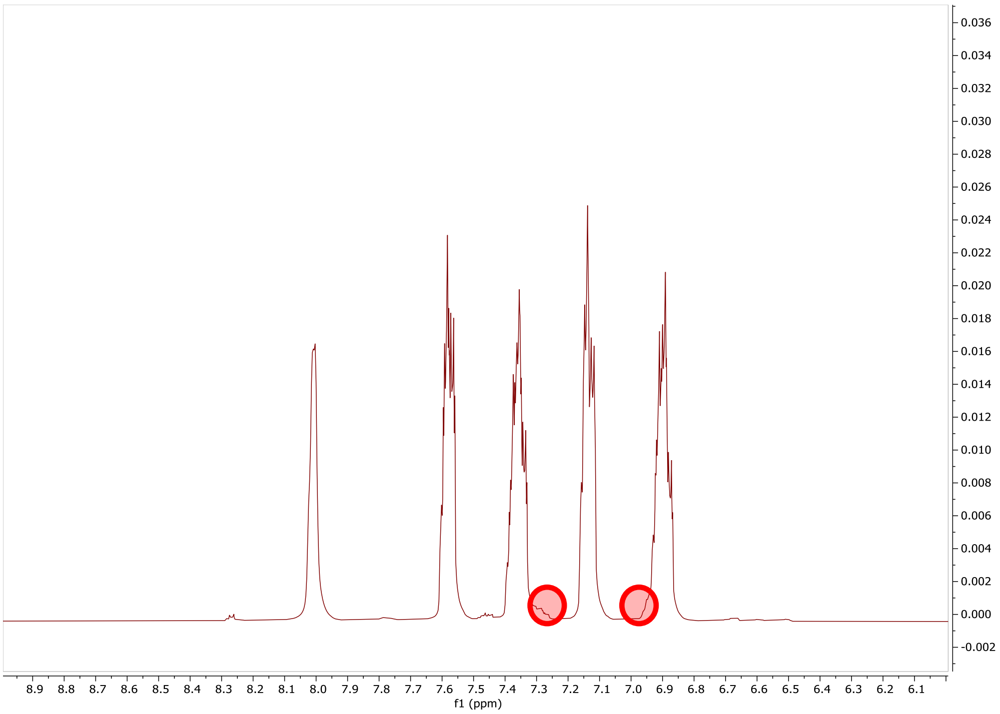

Figure S 89 ^{1}H NMR of the resulting mixture after reaction without the **DAE-2AH1**. We can clearly see the there is no trace of the product thus the **DAE-2AH1** is truly responsible for the successful dehalogenation.

12 CRYSTALLOGRAPHIC DATA FOR AH5

M = 286.38 g.mol^{-1}, monoclinic system, space group $P2_1/n$, a = 11.5536 (3) Å, b = 14.1661 (4) Å, c = 16.4150 (5) Å, β = 95.1406 (11)°, Z = 8, V = 2675.83 (13) Å^3, D_c = 1.422 g.cm^{-3}, μ(CuK-α) = 3.54 mm^{-1}, crystal dimensions of 0.42 × 0.36 × 0.21 mm. Data was collected at 180 (2) K on a Bruker D8 Venture Photon CMOS diffractometer with Incoatec microfocus sealed tube and Cu-$K\alpha$ radiation. The data reduction, scaling and absorption correction were performed in Apex4 (Bruker (2021). APEX4, SAINT and SADABS. Bruker AXS Inc., Madison, Wisconsin, USA). The phase problem was solved by charge flipping methods.[17] The structure was anisotropically refined by full matrix least squares on F^2 using the CRYSTALS[18] to final value R = 0.033 and wR = 0.087 using 5105 independent reflections (ϑ_{max} = 70.6°), 351 parameters and 8 restrains. The hydrogen atoms bonded to carbon atoms were placed in calculated positions refined with riding constraints, while hydrogen atoms bonded to nitrogen atoms were refined using soft restraints. The structure model was visualized using Diamond 3 (Brandenburg, K. (1999). DIAMOND. Crystal Impact GbR, Bonn, Germany), and Mercury 4.0.[19] The structure was deposited into Cambridge Structural Database under number CCDC 2345919.

The acylhydrazone **AH5** crystallized in monoclinic system in centrosymmetric space group $P2_1/n$. The asymmetric unit consists of two symmetry independent molecules of **AH5**, see Figure S 90. The bond lengths and angles in both molecules are very similar, with the largest difference in bond length being 0.009 Å for bond lengths C15–C16 and C35–C36 and the largest difference for the bond angles being 2.85 ° for N10–C11–C12 and N30–C31–C32. Although all atoms in the structure adopt sp^2 hybridization, the bonds in the bridge between phenyl and thieno[3,2-b]thiophene appear localized, with C1–C7, C7–N9, N9–N10 and C11–C12 having bond lengths very close to values expected for single bonds and N10–C11 having bond length close to value expected for a double bond. For further information on bond lengths, see Table S 6. The significant difference between the molecules can be found in their twisting. The molecule 1 (numbering from C1-C19) is twisted anticlockwise when viewed from C1–C7 single bond, while the molecule 2 (numbering from C21-C39) is twisted clockwise, when viewed from C21–C27 single bond. The twist in molecule 1 is larger compared to molecule 2, with dihedral angles between phenyl and thieno[3,2-b]thiophene of 66.43(6) and 35.14(6) ° respectively. The difference is caused by the rotation about the C1–C7 single bond, with C2–C1–C7–N9 torsion angle being 143.80(14) ° for molecule 1 and -170.48(12) ° for the same angle in molecule 2. For further details on torsion angles, see Table S 7.

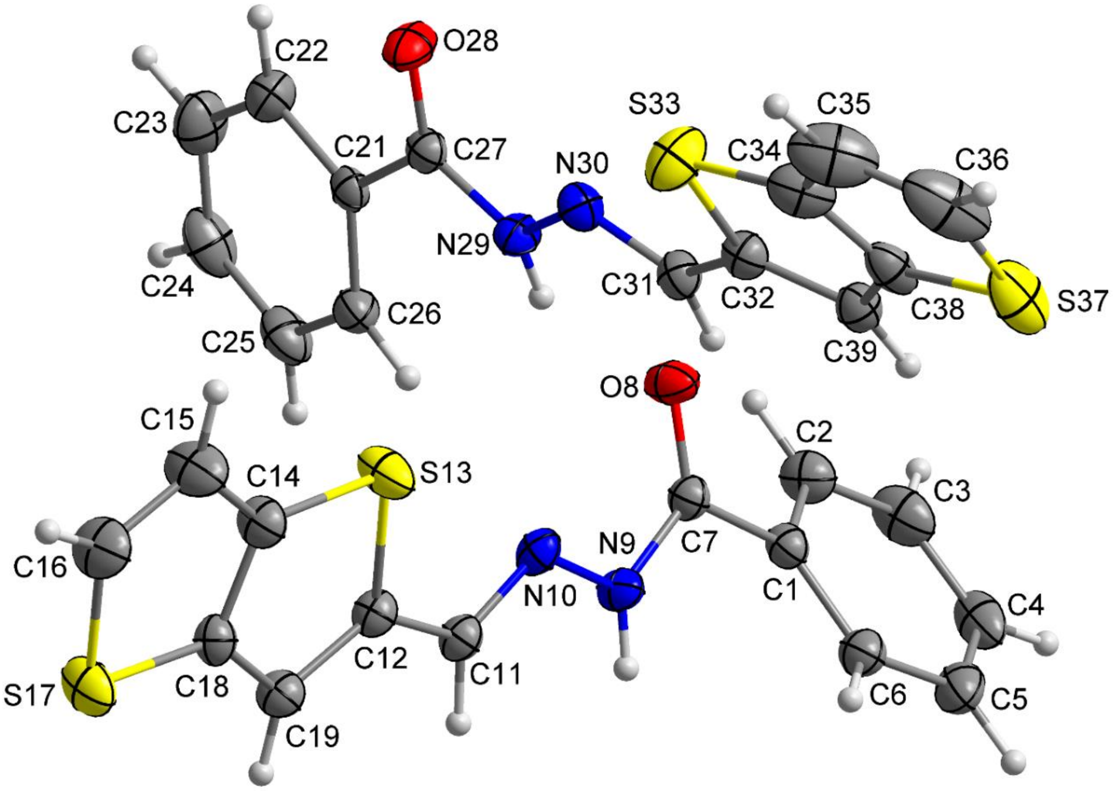

Figure S 90 The numbering scheme of crystal structure **AH5**, the ADP eplipsoids drawn at 50% probability level.

Table S 6 Selected bond lengths with expectation values for single and double bonds.

X–Y	X–Y (Å) (mol 1)	X–Y (Å) (mol 2)*	Expected bond (Å)[20]
C1–C7	1.4916(19)	1.4920(19)	Single 1.500
C7–N9	1.3525(18)	1.3558(18)	Single 1.355
N9–N10	1.3817(16)	1.3790(16)	Single 1.336
N10–C11	1.2819(19)	1.2761(19)	Double 1.279
C11–C12	1.4414(19)	1.448(2)	Single 1.470

Table S 7 Selected torsion angles.

W–X–Y–Z	W–X–Y–Z (°) (mol 1)	W–X–Y–Z (°) (mol 2)*
C2–C1–C7–N9	143.80(14)	-170.48(12)

C1–C7–N9–N10	172.91(11)	-174.11(11)
C7–N9–N10–C11	169.00(12)	-168.77(12)
N9–N10–C11–C12	176.51(12)	-176.30(12)
N10–C11–C12–C19	173.48(14)	-172.31(14)

[*] Molecule 2 is numbered with addition of 20.

The most prominent feature in crystal packing is formation of hydrogen bond chain in direction of *b* axis. The molecule 1 participates in the chain formation with one N–H···O hydrogen bond, while molecule 2 participates with one N–H···O(N) bifurcated hydrogen bond. Both bond direction and interatomic distances heavily favor the N29–H291···O8 hydrogen bond; however, the presence of weaker N29–H291···N10 hydrogen bond cannot be disregarded. In absence of other strong hydrogen bond donors, the chain is further supported by weaker C–H···O and C–H···N hydrogen bonds, see Figure S 91. The chains are connected together by weak C–H···π, C···S and S···S interactions. For further information on hydrogen bonding, see Table S 8.

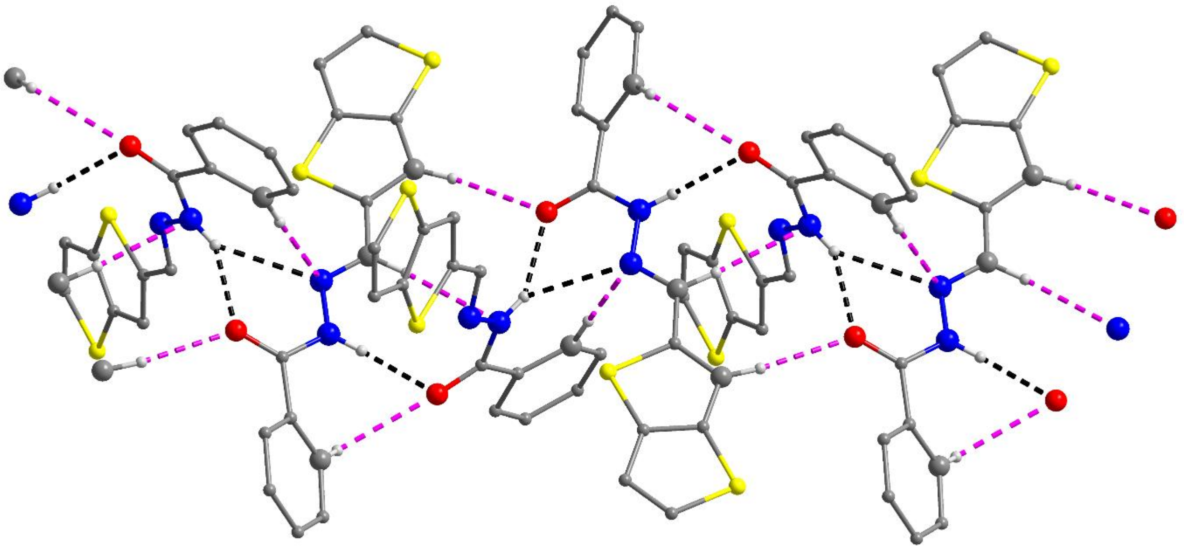

Figure S 91 The hydrogen bond chain in structure **AH5**, with stronger hydrogen bonds depicted as black dashed lines, weaker C–H···O(N) hydrogen bonds depicted in pink. The atoms are displayed as balls with arbitrary radii.

Table S 8 Selected hydrogen bonds in structure of **AH5**.

D–H···A	D–H (Å)	H···A (Å)	D···A (Å)	D–H···A (°)
N9–H91···O28^{i}	0.844(14)	2.123(15)	2.937(2)	161.9(16)
N29–H291···O8	0.851(14)	2.132(15)	2.909(2)	151.8(16)
N29–H291···N10	0.851(14)	2.660(17)	3.340(2)	137.9(14)
C6–H61···O28^{i}	0.93	2.65	3.281(2)	126
C11–H111···N29^{i}	0.97	2.53	3.485(2)	170
C19–H191···O8^{i}	0.93	2.46	3.372(2)	169
C26–H261···N10	0.97	2.65	3.620(2)	174

Symmetry code: (*i*) -*x*+0.5, *y*-0.5, -*z*+1.5.

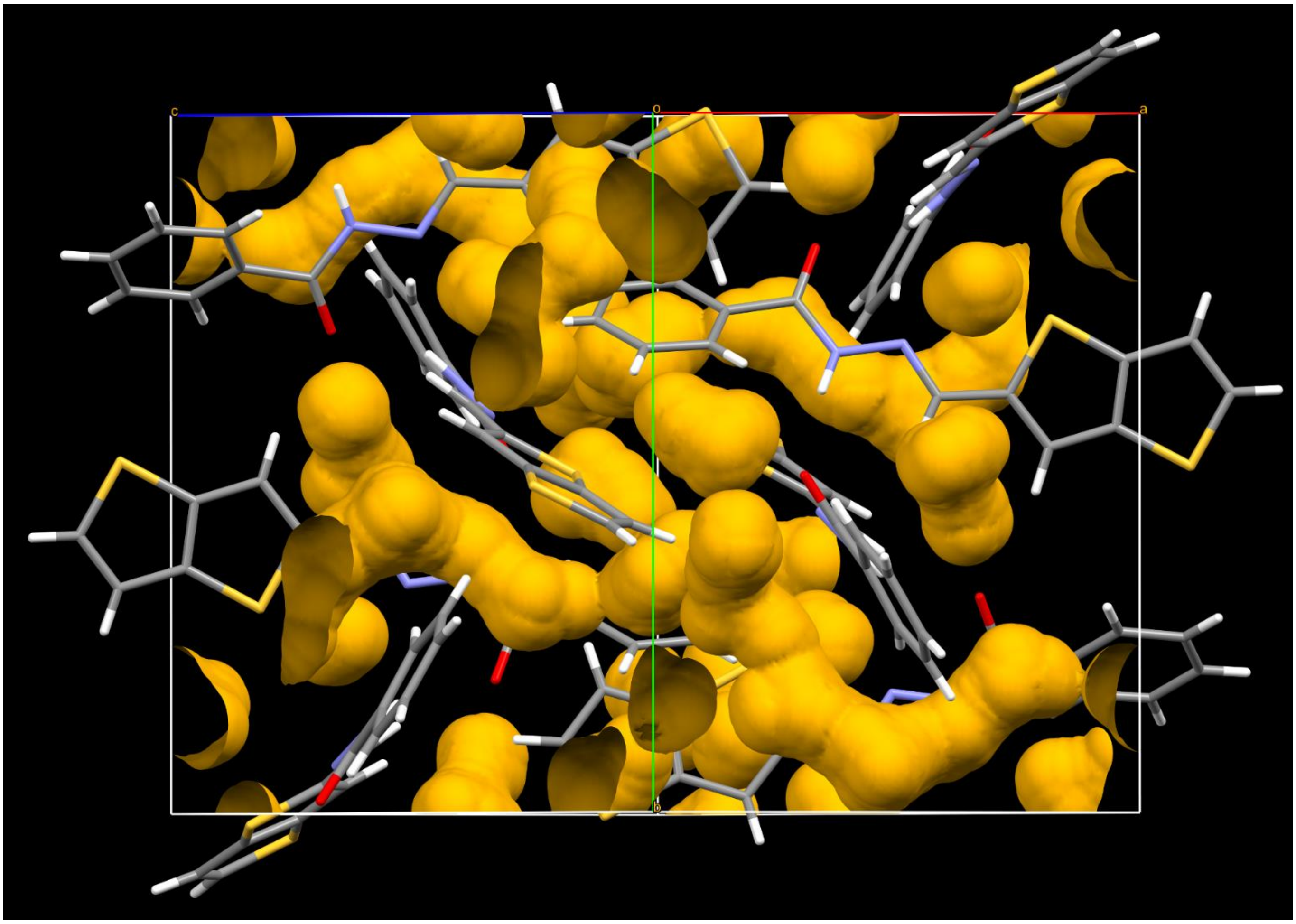

Figure S 92 The voids in structure **AH5** visualized with probe radius 0.8 Å and grid spacing 0.1 Å.

REFERENCES

1 H. E. Gottlieb, V. Kotlyar and A. Nudelman, *J. Org. Chem.*, 1997, **62**, 7512–7515.

2 J. Podlesný, O. Pytela, M. Klikar, V. Jelínková, I. V. Kityk, K. Ozga, J. Jedryka, M. Rudysh and F. Bureš, *Org. Biomol. Chem.*, 2019, **17**, 3623–3634.

3 M. Firstenberg, K. N. Shivananda, I. Cohen, O. Solomeshch, V. Medvedev, N. Tessler and Y. Eichen, *Adv. Funct. Mater.*, 2011, **21**, 634–643.

4 S.-H. Kang, H. R. Lee, G. K. Dutta, J. Lee, J. H. Oh and C. Yang, *Macromolecules*, 2017, **50**, 884–890.

5 M. Almáši, M. Walko, J. Boržíková and R. Gyepes, *Inorganica Chim. Acta*, 2020, **512**, 119879.

6 M. Kathan, P. Kovaříček, C. Jurissek, A. Senf, A. Dallmann, A. F. Thünemann and S. Hecht, *Angew. Chem. Int. Ed.*, 2016, **55**, 13882–13886.

7 R. Singh, H.-Y. Wu, A. Kumar Dwivedi, A. Singh, C.-M. Lin, P. Raghunath, M.-C. Lin, T.-K. Wu, K.-H. Wei and H.-C. Lin, *J. Mater. Chem. C*, 2017, **5**, 9952–9962.

8 D. J. van Dijken, P. Kovaříček, S. P. Ihrig and S. Hecht, *J. Am. Chem. Soc.*, 2015, **137**, 14982–14991.

9 C. G. Hatchard, C. A. Parker and E. J. Bowen, *Proc. R. Soc. Lond. Ser. Math. Phys. Sci.*, 1997, **235**, 518–536.

10 M. Montalti, A. Credi, L. Prodi and M. T. Gandolfi, *Handbook of Photochemistry*, CRC Press, Boca Raton, 3rd edn., 2006.

11 J.-D. Chai and M. Head-Gordon, *J. Chem. Phys.*, 2008, **128**, 084106.

12 A. Schäfer, H. Horn and R. Ahlrichs, *J. Chem. Phys.*, 1992, **97**, 2571–2577.
13 A. Schäfer, C. Huber and R. Ahlrichs, *J. Chem. Phys.*, 1994, **100**, 5829–5835.
14 V. Barone and M. Cossi, *J. Phys. Chem. A*, 1998, **102**, 1995–2001.
15 F. Neese, *WIREs Comput. Mol. Sci.*, 2012, **2**, 73–78.
16 F. Neese, *WIREs Comput. Mol. Sci.*, 2022, **12**, e1606.
17 L. Palatinus and G. Chapuis, *J. Appl. Crystallogr.*, 2007, **40**, 786–790.
18 P. W. Betteridge, J. R. Carruthers, R. I. Cooper, K. Prout and D. J. Watkin, *J. Appl. Crystallogr.*, 2003, **36**, 1487–1487.
19 C. F. Macrae, I. Sovago, S. J. Cottrell, P. T. A. Galek, P. McCabe, E. Pidcock, M. Platings, G. P. Shields, J. S. Stevens, M. Towler and P. A. Wood, *J. Appl. Crystallogr.*, 2020, **53**, 226–235.
20 F. H. Allen, O. Kennard, D. G. Watson, L. Brammer, A. G. Orpen and R. Taylor, *J. Chem. Soc. Perkin Trans. 2*, 1987, **12**, S1–S19.